FUNCTIONAL ANALYSIS OF PUTATIVE THIOL-DISULFIDE OXIDOREDUCTASES IN GROUP A STREPTOCOCCUS

By

Lydia Li

Submitted in partial fulfilment of the requirements
for the degree of Master of Science

at

Dalhousie University
Halifax, Nova Scotia
July 2018

Table of Content

List of Tables

List of Figures

Abstract

Group A *Streptococcus* (GAS) is a pathogenic bacterium that strictly infects humans, causing a diverse range of diseases from severe toxic shock syndrome to moderate strep throat infection, especially in children. GAS produces certain virulence factors that are structurally held together by complex molecular linkages, including covalent disulfide bonds formed between cysteine residues. Disulfide bonds are essential for protein stability and function, and are formed *in vivo* by enzymes called thiol-disulfide oxidoreductases (TDORs). Remarkably, disulfide bond formation pathways have not been studied in the context of GAS pathogenesis and could be an excellent approach to better understanding the structure and regulation of virulence factors in GAS. An *in silico* approach was used to identify five putative TDORs in GAS which were individually mutated and their subsequent biological functions characterized. Our results have identified 2037 as a novel TDOR enzyme in GAS. The *Δ2037* mutant showed significantly increased sensitivity to oxidative stress-promoting compounds and was more susceptible to phagocytic death by murine macrophages, indicating a role for 2037 in maintaining thiol balance at the cell surface through an unknown mechanism. Most notably, 2037 is needed for proper disulfide bond formation in an important GAS exotoxin: streptococcal pyrogenic exotoxin A (SpeA). Redox state analysis of SpeA secreted by the parent culture showed the presence of a disulfide linkage (oxidized form) whereas this disulfide bond was broken (reduced form) in *Δ2037* cultures. The *2037*-complemented mutant restored SpeA to the oxidized state, implicating 2037 as a direct player in forming the disulfide bond of SpeA. Consistent with these data, 2037 exhibited functional oxidase activity *in vitro* and disulfide exchange reactions showed recombinant SpeA changed from its initial reduced form to an oxidized form following incubation with oxidized recombinant 2037 but not reduced 2037. Furthermore, preliminary point mutation data suggests that the active site 2037 cysteines 46 and 49 have different reactivites, with the N-terminal Cys46 possibly playing a distinct mechanistic role during protein complex formation with SpeA. This is the first report of an enzyme being directly involved in the proper folding of a superantigenic toxin. Our findings highlight the importance of studying disulfide pathways in modifying virulence factors secreted by pathogenic bacteria, and pave the way for new drug targets and vaccine development strategies that offer an alternative to antibiotics.

List of Abbreviations Used

β	Beta
Ω	Ohms
°C	Degree Celsius
µF	Microfarad
µg	Microgram
µl	Microliter
µM	Micromolar
nmol	Nanomolar
x g	Times gravity
Δ	Deletion
AhpC	Alkyl hydroperoxide reductase
Amp	Ampicillin
AP	Alkaline phosphatase
APC	Antigen presenting cell
APS	Ammonium persulfate
ARF	Acute rheumatic fever
BCIP	5-bromo-4-chloro-3-indoyl phosphate
BHI	Brain heart infusion
Bp	Base pair
cCMP	Cytidine 2':3'-cyclic monophosphate monosodium salt
CFU	Colony forming unit
CHAP	Cysteine, histidine-dependent amidohydrolase/peptidase

cm	Centimeter
Cys	Cysteine
DNA	Deoxyribonucleic acid
dNTP	Deoxynucleotide triphosphate
DTT	Dithiothreitol
EB	Electroporation buffer
EDTA	Ethylenediaminetetraacetic acid
Ery	Erythromycin
FBS	Fetal bovine serum
GAS	Group A *Streptococcus*
GpoA	Glutathione peroxidase
GTE	Glucose-Tris-EDTA
GSH	Reduced glutathione
GSSG	Oxidized glutathione
HA	Hyaluronic acid
HEPES	4-(2-hydroxyethyl)-1-piperazineethanesulfonic acid
HF	High-fidelity buffer, for Phusion polymerase
His_6	Hexahistidine
HTVG	HEPES-buffered tryptone-vitamins glucose media
INFγ	Interferon gamma
IL	Interleukin
IPTG	Isopropyl-β-D-thiogalactoside
KAc	Potassium acetate

Kan	Kanamycin
Kb	Kilobase
kDa	Kilo dalton
L	Litre
LB	Luria-Bertani
Mal	Maleimide
MHC	Major histocompatibility complex
mA	Milliampere
ml	Milliliter
mm	Millimeter
mM	Millimolar
NADPH	Nicotinamide adenine dinucleotide phosphate (reduced form)
NBT	Nitro-blue tetrazolium
OD	Optical density
PBP	Penicillin binding protein
PCR	Polymerase chain reaction
PHAC	Public Health Agency of Canada
pKa	Acid dissociation constant, logarithmic scale
PBS	Phosphate-buffered saline
PBST	Phosphate-buffered saline with Tween-20
PCR	Polymerase chain reaction
PEG	Polyethylene glycol
RBC	Red blood cell

RNA	Ribonucleic acid
RNaseA	Ribonuclease A
ROS	Reaction oxygen species
Rpm	Revolutions per minute
RPMI	Roswell Park Memorial Institute medium
SAg	Superantigen
SDS	Sodium dodecyl sulphate
SDS-PAGE	Sodium dodecyl sulphate polyacrylamide gel electrophoresis
SE	Staphylococcal enterotoxins
SEC	Size exclusion chromatography
SEI	Staphylococcal enterotoxin-like proteins
SLO	Streptolysin S
SLS	Streptolysin O
SmeZ	Streptococcal mitogenic exotoxin Z
Sod	Superoxide dismutase
SpeA	Streptococcal pyrogenic exotoxin A
SSA	Streptococcal superantigen
STSS	Streptococcal toxic shock syndrome
T_m	Melting temperature
TAE	Tris-acetate-EDTA
TCA	Trichloroacetic acid
TCR	T cell receptor
TDOR	Thiol-disulfide oxidoreductase

TE	Tris-EDTA
TEMED	Tetromethylenediamine
TNFα	Tumor necrosis factor alpha
Tris	Tris (hydroxymethyl) aminomethane
TrxR	Thioredoxin reductase
TSST-1	Toxic shock syndrome toxin-1
U	Unit
V	Volts
Vβ	Variable beta chain
v/v	Volume per volume
w/v	Weight per volume

Acknowledgments

First and foremost, I would like to thank my supervisors Dr. Song Lee and Dr. Scott Halperin who have been incredibly supportive throughout my Masters program. Their advice and mentorship have both motivated and inspired me as a trainee. Thank you to the John McCormick lab at Western University, London ON Canada, for sharing their plasmids and knowledge on the MGAS8232 strain with us. I would also like to extend my gratitude to Dr. Nikhil Thomas and Dr. Jason LeBlanc for serving on my supervisory committee and for providing valuable insight on my project. Special thanks to Naif Jalal, the CCfV staff, as well as other present and past members of our lab who have helped me along my 2 year journey. Your contribution to my project, whether big or small, did not go unnoticed. Funding support from the IWK Graduate Student Scholarship and McCarlie Award is also acknowledged.

CHAPTER 1: Introduction

1.1 Group A Streptococcus

Streptococcus pyogenes, commonly known as Group A streptococcus (GAS), is a pathogenic Gram-positive bacterium that strictly infects humans, setting it apart from many other streptococcal species. GAS is spherical in morphology, characteristically forming chains of cocci that are non-motile (Bisno, 1991). Classifications of streptococcal species are initially based on the traditional Lancefield system; this involves grouping streptococci according to the reaction of antiserum raised against variable cell wall antigens and polysaccharides (Bessen, 2010; Lancefield, 1962). More than 20 serologic groups were identified and designated by letters (i.e. A, B, C, etc). In addition to Group A streptococci, Group B streptococcus is another established human pathogen that can cause neonatal pneumonia and meningitis; disease caused by Group C and group G streptococci are also described in the literature (Quach et al., 2009; Zaoutis, Attia, Gross, & Klein, 2004).

Isolates within the Group A streptococci classification are further divided into serotypes based on antigenic differences in the M protein molecule. The M protein is an anti-phagocytic surface protein that plays a major role in virulence. It is present in all isolates, displaying a high level of sequence polymorphism (Cole et al., 2010; Steer et al., 2009). In other words, every strain has a slightly different M protein. During *S. pyogenes* infection, Lancefield (1962) found that antibodies developed against strain-specific M proteins led to killing by opsonophagocytosis and immunity against reinfection; however, antibodies raised against the M protein of one strain often failed to protect against infection by another. Strong protective immunity is therefore M

type-specific (Lancefield, 1962). The development of antiserum directed to M proteins was the foundation of the serologically-based scheme known as M typing.

To better characterize and measure the growing genetic diversity among isolates of *S. pyogenes*, an extension of the Lancefield system through *emm* sequence typing is routinely used today (Facklam et al., 2002; Steer et al., 2009). This involves sequencing the 5' end of the *emm* gene, encoding for the M protein (Steer et al., 2009). To date, there are more than 200 *emm* types described (i.e., M1, M12, M18, M24, etc) (Bessen, 2010). Collectively, these classification systems serve as valuable epidemiological markers and provide a reference point for investigating outbreaks of *S. pyogenes* disease.

1.1.1 Prevalence of GAS

On the global scale, *S. pyogenes* is associated with significant morbidity and mortality, accounting for at least 517, 000 deaths each year worldwide (Carapetis, Steer, Mulholland, & Weber, 2005). It was ranked ninth among individual pathogens causing the highest estimated deaths, as reported in 2002 by the World Health Organization (Carapetis et al., 2005). Although quantifying an accurate disease burden remains challenging and available epidemiological data from 2005 may require revision, GAS is responsible for an estimated 616 million cases of throat infection (pharyngitis, tonsillitis) worldwide each year, and 111 million cases of skin infection in children of under-developed countries (Carapetis et al., 2005). While in high-income countries GAS infection predominantly raises public health concerns for pharyngitis and invasive diseases, low-income countries have a higher prevalence of rheumatic fever, rheumatic heart disease and glomerulonephritis (Steer et al., 2009). Indeed, the greatest burden of streptococcal diseases is encountered in low-income countries (Steer et al., 2009). Distribution differences of *S. pyogenes* serotypes vary both year-to-year and geographically, with certain M serotypes of GAS linked to

the high income countries that are scarcely seen in lower income nations. This inevitably represents a great obstacle in designing an effective GAS vaccine.

In Canada, GAS infections have also been the subject of public health concern. According to data from the Public Health Agency of Canada (PHAC), the number of reported cases of severe GAS infection in Canada has been rising steadily over the last 15 years (PHAC, 2014). Local media have reported extensively on recent outbreaks of a particularly invasive GAS strain that has affected Toronto, Montreal, Vancouver, Ottawa and other cities, with nine dead in the London Ontario area since 2016 (Ireland, 2017; Picard, 2018). The underlining causes of these outbreaks remains unknown, but are also reminiscent of other epidemic outbreaks in history, such as invasive strains affecting Los Angeles County, USA in the 1980s and parts of Norway and Sweden from 1987-1989 (Bisno, 1991).

1.1.2 Superficial colonization and infection

Outside of the human host, there is no known reservoir for GAS (Wilkening & Federle, 2017). This bacterium primarily colonizes the mucosal epithelium of the oropharynx and the epidermal layer of the skin (Bessen, 2010). It is at these two niche sites that the organism most often enters and exits its biological host. Upon initial invasion, GAS tends to reside extracellularly as it attempts to replicate and persist while overcoming human immune system defenses (Bessen, 2010).

The presence of GAS does not always result in symptomatic infection. In fact, GAS is carried asymptomatically in 5–20% of school-age children during seasonal peaks and 25% of adults with household contact of infected school-age children (Bessen, 2010; Bisno, 1991). This quiescent carrier state elicits little or no immune response to streptococcal antigens.

Asymptomatic throat carriage can persist for weeks or months while carriage at the skin is less well understood, and may be only transient (Bessen, 2010; Kaplan, 1980).

When a productive infection does occur, GAS is often clinically associated with impetigo and streptococcal pharyngitis (strep throat) (Bessen, 2010). Impetigo is a topical skin infection that results in honey-colored crusted skin lesions and mainly affects children between the ages of 2-6 years old (Parks, Smeesters, & Steer, 2012). This contagious disease is spread through direct contact with open wounds and sores on the skin from infected individuals (Bessen, 2010; Walker et al., 2014). Strep throat is infection of the pharynx, which results in swelling of the tonsils and mucus production, usually accompanied by fever (Parks et al., 2012). Other common symptoms include malaise, headache, nausea, abdominal pain, and vomiting (Walker et al., 2014). GAS pharyngitis is generally self-limiting but is highly communicable person-to-person through mucous secretions and saliva droplets (coughing) (Walker et al., 2014). Children aged 5-15 years are especially susceptible to infection (Wilkening & Federle, 2017). Both impetigo and pharyngitis are examples of well-characterized moderate-to-mild cases of GAS infection routinely treated with antibiotics.

1.1.3 Invasive diseases

Rare invasive GAS infections also occur, which are the consequence of the bacteria migrating to normally sterile sites, such as the bloodstream and deep tissues. (Bisno, 1991; Walker et al., 2014). This intrusive migration can lead to tissue destruction, bacterial dissemination, and hyper-inflammation (Walker et al., 2014). Despite representing a minority of cases, invasive illnesses have long been the focal point of GAS research (Wilkening & Federle, 2017). Invasive diseases range from less severe forms of cellulitis and bacteremia, to more

severe cases of necrotizing fasciitis (flesh-eating disease) and streptococcal toxic shock syndrome (STSS) (Cunningham, 2008; Walker et al., 2014).

GAS infections that originate in the skin, such as impetigo, may penetrate the epidermis to cause cellulitis (Walker et al., 2014). Cellulitis is an infection of the subcutaneous tissues and manifests as redness and inflammation of the skin with associated pain and swelling (Walker et al., 2014). Bacteremia is the presence of GAS in the bloodstream and is often characterized by high fever, nausea, and vomiting as a result of a robust pro-inflammatory cytokine response (Bessen, 2010). As reviewed by Walker et al. (2014), GAS strains may be introduced directly into the bloodstream from childbirth, or may be introduced as a consequence of superficial infection of the throat or skin.

Necrotizing fasciitis is a severe invasive GAS infection of the skin, subcutaneous tissue, fascia, and muscle (Walker et al., 2014). This flesh-eating disease has high mortality rates due to the rapidly progressive nature of the infection. (Cunningham, 2008). As the name implies, GAS invades and spreads along the fascial sheaths that separate adjacent muscle groups, which in turn are breached, resulting in severe necrosis of the adjacent tissues (Cunningham, 2008; Walker et al., 2014). Symptoms commonly present as localized pain, chills, fever, sore throat, rash and vomiting (Cunningham, 2008). While GAS is the most common cause of flesh-eating disease, this disease state is frequently polymicrobial in nature (Wilkening & Federle, 2017).

1.1.4 Toxin-mediated diseases

The pathogenesis of streptococcal toxic shock syndrome is related in part to the ability of certain streptococcal pyrogenic exotoxins released by GAS that function as superantigens (SAgs) (Parks et al., 2012; Walker et al., 2014). In STSS, SAgs cause activation of a large numbers of T

cells in an antigen-independent manner. The result is a massive cytokine response by T cells (IL-2, IFN-γ) and antigen-presenting cells (TNF-α, IL-1β, and IL-6) (Walker et al., 2014; Xu & McCormick, 2012). STSS often occurs in conjunction with other invasive streptococcal diseases and rapid onset can result in hypotension, widespread tissue damage and fatal multiple-organ failure (Steer et al., 2009). Additionally, the lack of anti-SAg antibodies has been associated with an increased risk of STSS (Breiman et al., 1993).

GAS strains that secrete streptococcal pyrogenic exotoxins are also the causative agent of clinical scarlet fever (Bessen, 2010). Scarlet fever is characterized by a distinct red sandpaper rash, fever and swelling of the tongue that gives a strawberry appearance (Parks et al., 2012). However, scarlet fever only affects a small number of individuals who have strep throat or streptococcal skin infections. The rash may persist for more than a week and can manifest in either mild or severe infections (Bisno, 1991).

1.1.5 Non-pyrogenic diseases

Prior GAS infections that were not properly treated may result in a number of post-infectious sequelae (Bisno, 1991). These non-suppurative complications of GAS infections include rheumatic fever and glomerulonephritis (Ferretti, Stevens, & Fischetti, 2016; Walker et al., 2014).

Acute rheumatic fever (ARF) is a delayed inflammatory complication of pharyngitis, appearing 2-5 weeks later, with symptoms such as fever, multiple painful joints and involuntary muscle movements (Steer et al., 2009). While the pathogenesis of ARF is still being actively studied, symptoms are auto-immune in nature and likely due to antibody cross-reactivity against shared epitopes from the streptococcal M-protein similar to epitopes found in cardiac myosin,

synovial, and neuronal tissues (Bisno, 1991). Cross-reactivity of self-antibodies that target and damage the heart valve antigens is known as rheumatic heart disease (Steer et al., 2009). Rheumatogenic serotypes associated with documented epidemiologically outbreaks include M1, 3, 5 and 18 (Bisno, 1991). Similarly, post-streptococcal glomerulonephritis is the immune-mediated swelling of and subsequent damage to the kidneys, which may eventually result in kidney failure (Cunningham, 2008). GAS M12 and M49 serotypes have most commonly been related to glomerulonephritis which typically affect children the most (Cunningham, 2008; Wilkening & Federle, 2017).

Taken together, *S. pyogenes* produces infections of varying clinical severities, with genetically identical strains even causing both severe and non-severe human diseases (Bessen, 2010). This points to an important role for both bacterial and host factors in determining the clinical outcome of streptococcal infections.

1.2 Dynamic regulation of GAS virulence factors

GAS virulence factors work in a highly coordinated fashion to help establish a successful infection in the human pharynx, a challenging environment for bacterial colonization. Virulence factors are produced by bacteria to aid in invading and multiplying within the host; this includes surface adherence proteins, secreted exotoxins, production of a protective capsule and growth factors (Cross, 2008). Work done in evolutionary biology points to complex virulence regulation and quorum-sensing pathways as playing key roles in bypassing primary pharyngeal defences (Bessen, 2010). These mechanisms allow rapid and dynamic alterations in gene expression without requiring a fixed mutation in the genome. When misregulated however,

these pathways could have counter-productive consequences if host immune responses become stimulated, which work to kill any GAS bacteria (Wilkening & Federle, 2017). This GAS host-pathogen interaction is the focus of on-going research with the mechanisms from both sides lacking in full understanding.

Two well-studied virulence regulators in *S. pyogenes* are the stand-alone regulator Mga and the CovRS two-component system (Kasper, 2013; Kreikemeyer, McIver, & Podbielski, 2003). All GAS serotypes have the transcriptional activator Mga which regulates genes required for growth, adaptation into new tissue sites and expression of surface associated molecules such as the M protein and C5a peptidase (Kreikemeyer et al., 2003). The CovRS two-component system is comprised of a sensory histidine kinase (CovS) that auto-phosphorylates in response to an environmental signal, and transfers the phosphate to a response regulator (CovR), which then influences the transcription of approximately 15% of genes in GAS (Kreikemeyer et al., 2003). The CovRS system controls genes involved in stress adaptation and virulence, including the hyaluronic acid synthesis operon, streptokinase, cysteine protease, mitogenic factor, capsule and streptolysin S (Kreikemeyer et al., 2003; Wilkening & Federle, 2017). Indeed, other regulators also exist that are less well-defined in the context of GAS pathogenesis.

1.2.1 Hemolysins

In the early stages of infection, streptolysin O (SLO) and streptolysin S (SLS) are two potent toxins expressed by almost all GAS strains (Fontaine, Lee, & Kehoe, 2003). These proteins lyse mammalian erythrocytes, or red blood cells (RBCs), and are responsible for the zone of beta (β)-hemolysis observed on blood agar plates (Molloy, Cotter, Hill, Mitchell, & Ross, 2011). SLO is a 540-amino-acid secreted protein toxin that is also highly immunogenic.

SLO binds to cholesterol in eukaryotic cell membranes, where it ultimately oligomerizes to produce large transmembrane pores, leading to cell lysis (Fontaine et al., 2003).

On the other hand, active SLS is a 2.7 kDa peptide that is cytolytic only when associated with the bacterial cell surface or in the presence of certain carrier molecules (Molloy et al., 2011; Theodore & Calandra, 1981). SLS is extensively post-transcriptionally modified, resulting in the formation of distinctive heterocycles, prior to export from the cell. Previous studies of transposon mutants of GAS that lacked SLS production revealed that the *sagA* gene encodes a 53-amino acid SLS precursor, called SagA (Betschel, Borgia, Barg, Low, & De Azavedo, 1998; Molloy et al., 2011). In contrast to SLO, SLS is not immunogenic in the course of natural infection, however, isolation of the mature SLS toxin and elucidation of its molecular structure has proven to be challenging (Fontaine et al., 2003).

1.2.2 Bacteriocins

GAS is able to compete with the highly complex microbiota of the human upper respiratory tract during infection, including many other species of streptococci, by producing bacteriocins. Bacteriocins are small, ribosomally synthesized antimicrobial peptides that typically demonstrate activity against closely related organisms (Armstrong et al., 2016). There are three major classes of bacteriocins: Class I bacteriocins that undergo post-translational modification to incorporate lanthionine or β-methyllanthionine residues into the active peptide; Class II bacteriocins that are typically not post-translationally modified except for leader peptide cleavage and disulfide bond formation; and Class III bacteriocins (Armstrong et al., 2016). Of importance to bacteriocin regulation is the streptococcal invasion locus (*sil*), a quorum-sensing locus which is activated by the auto-inducer peptide SilCR through the two-component system SilA-SilB (Belotserkovsky et al., 2009). Recent studies of the invasive GAS strain JS12 show

that upon sensing asparagine released by host cells, GAS upregulates expression of the SilCR; this auto-induction process propagates throughout the GAS population, resulting in bacteriocin production (Hertzog et al., 2018). While *sil* has been linked to bacteriocin production and increased virulence in GAS, only 18% of clinical GAS isolates have an intact *sil* locus, suggesting a more complex explanation (Hertzog et al., 2018). In the M18 strain, for example, the SilD/E transporter is inactivated, and a promoter element is highly induced within the mouse nasopharynx, which might account for bacteriocin production *in vivo* (Armstrong et al., 2016; Hertzog et al., 2018).

1.2.3 Cell-membrane and cell-wall integrity

As mentioned, the CovRS two-component signal transduction regulatory system in GAS represses roughly 15% of the GAS genome, including virulence-associated genes, in response to the environment (Cole et al., 2010; Dalton & Scott, 2004). Under mild stress conditions, CovS reportedly dephosphorylates CovR, either directly or indirectly, leading to its inactivation; the dephosphorylated CovR then dissociates from the regulatory promoter sequences to which it usually binds (Dalton & Scott, 2004). CovR inactivation therefore relieves repression of many GAS genes. This allows transcription of genes needed for growth of GAS under general stress conditions such as low iron, elevated temperatures (40°C), pH changes, and growth in the presence of saline (Cole et al., 2010; Dalton & Scott, 2004). Along the same lines, other one-component Ser/Thr kinase-mediated regulatory systems in GAS have been reported to mediate proteins containing a CHAP (cysteine and histidine-dependent aminohydrolases/peptidases) domain (Pancholi, Boël, & Jin, 2010). Proteins with CHAP domains are mainly involved in peptidoglycan hydrolysis, thus making them important in the regulation of cell division, growth, and virulence (Pancholi et al., 2010).

Maintaining a healthy cell-wall and cell-membrane are crucial for GAS survival and current treatments for GAS infections involve antibiotics, specifically those that target the bacterial cell wall. GAS is most often treated with β-lactam antibiotics such as penicillins (i.e. penicillin or amoxicillin) (Eneli & Davies, 2007; Parks et al., 2012). Penicillin and other β-lactam antibiotics inhibit the formation of peptidoglycan cross-links in the bacterial cell wall by binding transpeptidase, also called penicillin binding proteins (PBPs) for their known affinity for penicillin (Sauvage, Kerff, Terrak, Ayala, & Charlier, 2008). Fortunately, resistance to penicillin has not emerged in *S. pyogenes*, perhaps due to the essential role of PBPs involved in cell wall synthesis where any mutations that lower their affinity for penicillin may have low survival fitness (Bessen, 2010). In the case of penicillin allergy, clindamycin or macrolide antibiotics are used as alternatives (Eneli & Davies, 2007; Kaplan, 2004; Spellerberg & Brandt, 2016).

1.2.4 Capsule

GAS must first pass through a mucus layer to reach and attach to the epithelial cells of the pharynx during human infection. The streptococcal cell wall is surrounded by a capsule composed of hyaluronic acid (a high-molecular-mass polysaccharide comprised of glucuronic acid and N-acetylglucosamine), which has both advantageous and disadvantageous features (Cole et al., 2010). While the hyaluronic capsule may aid in passing though mucus, it has also been reported that the negatively charged capsule likely repels surface interactions with epithelial cells and could provide a reason why hyper-encapsulated strains are impaired in host colonization (Flores, Jewell, Fittipaldi, Beres, & Musser, 2012). According to Flores et al. (2012), GAS serotypes M4 and M22 multiplied extensively *ex vivo* in human blood despite lacking a hyaluronic acid capsule and it is speculated that these strains have alternative, compensatory mechanisms that promote virulence. It has also been hypothesized that hyper-

encapsulation may impede surface attachment by masking other bacterial adhesins, as is the case for M3 isolates where loss of capsule is beneficial (Bisno, 1991).

However, Lynskey et al. (2013) found the opposite to be true in a hyper-encapsulated M18 serotype, which appears to be anti-phagocytic and has an advantage in whole-blood survival and murine nasopharyngeal carriage. Given that CovR is an important transcriptional repressor of the capsule synthesis operon (*has* operon), a positive regulator of CovR, called RocA, has been reported to upregulate *covR* transcription with subsequent enhanced repression of capsule synthesis (Dalton & Scott, 2004; Lynskey et al., 2013). The highly mucoid M18 strain was found to have a protein truncation in RocA leading to decreased *covR* expression, which thus limited repression of the capsule biosynthesis *has* operon (Lynskey et al., 2013). These mechanistic findings are supportive of observations that hypermucoid M18 isolates were largely responsible for outbreaks of rheumatic fever occurring in a number of areas in the USA between 1985 and 1987, and once again between 1997 and 1999 (Bisno, 1991; Smoot et al., 2002; Wilkening & Federle, 2017). GAS regulation of hyaluronic capsule production impacts success during colonization and serves as an accessory virulence factor.

1.2.5 Superantigens

Bacterial SAgs are a diverse family of potent immunostimulatory exotoxins classically associated with food poisoning and toxic shock syndrome (TSS) (Sriskandan, Faulkner, & Hopkins, 2007; Wilkening & Federle, 2017). They are commonly encoded on mobile genetic elements (Wilkening & Federle, 2017). SAgs act by simultaneously binding to major histocompatibility complex (MHC) class II molecules on host antigen-presenting cells (APCs) and the T-cell receptor (TCR) variable β-chain, resulting in non-specific activation of a large number of T-cells, massive cytokine release and systemic inflammation (Xu, Kasper, Zeppa, &

McCormick, 2015). GAS can produce at least 14 SAgs but there is surprisingly little known about their genetic regulation (Sriskandan et al., 2007; Wilkening & Federle, 2017). Previous reports have highlighted SAgs as being critical for the invasive qualities of M1 serotypes that have been linked to major outbreaks worldwide (Bisno, 1991; Wilkening & Federle, 2017). During the early stages of infection, the potent SAgs released by GAS are responsible for the clinical symptoms of STSS and scarlet fever.

1.3 Protein disulfide bonds

From a structural perspective, bacterial virulence proteins are held together by complex molecular linkages and must be folded properly to function. One type of linkage is called a disulfide bond, which is important for the stability of many extracellular proteins (Daniels et al., 2010). Disulfide bonds are covalent bonds formed between sulfur atoms of cysteine (Cys) residues (Daniels et al., 2010). They are formed through an oxidation reaction that involves the loss of two electrons and are broken by a reduction reaction where cysteines conversely gain two electrons (Heras et al., 2009). In proteins with more than two cysteines, an incorrect disulfide bond could be made which requires reshuffling or rearranging of the non-native bond through an isomerization reaction (Heras et al., 2009).

While spontaneous disulfide bond formation *in vivo* is possible, the process is extremely slow (Heras et al., 2009). Instead, a family of enzymes called thiol-disulfide oxidoreductases (TDORs) catalyzes the oxidation, reduction and isomerization of protein disulfide bonds (Heras et al., 2009). These TDOR enzymes typically have a distinct active site motif with 2 Cys residues separated by two amino acids (CXXC) and often function by coupling the redox of their own

active site cysteines with those of their substrates, forming a mixed disulfide intermediate, in a thiol-disulfide exchange reaction (Heras et al., 2009; Lee & Davey, 2017). While cytoplasmic TDORs, such as thioredoxin, maintain a reducing environment inside the cell, extracytoplasmic TDORs in the cell envelope play a role in a variety of physiological processes, including disulfide bond formation, oxidative stress resistance, energy generation, sporulation, and regulation of virulence factors (Davey, Halperin, & Lee, 2016). Any disruptions in the natural protein folding mechanisms of bacteria lead to abnormal misfolded proteins, which are dysfunctional and quickly degraded by proteases. Because of this, there is particular interest in understanding and targeting these bacterial protein folding pathways to potentially reduce the production of harmful proteins.

1.3.1 Disulfide bond formation in Gram negative bacteria

Disulfide bond formation pathways have been extensively studied in Gram-negative bacteria. In fact, the best-characterized extracytoplasmic TDOR enzymes belong to the Dsb pathway in *Escherichia coli*. As reviewed by Heras et al. (2009), the *E. coli* oxidase DsbA introduces disulfide bonds into newly synthesized substrate proteins that are translocated from the reducing environment of the cytoplasm to the periplasm, a space between the inner and outer cell membranes. The active site of DsbA contains a pair of redox-active cysteines that are disulfide bonded (C_{30}–P_{31}–H_{32}–C_{33}; CPHC motif), and this disulfide bond is transferred to substrate proteins. After each reaction, DsbA is left in a reduced state and its redox partner, DsbB, is required to reoxidize DsbA back to its active state, allowing the catalytic cycle to continue. *E. coli* expresses over 250 proteins containing at least two cysteine residues that are predicted to enter the periplasm and it is reported that DsbA has broad substrate specificity, with DsbA-homologs widely distributed among Gram-negative bacteria (Heras et al., 2009). The

disulfide isomerase, DsbC, with its redox partner DsbD, as well as the reductase, DsbE, with its redox partner DsbD are additional well-known components of the *E. coli* disulfide bond formation pathway (Heras et al., 2009).

The thermodynamic mechanisms of DsbA interaction have been well-documented in the literature. DsbA has greater thermodynamic stability in its reduced form compared to its oxidized form (Heras et al., 2009). The disulfide bond that forms reversibly in the DsbA active site (between Cys30–Cys33) is believed to be very unstable and is 10^3-fold more reactive toward thiol groups than normal, thus giving rise to its highly oxidizing activity (Inaba & Ito, 2008; Nelson & Creighton, 1994). In fact, the two cysteine residues of DsbA are markedly different in their chemical properties in the native conformation, whereas they have similar and normal properties in the unfolded protein (Nelson & Creighton, 1994). The Cys30 residue is solvent exposed with its thiol group highly reactive toward alkylating reagents even at acidic pH environments. In contrast, the sulfur atom of the Cys33 residue is buried in the folded conformation of oxidized DsbA, with the thiol group being less reactive and ionizes less readily than normal. It is therefore the sulfur atom of Cys30 that preferentially reacts with an external thiol group of *E. coli* substrates, and Cys33 can react only with the sulfur atom of Cys30 (Nelson & Creighton, 1994). In-depth studies focused on cysteine point mutations and the pKa values of the thiol groups have been able to model and reflect the intrinsic chemical reactivates of protein sulfur atoms, providing insights on the rate of thiol-disulfide exchange (Inaba & Ito, 2008; Nelson & Creighton, 1994). In DsbA, the instability of the disulfide bond makes it ideally suited to react with the cysteine residues of newly-synthesized proteins to join them with disulfide bonds when appropriate.

1.3.2 Disulfide bonds in Gram positive bacteria

Very little is known about disulfide bond formation in Gram-positive bacteria, with the majority of TDORs identified only within the last 5 years. This discrepancy in knowledge and understanding is likely due to a combination of factors. For example, Gram-positive bacteria are predicted to have a lower prevalence of disulfide-bonded proteins and tend to generally exclude cysteines from their exported proteins (Daniels et al., 2010; Davey, Halperin, et al., 2016). Additionally, they lack the structural periplasmic compartment of Gram-negative species that serves as an optimum environment for redox reactions to occur, and instead use TDORs located at the cell wall (Heras et al., 2009).

Nevertheless, several DsbA-like disulfide bond catalysts have been discovered in the phylum Actinobacteria. As reviewed by Reardon-Robinson & Ton-That (2016), current data has largely focused on *Mycobacterium tuberculosis*, *Corynebacterium diphtheriae* and *Actinomyces oris*. Dsb-like factors identified in *M. tuberculosis* include MtbDsbA, MtbDsbE, and MtbDsbF (Chim, Harmston, Guzman, & Goulding, 2013). While *in vitro* analyses of these enzymes have been extensive, their biological functions are not clear and studying *in vivo* activity is challenged by the slow-growth phenotype of *M. tuberculosis* and a lack of consistent established genetic techniques (Chim et al., 2013; Reardon-Robinson & Ton-That, 2016). The membrane-localized oxidoreductase MdbA was identified in oral pathogens *C. diphtheriae* and *A. oris*, which are used as alternative models to study disulfide bond formation systems in Actinobacteria (Reardon-Robinson et al., 2015). Notably, *mdbA* mutants exhibit severe morphological defects, have defective toxin production, and poor pilus assembly; this suggests that MdbA is important for growth and may serve as a powerful target for new bactericidal drugs (Reardon-Robinson & Ton-That, 2016).

Recent studies of the Gram-positive phylum Firmicutes have identified TDORs belonging to aerobic species *Bacillus* and *Staphylococcus*. *B. subtilis* has a main extracytoplasmic TDOR, called BdbD, which is broadly similar to *E. coli* DsbA, and two DsbB-like proteins, named BdbB and BdbC (Meima et al., 2002). Unlike *Bacillus*, only one TDOR has been identified in *S. aureus*: a single DsbA-like protein called SaDsbA that is predicted to be conserved among staphylococci (Dumoulin, Grauschopf, Bischoff, Thöny-Meyer, & Berger-Bächi, 2005). The target substrate proteins of SaDsbA are still unclear. SaDsbA has been proposed to function autonomously, without a redox partner, and this has been attributed to the unusual structural stability of its active site cysteines. While the active site cysteines in similar TDORs form an unstable bond and require a redox partner to achieve the energetically unfavorable conformation, as is the case for *E. coli*, the reduced and oxidized forms of SaDsbA have equivalent thermodynamic stabilities and likely allow oxidation through a different mechanism (Heras et al., 2008). It is also possible that SaDsbA might use a redox partner that has not been identified yet.

1.3.3 Disulfide bonds in streptococcal species

Unlike the aforementioned Gram positive species, facultative anaerobic streptococci lack homologs to *E. coli* DsbA and the TDORs identified share low sequence identity with known enzymes. Previously published work in our laboratory has notably identified a novel TDOR enzyme in *Streptococcus gordonii*, called SdbA (Davey, Ng, Halperin, & Lee, 2013). Compared to parent, the *ΔsdbA* mutant displays a range of phenotypic defects including thick biofilms, and impaired extracellular DNA production, genetic competence, bacteriocin production, and autolysis (Davey et al., 2013). Mutation of *sdbA* even triggered upregulation of the CiaRH two-component signaling system in *S. gordonii*, which contributes to cell wall homeostasis (Davey,

Halperin, & Lee, 2016). SdbA was found to catalyze disulfide bonds in the major autolysin AtlS and it is possible that SdbA has additional natural substrates not yet identified (Davey, Halperin, et al., 2016). While the underlying mechanisms for many of these phenotypes is not well understood, it appears to be a combination of SdbA substrates lacking their disulfide bonds, along with a general stress response (Davey, Halperin, et al., 2016). Together, this highlights the importance of investigating TDORs, even in bacteria that are predicted to have few disulfide-bonded proteins.

1.4 Reducing pathways

Aside from oxidation pathways, there are also specialized TDORs required to maintain proteins in a reduced conformation. Broadly speaking, reducing pathways in bacteria consist of systems that work by transferring electrons originating from cytoplasmic NADPH via possibly thioredoxin or membrane proteins to extracellular TDORs. These electrons serve as reducing equivalents needed to catalyse the reduction of substrate disulfide bonds (Cho & Collet, 2013). The function of reducing pathways provides electrons to a variety of cellular process and are important for oxidative stress resistance in some species, although a better holistic understanding is required in both Gram negative and positive bacteria.

1.4.1 Reducing pathways in Gram positive bacteria

As reviewed by Davey et al. (2016b), *B. subtilis* has a cell envelope-associated reducing pathway and this system works by transferring electrons from the cytoplasm across the membrane through an integral membrane protein called CcdA, which functions similar to the transmembrane domain of *E. coli* DsbD. Electrons are passed from cysteines in CcdA to the

extracellular TDORs called ResA and StoA, both of which reduce downstream substrates (Möller & Hederstedt, 2008). ResA and StoA are membrane-anchored TDORs required for cytochrome *c* maturation and sporulation respectively. On the other hand, *B. cereus* and *B. anthracis* have two CcdA proteins (CcdA1 and CcdA2) and these enzymes are involved in processes such as cytochrome *c* biogenesis and toxin production (Han & Wilson, 2013).

Reducing pathways of streptococci have recently been characterized in *S. pneumoniae* and are important for oxidative stress resistance, involving CcdA proteins CcdA1 and CcdA2 (Davey et al., 2016; Saleh et al., 2013). To counter oxidative stress at the cell envelope, *S. pneumoniae* uses an extracellular methionine sulfoxide reductase, termed MsrAB2 (Saleh et al., 2013). MsrAB2 repairs protein damage caused by the oxidation of methionine to methionine sulfoxide, by reducing methionine sulfoxide and thus restoring its original state (Cho & Collet, 2013; Saleh et al., 2013). Following the flow of electrons from inside to outside, *S. pneumoniae* CcdA1 and CcdA2 pass electrons from the cytoplasm to two extracellular TDORs called Etrx1 and Etrx2; Etrx1 and Etrx2 then reduce different domains of MsrAB2, which then reduce methionine sulfoxide (Saleh et al., 2013). In fact, mutants lacking both Etrx1 and Etrx2 were more sensitive to killing by hydrogen peroxide (H_2O_2), reinforcing their role in oxidative stress resistance and showing their partial redundancy (Gennaris & Collet, 2013). The role for CcdA-Etrx-MsrAB2 in oxidative stress resistance is particularly important for *S. pneumoniae* because it produces H_2O_2 as a metabolic by-product and lacks catalase, similar to GAS.

1.4.2 Thiol-dependent antioxidant systems

Different bacteria are equipped with various types of antioxidant systems. The three major systems are thioredoxin-dependent, glutathione-dependent and catalase-driven. Thioredoxins (Trx) are typically 12 kDa small cytoplasmic reductases that maintain thiol-

disulfide bond balance by directly repairing oxidized protein cysteines in the cytosol or by providing reducing equivalents to upstream enzymes (Lu & Holmgren, 2014). Reduction of Trx depends on thioredoxin reductase (TrxR). The reaction mechanism therefore involves the transfer of electrons from cytoplasmic NADPH → TrxR → Trx → CcdA-like proteins or other repair enzyme families such as peroxidases, which convert harmful peroxides to alcohols (Lu & Holmgren, 2014). Catalase, for example, is an important heme-dependent enzyme that rapidly degrades H_2O_2 to water (H_2O) and oxygen (O_2) (Seaver & Imlay, 2001). Similarly, the glutathione (GSH) system involves the transfer of electrons from NADPH → glutathione reductase → GSH → glutaredoxin → upstream repair enzymes (Lu & Holmgren, 2014). Trx and GSH antioxidant systems have many overlapping complementary functions, and indeed, these systems have been extensively studied in *E. coli* but little is known in Gram-positive species (Lu & Holmgren, 2014). While Trx is ubiquitous in bacteria, GSH or catalase is lacking in some bacteria.

1.4.3 Antioxidant systems in GAS

GAS must avoid and counteract host immune clearance mechanisms in order to survive. At the infection site, innate immune cells such as neutrophils and monocytes phagocytose microbes, thus causing oxidative burst and release of reactive oxygen species (ROS) (Henningham, Döhrmann, Nizet, & Cole, 2015). ROS are the highly reactive and toxic by-products of oxygen metabolism, such as H_2O_2, superoxide anions and hydroxyl radicals which can easily damage bacterial nucleic acids, proteins and cell membranes (Henningham et al., 2015). GAS navigate the subsequent harsh oxidative stress conditions by expressing surface-associated ROS resistance factors, intracellular and secreted enzymes involved in ROS detoxification or repair of ROS-damaged proteins (Henningham et al., 2015). For example, the

surface M protein and hyaluronic acid capsule of GAS act as initial defences, due to their anti-phagocytic properties, resistance against H_2O_2, and the ability to structurally mimic human tissues containing identical hyaluronic acid, therefore avoiding detection (Henningham et al., 2015).

In contrast to Gram-positive *S. aureus*, GAS lacks catalase. Because of this, the antioxidant function mainly relies on a thiol-dependent system, which makes the bacteria easy to be attacked by thiol reacting agents (Lu & Holmgren, 2014). In spite of this, GAS can repair and cope with oxidative stress through enzymes such as superoxide dismutase (Sod), alkyl hydroperoxide reductase (AhpC) and glutathione peroxidase (gpoA) as reviewed by Henningham et al. (2015).

GAS has a single Mn^{2+}-dependent superoxide dismutase, designated SodA, which enhances growth under aerobic conditions and protects against superoxide stress by converting superoxide anion ($O_2^{\bullet-}$) into H_2O_2 and O_2. According to King et al. (2000), GAS AhpC is an NADH-dependent H_2O_2-degrading peroxidase that is up-regulated in response to oxidative stress. An in-frame *ahpC* deletion mutant was found to be more susceptible to a 5–10 mM range of methyl viologen (paraquat), which is a redox-cycling agent that augments intracellular levels of superoxide. GAS *ahpC* mutants were also more susceptible than wild-type to 5–20% cumene hydroperoxide, as measured by zone of growth inhibition in disk diffusion assays, and catalase treatment rescued the *ahpC* mutant phenotype, indicating that AhpC enhances GAS resistance to H_2O_2. A role for AhpC in scavenging intracellular H_2O_2 was seen in catalase-deficient *E. coli ahp* mutant which accumulated more H_2O_2 intracellularly (Seaver & Imlay, 2001). Similarly, Gpo is an oxidoreductase important for maintaining cellular redox homeostasis and for protecting cells from host released ROS (Arthur, 2001). Studies from the in-frame *gopA* mutant

in serotype M14 GAS strain HSC5 found it to be important for resistance against 5–10 mM paraquat, but not sensitive to direct challenge with H_2O_2 (Henningham et al., 2015).

There have also been previous reports that *S. pyogenes* has both Trx and GSH systems as *E. coli*, but the major thiol-dependent peroxidase system is understudied and unclear (Lu & Holmgren, 2014).

1.5 Virulence factors have disulfide bonds

Disulfide bonds are known to be crucial components of some Gram-positive virulence factors yet the mechanism of this bond formation remains a mystery. The potent human clostridial neurotoxins, including tetanus toxin from *Clostridium tetani*, and botulinum neurotoxin from *C. botulinum*, are di-chain proteins linked by a disulfide bridge that is vital for function (Zuverink, Chen, Przedpelski, Blum, & Barbieri, 2015). These toxins cause human paralysis by targeting motor neurons. An intact disulfide bond is required for and dictates the outcome of the protein light chain translocation into host neuronal cells (Fischer & Montal, 2007; Zuverink et al., 2015).

Diphtheria toxin, a potent exotoxin secreted by *Corynebacterium diphtheriae*, is composed of two subunits linked by a single disulfide bridge and is also known as an A-B toxin (Reardon-Robinson & Ton-That, 2016). Diphtheria toxin is infamous for causing diphtheria, a deadly disease for unvaccinated individuals. It was hypothesized that *C. diphtheriae* MdbA, a TDOR previously mentioned, is involved in the folding of cysteine-containing exported proteins such as this toxin. Work done by Reardon-Robinson et al. (2015) showed that deletion of *mdbA* was associated with the release of reduced and degraded diphtheria toxin. This phenotype, along

with the lack of adhesive pili, had clear consequences on *C. diphtheriae* pathogenesis, as the Δ*mdbA* mutant was attenuated in a guinea pig model of diphtheritic toxemia. While the mechanism is still unclear, the combined data is indicative of MdbA being important for the disulfide bond formation in diphtheria toxin and general folding of other secreted virulence factors (Reardon-Robinson & Ton-That, 2016).

S. aureus has multiple disulfide bonded virulence factors that are independent of SaDsbA, including up to 23 superantigens. Staphylococcal superantigens include the staphylococcal enterotoxins (SEs) A, B, $C_{1–3}$, D, E, G, H, I, R, and T; the staphylococcal enterotoxin-like (SEls) proteins; and toxic shock syndrome toxin-1 (TSST-1) (Xu & McCormick, 2012). Based on previously reported three-dimensional crystal structure analyses, a disulfide loop is present in all staphylococcal superantigens except TSST-1, which does not possess any cysteine residues (Hovde et al., 1994; Papageorgiou et al., 1999; Spaulding et al., 2013). This cysteine loop has a varying 10- to 19-amino-acid sequence separating the cysteine residues and importantly, the disulfide loop is required for emetic activity, or causing clinical vomiting. However, it has been previously shown in staphylococcal enterotoxin C (SEC) that changing the two cysteine residues to alanine resulted in loss of functional emetic activity, but changing the residues to serine does not (Hovde et al., 1994; Papageorgiou et al., 1999). Thus, the overall conformation of the SE structure, as regulated by the disulfide loop amino acids, may be more important than the actual presence of the cysteine bond itself (Spaulding et al., 2013). Remarkably, there is no knowledge on how these toxin disulfide bonds are formed. If there are TDOR pathways involved in forming and breaking these bonds, these enzymes could be targets for novel drug development strategies in the clinical setting.

1.6 Evidence of disulfide bonded proteins in Group A streptococcus

TDOR pathways have yet to be studied in the context of *S. pyogenes* pathogenesis. Interestingly, there is evidence of disulfide-bonded proteins produced by GAS. Similar to *S. aureus*, GAS can produce up to 14 superantigens including streptococcal pyrogenic exotoxins (SPEs) (A, C, G-M); streptococcal superantigen (SSA); and streptococcal mitogenic exotoxin Z_n ($SMEZ_n$) depending on the strain. Excluding SpeG and SMEZ which are encoded on the core chromosome, all of the streptococcal superantigens are encoded by genes located within bacteriophages (Spaulding et al., 2013). Of particular interest is SpeA, which has been linked to clinical symptoms of scarlet fever rash, hypotension and severe infection associated with STSS and high mortality rate (Hoge et al., 1993; Maamary et al., 2012; Sriskandan, Unnikrishnan, Krausz, & Cohen, 1999). The *speA* gene is present in 40–90% of *S. pyogenes* strains associated with invasive streptococcal disease and TSS, but in only 15–20% of non-invasive strains (Yu & Ferretti, 1989). Undoubtedly, SpeA plays a key role in GAS pathogenesis and acquiring a better understanding of its mode of action is essential.

Notably, crystal structure analysis of SpeA revealed its overall structure is similar to that of other prototype microbial superantigens, either of staphylococcal or streptococcal origin. SpeA has greatest similarity to *S. aureus* SEC2 (Papageorgiou et al., 1999). The crystallized allelic form of this toxin, SpeA1, contains three cysteine residues; two of them (Cys87 and Cys98) form a disulfide bridge, while the third cysteine (Cys90) is accessible to solvent and is part of the disulfide loop. The SpeA1 disulfide loop is comprised of 10 residues and is shorter than the corresponding loops in SEB and SEC (19 and 16 residues respectively), but is of similar length to that of SEA (9 residues) (Papageorgiou et al., 1999).

Mutational analysis of SpeA through single- and double-site mutants by Roggiani et al. (1997), found that 2 cysteine mutants (C87S and C98S) failed to stimulate proliferation of murine lymphocytes. In other words, they were less mitogenic than native SpeA. Therefore, cysteine residues 87 and 98, which are now known to form a disulfide bond, were important for the lymphocyte proliferative activity of SpeA. This is supportive of the idea that the SpeA disulfide linkage confers conformational stability as well as protease resistance to this exotoxin (Roggiani et al., 1997).

1.7 Hypothesis and Objective

There are still many unanswered questions surrounding the mechanisms of GAS virulence and its interaction with host factors during infection. Given the clinical importance of GAS and the evidence of disulfide-bonded toxins produced, further investigation of disulfide bond formation pathways could be an excellent approach to better understanding the regulation of GAS virulence factors at the molecular level.

It was **hypothesized** that GAS has a disulfide bond formation pathway mediated by a TDOR. To test this hypothesis, 3 main **objectives** were designed:

Aim 1: Identification of candidate TDORs and natural TDOR substrates in GAS

Aim 2: Construction of TDOR mutants and functional analysis of their role in *in vitro* and *in vivo* phenotypic assays compared to parent

Aim 3: Analysis of enzymatic functions and activities of recombinant TDOR proteins

CHAPTER 2: Materials and Methods

2.1 Bacteria and Culture Conditions

2.1.1 *S. pyogenes* growth conditions

S. pyogenes strains used in this study are listed in Table 1. Unless otherwise specified, *S. pyogenes* cultures were grown in Brain Heart Infusion broth (BHI) (Wisent, QC) supplemented with 0.2% (w/v) yeast extract (Wisent) at either 30°C, 37°C or 40°C, 5% CO_2 incubation without shaking. Culture medium was prepared to contain 1 µg/ml erythromycin (Sigma-Aldrich, St. Louis MO, USA) for growth with plasmids as necessary. All antibiotics were filter sterilized through a 0.2 µm syringe filter. *S. pyogenes* stocks were maintained and stored in 1 ml aliquots of BHI containing appropriate antibiotics and 25% (v/v) glycerol (Fisher Scientific, USA) at -80℃.

2.1.2 *E. coli* growth conditions

E. coli strains used in this study are listed in Table 1. All *E. coli* cultures were grown aerobically in Luria-Bertani (LB) broth [1% tryptone (Wisent), 0.5% yeast extract, 1% NaCl (Fisher Chemicals) (w/v)] at 37°C with shaking at 180 rpm, or on LB or BHI agar (1.5%) (w/v). Media were prepared to contain antibiotics appropriate to the plasmids within those strains: ampicillin (amp) (BioShop, Burlington ON, CAN) was used at a concentration of 100 µg/ml, erythromycin (ery) at 200 µg/ml (Sigma) and kanamycin (kan) at 50 µg/ml (Bioshop). *E. coli* stocks were maintained and stored in 1 ml aliquots of LB containing appropriate antibiotics and 25% (v/v) glycerol at -80℃.

Table 1: Bacterial strains used in this study.

Strains	Relevant Characteristics	Source
S. pyogenes		
S. pyogene MGAS8232 wild-type	M18 serotype associated with acute rheumatic fever outbreaks in USA; Isolated from acute rheumatic fever patient in Utah, 1987	Smoot et al. (2002)
S. pyogenes 40/58	M1 serotype, reference strain WHO, Prague	Koroleva et al. (1998)
S. pyogenes 10/69	M22 serotype, reference strain WHO, Prague	Koroleva et al. (1998)
S. pyogenes Δ2037	Strain MGAS8232 *2037::erm*	This study
S. pyogenes ΔahpC	Strain MGAS8232 *ahpC::erm*	This study
S. pyogenes Δ982	Strain MGAS8232 *982::erm*	This study
S. pyogenes Δ2138	Strain MGAS8232 *2138::erm*	This study
S. pyogenes Δ1572	Strain MGAS8232 *1572::erm*	This study
S. pyogenes 2037 complement	Strain MGAS8232 *Δ2037::2037, kan*	This study
E. coli		
E. coli XL-1 Blue	Alpha complementation	Stratagene
E. coli SpeA	XL-1 Blue carrying pQE-30- *SpeA1*	Lee, unpublished
E. coli 2037	XL-1 Blue carrying pQE-30- *2037*	This study
E. coli 2037_{C46A}	XL-1 Blue carrying pQE-30- *2037* coding for cysteine 46 to alanine point mutation (AXXC)	This study
E. coli 2037_{C49A}	XL-1 Blue carrying pQE-30- *2037* coding for cysteine 49 to alanine point mutation (CXXA)	This study
Other		
Lactococcus lactis MG1363	Indicator strain for bacteriocin assay	Amiri-Jami, Lapointe, & Griffiths, (2014); Wegmann et al. (2007)

2.2 Genetic DNA Manipulations

2.2.1 Genomic DNA isolation

Chromosomal DNA for polymerase chain reaction was obtained from *S. pyogenes* through a rapid chloroform extraction procedure. Cultures (3 ml) were grown overnight and cells were harvested by centrifugation at 10 000 x g, 5 min. Resulting pellets were suspended in 200 µl TE buffer (10 mM Tris, 10 mM EDTA, pH 8.0), 200 µl chloroform (Fisher Scientific), and 100 mg glass beads (400 µm, Sigma), and vortexed for 1 min. Cell debris was removed by centrifugation at 10 000 x g, 5 min and the top aqueous layer transferred to new 1.5 ml tubes. Extracted DNA was kept at 4°C for immediate use or stored at -20°C.

2.2.2 Plasmid DNA isolation

Plasmids were isolated from *E. coli* by the alkaline lysis method (Birnboim & Doly, 1979). Cells were grown overnight in 2 ml LB with appropriate antibiotics and harvested by centrifugation at 14 000 x g, 5 min. Cell pellets were resuspended in 100 µl GTE buffer (50 mM glucose, 25 mM Tris, 10 mM EDTA, pH 8.0), 186 µl MilliQ water, 2 µl RNase A (10 mg/ml), 10 µl of 20% SDS, 4 µl NaOH (10 M). The tubes were gently mixed by inversion and incubated at room temperature for 5 min. The pH was neutralized with 150 µl of cold potassium acetate solution (60% (v/v) 5 M potassium acetate, 28.5% (v/v) MilliQ H_20 and 11.5% (v/v) glacial acetic acid), mixed gently again by inversion, and incubated on ice for 10 min. This was followed by centrifugation at 14 000 x g, 10 min, at 4°C. Supernatants were transferred to new 1.5 ml tubes and extracted with vigorous vortexing using an equal volume of chloroform for 2 min. The mixture was centrifuged at 14 000 x g for 5 min. Top aqueous layers were then precipitated with 95% ethanol containing 2.5% potassium acetate for at least 30 min at -80°C.

DNA was sedimented by centrifugation at 14 000 x g, 10 min, 4˚C, and washed with 70% ethanol. The resulting pellets were carefully vacuum dried and dissolved in 20 µl TE buffer. To quantify the amount of plasmid DNA, 1 µl was separated by gel electrophoresis and the concentration was estimated using ImageJ analysis of pixel intensity compared to a known standard (1 kb DNA ladder N3232S, New England Biolabs).

2.2.3 DNA restriction digestions

Endonuclease restriction digestions were performed in a 10 µl reaction volume containing 0.5-1 µl of each restriction enzyme in the appropriate 1 X reaction buffer and incubated following the manufacturer's recommended conditions. Enzymes were purchased from New England Biolabs (Ipswich MA, USA, Whitby ON, Canada) or Invitrogen (Burlington, ON, Canada). Digested DNA was subjected to agarose gel electrophoresis followed by excision of the DNA bands from the gel and purification using a DNA Fragment Extraction Kit (DNA Land Scientific, USA) according to the manufacturer's instructions.

2.2.4 DNA ligation

All ligations were performed in 10 µl reaction volumes containing 20 U of T4 DNA ligase (New England Biolab) and an excess of insert to vector ratio (10:1). Reactions were carried out overnight at room temperature.

2.2.5 Transformation of *E. coli*

To prepare competent cells, 1 ml of an overnight culture was inoculated to 45 ml of LB. Cultures were grown at 37°C, 180 rpm, to an OD_{600} close to 0.35, and cells were harvested by centrifugation at 10 000 x g, 10 min, 4°C. The cell pellet was washed with 50 ml of Transformation Buffer 1 (10 mM Tris, 150 mM NaCl, pH 7.5), followed by centrifugation. The

resulting pellets were resuspended in Transformation Buffer 2 (50 mM $CaCl_2$) and incubated on ice for 45 min. Cells were harvested by centrifugation and suspended in 3 ml of Transformation Buffer 2 and 2 ml of 50% glycerol. Aliquots of competent cells were stored at -80°C.

DNA was combined with 200 µl of competent cells and 100 µl Transformation Buffer 3 (10 mM Tris, 50 mM $CaCl_2$, and 10 mM, $MgSO_4$, pH 7.5) and incubated on ice for 45 min. The transformation mixture was heat shocked at 37°C for precisely 2 min, followed by incubation at room temperature for 10 min. Fresh LB (0.5 ml) was added and the cells were incubated for 1 h at 37°C. Transformants were grown for 24 h at 37°C on LB agar plates with appropriate antibiotics.

2.3 Agarose Gel Electrophoresis

DNA was electrophoresed on a 0.8% (w/v) agarose (Bioshop) gel placed in an apparatus filled with 1 X TAE buffer (Tri-acetate-EDTA buffer, 40 mM Tris base, 1 mM EDTA, and 0.1% (v/v) glacial acetic acid) containing 0.5 µg/ml of ethidium bromide (Sigma). DNA loading dye [5% glycerol, 0.04% (w/v) bromophenol blue (Fisher)] was mixed with each sample prior to loading onto the gel. An electric field was applied across the apparatus (125 V) to allow separation of differently sized DNA fragments. A 1 kilobase (kb) DNA molecular weight ladder (New England Biolabs) was included as a size standard. Visualization of DNA was done under UV light using the UVP BioDoc-It Imaging System (Upland CA, USA).

2.4 Polymerase Chain Reaction

2.4.1 Standard polymerase chain reaction method

Polymerase chain reaction (PCR) was performed in an Eppendorf Mastercycler EP S Thermo-Module. All oligonucleotide primers used were obtained from Alpha DNA (Montreal, QC). Reactions were prepared in 100 µl reaction volumes or master mixes containing: 1 µl template DNA, 0.5 µM of the forward primer, 0.5 µM of the reverse primer, 200 µM deoxyribonucleoside triphosphates (dNTP) mixture (DNA Land Scientific), sterile MilliQ H_2O and either 1 X high fidelity (HF) buffer (New England Biolabs) with 1 U of Phusion DNA polymerase (New England Biolabs), or 1 X ThermoPol Buffer (New England Biolabs) with 2.5 U of Taq DNA polymerase (New England Biolabs). General cycle conditions were as follows: 98°C for 5 min; 98°C for 15-30 sec; primer-specific annealing temperature which was in general the melting temperature (T_m) + 4°C for 30 sec; 68-72°C for a duration appropriate for the gene being amplified at 15 sec/1 kb (Phusion) or 60 sec/1 kb (Taq). PCR was typically performed for 35 cycles followed by a final extension at 72°C for 5 min.

2.4.2 Colony screening by polymerase chain reaction

To screen for *E. coli* transformants, colony PCR was performed. A standard master mix for PCR was prepared with the exception of added template DNA and aliquoted into 25 µl volumes across 0.2 ml PCR flat-capped reaction tubes (Corning, Axygen Scientific). Single colonies were picked from LB or BHI agar plates using individual sterile toothpicks and dipped into 0.5 ml tubes containing 100 µl TE buffer. From there, 1 µl was taken as template DNA for the prepared PCR reaction tubes. Resulting PCR amplified products were analyzed by agarose gel electrophoresis. Colonies showing the DNA bands of interest were grown and stored in appropriate media with necessary antibiotics.

2.5 Mutant Construction

2.5.1 Electroporation of *S. pyogenes*

Electrocompetent *S. pyogenes* cells were prepared by subculturing 1:100 of an overnight culture into pre-warmed BHI supplemented with 40 mM L-threonine (BDH Laboratory Supplies, Poole, UK). The culture was grown at 37°C until the OD_{600} reached 0.2, followed by centrifugation at 3 000 x g for 15 min. The resulting cell pellet was washed 3 times using 1 ml ice-cold filter-sterilized electroporation buffer (EB) (0.3 M sucrose, 1 mM $MgCl_2$, 5 mM sodium phosphate buffer, pH 7). Afterwards cells were resuspended in 2 ml of EB and kept on ice for at least 15 min.

Plasmids to be electroporated were ethanol precipitated (described previously), washed twice with 1 ml 70% ethanol, and dissolved in 20-25 µl of sterile MilliQ H_20. DNA (1-2 µg) was combined with 600 µl of prepared electrocompetent *S. pyogenes* cells in a sterile 4 mm-gap electroporation cuvette (Biorad). Cells were electroporated at 2500 V, 400 Ω, and 25 µF in a Biorad Gene Pulser X Cell electroporator. After electroporation, cells were transferred to a 1.5 ml tube and immediately placed on ice for 10 min, followed by addition of 800 µl of BHI. The tube was incubated at 30°C for 2 h then pelleted (10 000 x g, 10 min), resuspended and plated on BHI agar plates (1.5% w/v) with 1 µg/ml ery. Plates were incubated for up to 3 days at 30°C.

2.5.2 Insertional inactivation

The construction of the streptococcal TDOR mutants was made in a manner similar to the procedure reviewed in Maguin et al. (1996) and achieved through insertional inactivation. *S. pyogenes* were electroporated with a pG^+host5-based plasmid (Table 2) carrying an internal portion of the TDOR gene to be targeted. Bacterial transformants that grew on BHI + 1 µg/ml

ery plates at 30°C were picked and grown in 1 ml BHI, ery media at 30°C for 3 h. This was followed by incubation at 40°C for 3 h to facilitate integration of the plasmid into the TDOR gene via homologous recombination Following transformation, bacteria were plated on BHI, ery agar plates (1.5% w/v) and incubated at 40°C, 5% CO_2 for up to 3 days. Resulting colonies were picked and grown in BHI, ery media at 40°C. DNA was isolated by chloroform extraction and the insertional integration of the construct was analyzed by PCR. The PCR primers used for *S. pyogenes* mutations are listed in Table 3 and the mutagenesis strategy is depicted in Figure 1.

2.5.3 Site directed mutagenesis

A cysteine (TGT) to alanine (GCT) mutation was introduced in the 2037 enzyme active site at amino acid position 46. The point mutation was constructed by overlapping PCR using Phusion high-fidelity DNA polymerase and primer pairs SL1417 and SL1312 (upstream), and SL1418 and SL1311 (downstream) (Table 3). The two fragments were combined as template for overlapping PCR and amplified with the outside primers SL1311/SL1312. Standard PCR procedures were followed with the exception of forward/reverse primer solutions (0.5 μM) being omitted from the initial master mix preparation. After 5 amplification cycles, the reaction was paused, primers were added and amplification resumed. A second cysteine (position 49) to alanine point mutant was constructed using the same procedures except with the following primer pairs: SL1419/SL1312 (upstream), SL1420/SL1311 (downstream) (Table 3). Each resulting point mutant construct was then double digested with BamHI/HindII, and cloned into the pQE-30 plasmid backbone as described in Table 2.

Table 2: Plasmids used in this study.

Plasmid	**Description**	**Source**
pG$^+$host5	Erythromycin resistance, Gram-negative origin of replication, Gram-positive temperature-sensitive origin of replication	Appligene
pG$^+$host5 *Δ2037*	Internal 300 bp of *2037*, ery^R	This study
pG$^+$host5 *ΔahpC*	Internal 450 bp of *ahpC*, ery^R	This study
pG$^+$host5 *Δ982*	Internal 490 bp of *982*, ery^R	This study
pG$^+$host5 *Δ2138*	Internal 750 bp of *2138*, ery^R	This study
pG$^+$host5 *Δ1572*	Internal 310 bp of *1572*, ery^R	This study
pG$^+$host5 *2037* complement	Whole gene with predicted promoter sequence 675 bp of *2037*, kan^R	This study
pQE-30	Bacterial expression vector, T5 promoter, N-terminus 6X His tag, BamHI and Hind III cloning sits, amp^R	Qiagen
pQE-30 *r*SpeA	T5 promoter, N-terminus 6X His tag, *speA1* whole gene, amp^R	Lee, unpublished
pQE-30 *r*2037	T5 promoter, N-terminus 6X His tag, *2037* whole gene, amp^R	This study
pQE-30 *r*2037$_{C46A}$	T5 promoter, N-terminus 6X His tag, *2037* with cysteine 46 to alanine point mutation, amp^R	This study
pQE-30 *r*2037$_{C49A}$	T5 promoter, N-terminus 6X His tag, *2037* with cysteine 49 to alanine point mutation, amp^R	This study
pDL276	Contains kanamycin resistance cassette (*aphA3*), kan^R	Dunny et al. (1991)

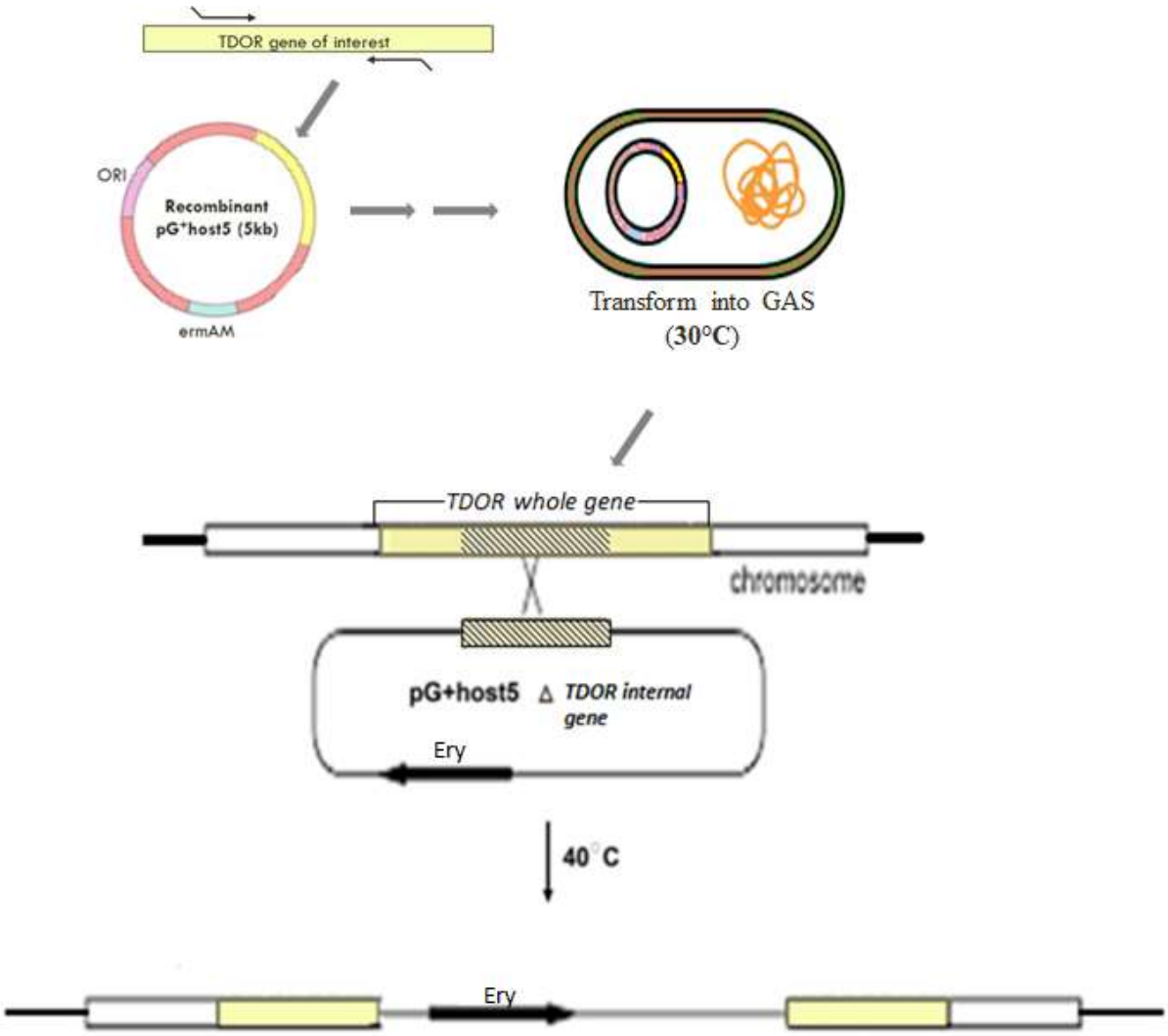

Figure 1: Insertional inactivation strategy to generate mutants in *S. pyogenes*. All constructs were made in pG+host5 (Table 2) by cloning PCR products containing internal regions of the TDOR gene target. Following electroporation, *S. pyogenes* transformants containing the plasmids were grown at 40°C with erythromycin to facilitate single cross-over integration of the plasmid into the streptococcal genome. Erythromycin-resistant *S. pyogenes* were screened for proper TDOR gene disruption by PCR using specific primers (Table 3).

Table 3: Primers used.

Primer	Gene	Direction	Description	RE*	Sequence (5' → 3')
SL1309	*2037*	For	Knockout	EcoRI	TACGAATTCCATGACATTTGAAGAAATCG
SL1310	*2037*	Rev	Knockout	HindIII	TACAAGCTTCACATACAGCCCTTTGGTG
SL1311	*2037*	For	Knockout	BamHI	TACGGATCCATGAGACCAAAAGAGAAGG
SL1312	*2037*	Rev	Knockout	HindIII	TACAAGCTTTTACTCACGAGTCAAAAAAG
SL1338	*ahpC*	For	Knockout	BamHI	TACGGATCCATCATGTTACAAATGAAG
SL1339	*ahpC*	Rev	Knockout	EcoRI	TACGAATTCTTTCCATTTAGCTGGACA
SL1340	*ahpC*	For	PCR		ATGTCTCTAATTGGAAAAGAA
SL1342	*0982*	For	Knockout	BamHI	TACGGATCCATATTGACAACAAAGAATG
SL1343	*0982*	Rev	Knockout	EcoRI	TACGAATTCACTTGATTTGGTTGGAG
SL1341	*0982*	For	PCR		ATGGCACAAAGAATCATTG
SL1345	*2138*	For	Knockout	BamHI	TACGGATCCTTGCTCTCTTGCAAGTAT
SL1346	*2138*	Rev	Knockout	XhoI	TACCTCGAGTTCAAAGAGTGGGCCATC
SL1344	*2138*	For	PCR		ATGGCATTAAGTCCTGATAT
SL1161	*1572*	For		BamHI	TACGGATCCGAAATAACTCAGGACA
SL981	*1572*	Rev		BamHI	GTAGGATCCTTCCTAATGTATACCTTTAAG
SL1116	*1572*	For	PCR		TAGGAGGGAAGCTTATGAAAAAAGGACTATTAGT
SL106	-40 universal primer		PCR		GTTTTCCCAGTCACGAC
SL728	*erm*	For	PCR		TTTGTAATTAAGAAGGAGTG
SL729	*erm*	Rev	PCR		TACGGATCCAGCGACTCATAGAATTATTT
SL1417	*2037*	For	2037 point mutants C46A		TCGAGCGCTCCTTATTGTCGCC

Primer	Gene	Direction	Description	RE*	Sequence (5' → 3')
SL1418	*2037*	Rev	2037 point mutants C46A		GGCGACAATAAGGAGCGCTCGA
SL1419	*2037*	For	2037 point mutants C49A		TCGAGCTGTCCTTATGCTCGCC
SL1420	*2037*	Rev	2037 point mutants C49A		GGCCAGCATAAGGACAGCTCGA
SL1421	*2037*	For	2037 complement	BamHI	TACGGATCCCATCAAACCAAAACACCAG
SL1421	*2037*	Rev	2037 complement	AscI	ATATGGCGCGCCTTACTCACGAGTCAAAAAAG
SL1129	*aphA3*	For	2037 complement	SphI	TAGGCATGCGCAAGGAACAGTGAATTGGA
SL802	*aphA3*	Rev	2037 complement	EcoRI	TACGAATTCCAGTTGCGGATGTACTTCAG

*Restriction enzyme cut site

All cysteine point mutations were confirmed by DNA sequencing (The McGill University and Génome Québec Innovation Centre).

2.5.4 Complemented mutant construction

Construction of a *2037*-complemented mutant was achieved by introducing a functional *2037* gene back into the chromosome. To this end, the entire 2037 reading frame, along with 300 bp of upstream DNA containing the predicted promoter and ribosomal-binding site sequences, was amplified with the primer pair SL1421/SL1422 (Table 3). This fragment was ligated to a kanamycin resistance cassette (*aphA3*) amplified from the plasmid pDL276. The ligated DNA was amplified by PCR using the primer pair SL1421/SL802 (Table 3) and double digested with BamHI and EcoRI, then cloned into the pG^{+}host5 plasmid. The resulting plasmid was transformed into *E. coli* and selected on BHI plates containing ery (150 μg/ml) and kanamycin (50 μg/ml). Colony PCR was done to confirm positive transformants. This was followed by plasmid DNA isolation from *E. coli* cells and then transformation into the *Δ2037* mutant by electroporation (previously described). Homologous recombination via single crossing-over resulted in a complement strain that has both the kanamycin resistance cassette and *ermAM* cassette. Transformants were selected on BHI with both kan (250 μg/ml) and ery (1 μg/ml), and analyzed for *2037* gene complementation by PCR.

2.6 Protein Analysis

2.6.1 Sodium dodecyl sulfate polyacrylamide gel electrophoresis

Proteins were analyzed by sodium dodecyl sulfate polyacrylamide gel electrophoresis (SDS-PAGE) followed by Coomassie blue staining according to the protocol developed by

Laemmli (1970). Samples were mixed with sample buffer (250 mM Tris-HCl, pH 6.8, 2% sodium dodecyl sulfate, 10% glycerol, 10% 2-mercaptoethanol, 0.01% bromophenol blue), boiled for 5 min, and then centrifuged at 10 000 x g, 5 min. For samples run under non-reducing conditions, 2-mercaptoethanol was omitted from the sample buffer preparation. The samples were electrophoresed on 15% SDS-PAGE gels using the buffer system of Laemmli (1970) (Mini PROTEAN electrophoresis system, Bio-Rad; 200 V, ~1 h). The gels were stained with Coomassie Brilliant Blue staining solution (0.1% (w/v) Coomassie brilliant blue R 250 (Fischer), 50% (v/v) isopropanol, 10% (v/v) glacial acetic acid, 40% (v/v) H_2O) and then destained for visualization (5% glacial acetic acid (Fischer)). The concentration of purified recombinant protein was quantified using a standard curve generated by bovine serum albumin (BSA, Sigma) standards (2, 1, 0.5, 0.25 μg) on the same gel with ImageJ software (National Institutes of Health, Bethesda, MD).

2.6.2 Western blotting

Unless otherwise specified, western blotting was performed according to the protocol of Towbin et al. (1979). *S. pyogenes* from 3 ml of overnight culture were pelleted by centrifugation (10 000 x g, 10 min, 4°C). Supernatants were collected and incubated with 9% (w/v) trichloroacetic acid (Sigma) with 0.18% (v/v) sodium deoxycholate (BDH Chemicals Ltd, Poole, England) (TCA precipitation) on ice for 30 min, followed by centrifugation (15 000 x g, 10 min, 4°C).The pelleted proteins were washed twice with ice-cold acetone. Protein samples were electrophoresed on 15% SDS-PAGE gels and then transferred to nitrocellulose membranes (Bio-Rad) at 200 mA for 60 min (Mini Trans-Blot, Bio-Rad). Membranes were blocked with 1% (w/v) gelatin (Bioshop) dissolved in PBS with 0.1% (v/v) Tween-20 (Bioshop) (PBST) for 1 h at room temperature followed by overnight incubation with primary antibodies diluted in PBST at

4°C. The blots were washed 4 × 1 min with PBST. Proteins were detected by adding secondary antibodies conjugated to alkaline phosphatase for 1 h. Membranes were then developed at room temperature using 33 µl of 5-bromo-4-chloro-3-indoyl phosphate (BCIP) (50% (w/v) BCIP (Bioshop) in dH2O) and 66 µl of nitroblue tetrazolium (NBT) (50% (w/v) NBT (Bioshop), 70% (v/v) dimethyl-formamide (Fischer)) in 10 ml of alkaline phosphatase buffer (0.01 mM $MgCl_2•6H_2O$, 0.1 M NaCl, and 0.2 M Tris-HCl, pH 9.8) until the desired band intensity was obtained. Antibodies used are given in Table 4.

2.7 Phenotypic Assays

2.7.1 Growth on selective agar plates

To test for hemolytic activity, *S. pyogenes* cultures were streaked on sheep blood agar (SBA) plates and incubated overnight at 37°C, 5% CO_2. Zones of hemolysis around single-cell colonies were observed.

Sensitivity to salt and copper were tested on BHI agar plates containing 0.4 M sodium chloride (NaCl) (Fisher Scientific), 0.2 M potassium chloride (KCl) (Bioshop) or 2 mM copper sulfate ($CuSO_4$) (Fisher). Overnight *S. pyogenes* cultures were adjusted to an OD_{600} of 0.2 using BHI and four serial dilutions were made in 1.5 ml tubes (dilutions: 10^{-1}-10^{-4}). Ten µl of each diluted culture tube was spotted onto the agar plates containing different salt and copper concentrations. The culture drops were allowed to air-dry and the plates were incubated at 37°C, 5% CO_2. After 24 h, bacterial growth was observed and compared between plates.

Table 4: Antibodies used in Western blot.

Antibody	**Characteristics**	**Dilution**	**Source**
Mouse anti-2037	Polyclonal, antiserum	1:8000	This study
Mouse anti-SpeA1	Polyclonal, antiserum	1:1000	This study
Goat anti-mouse IgG	Polyclonal, against the whole IgG, alkaline phosphatase conjugate	1:3000	Sigma-Aldrich
ExtrAvidin	Avidin-Alkaline phosphatase conjugate	1:60000	Sigma-Aldrich

2.7.2 Bacteriocin deferred-antagonism assay

A deferred antagonism bacteriocin assay was done as described by Hossain & Biswas (2011). *S. pyogenes* cultures were stabbed into BHI agar plates with a sterile toothpick and grown overnight (~18 h) at 37°C under microaerophilic conditions in candle jars. The indicator strain, *Lactococcus lactis* (Table 1), was incubated in 5 ml BHI at 30°C. The following day, 0.1 ml of the *L. lactis* indicator culture was mixed with 10 ml of BHI soft (0.4%, w/v) agar and overlaid on plates containing *S. pyogenes* stabs. The plates were then incubated overnight at 30°C in the same candle jars and the diameters of the zones of inhibition around the *S. pyogenes* stabs were observed.

2.7.3 Disc diffusion assay

Sensitivity to cell-wall or cell-membrane specific antibiotics were tested using a disc diffusion assay protocol. Overnight *S. pyogenes* cultures were adjusted to an OD_{600} of 0.2 in 1 ml of BHI, and transferred to agar plates using sterile cotton swabs to evenly distribute a bacterial lawn across the top. After air-drying briefly, tweezers were used to place sterile filter paper discs on the agar plate surface in an arrangement of 4 discs per plate evenly spaced. The following antibiotics and their final concentrations were tested: penicillin G (Sigma) (5, 2.5, 1.25, 0.625 µg/ml), vancomycin (Sigma) (100, 50, 25, 12.5 µg/ml), bacitracin (Sigma) (100, 50, 25, 12.5 U/ml), polymyxin (Bioshop) (200, 100, 50, 25 mg/ml). Antibiotics were then pipetted directly on top of the sterile discs at a volume of 10 µl. Plates were incubated at 37°C, 5% CO_2 and examined after 24 h for growth inhibition zones surrounding the antibiotic discs. Zones were measured in centimeters (cm) using a ruler. Discs containing no antibiotic treatment were also used on agar plates and included as a negative control (data not shown).

Sensitivity to hydrogen peroxide (H_2O_2) was assessed using the same disc diffusion assay. The concentrations of H_2O_2 (Sigma) used were 0.5%, 1%, 1.5% and 2%.

2.7.4 Autolytic activity

Autolysis was tested as described by Ahn & Burne (2006) with the following modifications. Overnight cultures of *S. pyogenes* were diluted 1:5 into HTVG media (per 100 ml: 0.5 g glucose, 3.5 g tryptone, 100 mM HEPES, 4 mg *p*-aminobenzoic acid, 20 mg thiamine-HCl, 0.1 mg nicotinamide and 0.02 mg riboflavin, pH 7.6) and grown at 37°C, 5% CO_2, to an OD_{600} of 1.0. The cells were pelleted by centrifugation (3000 x g, 10 min, 4°C) and then suspended in pre-warmed (44°C) 20 mM potassium phosphate buffer (pH 6.5) containing 1 M KCl, 1 mM $CaCl_2$, 1 mM $MgCl_2$, 0.4% sodium azide, and 0.2% Triton X-100. The cell suspensions were incubated in a 44°C water bath and autolytic activity monitored by measuring the OD_{600} at 0, 1, 2, 3 and 4 h.

2.7.5 Capsule production

To quantify the amount of hyaluronic acid (HA) capsule produced by each GAS strain, the Stain-All protocol was used similar to that described by Crater & Van de Rijn (1995) and Moses et al. (1997). Overnight *S. pyogenes* cultures were subcultured 1:10 in BHI and incubated to mid-log phase of growth (~OD_{600} = 0.7). The volume of culture equivalent to an OD_{600} of 2 was centrifuged at 10 000 x g, 5 min. Pelleted cells were washed twice with water and the pellet resuspended with 500 µl MilliQ H_20 in a 1.5 ml tube. Chloroform (1 ml) was added and the tubes were vortexed for 2 min to extract the capsule. The mixtures were centrifuged (10 000 x g, 10 min, 4°C). The top aqueous layers were saved in new tubes, kept on ice, and diluted 1/10 with MilliQ H_20. In a 96-well plate, 50 µl of the each diluted aqueous layer was combined with 150 µl

of Stain-All solution (20 mg Stains-All powder (Sigma, USA), 50% formamide (Bioshop), 0.06% glacial acetic acid (Fisher) in a final volume of 100 ml). Absorbance was measured at 640 nm using a microplate reader (Synergy HT; BioTeK®, USA) and the total amount of hyaluronic acid was determined using a standard curve generated with known concentrations of hyaluronic acid (Alfa Aesar, Ward Hill MA, USA).

2.7.6 Paraquat and dithiothreitol sensitivity assay

Sensitivity to the oxidative-stress-promoting compound methyl viologen (paraquat) was performed according to King et al. (2000). Briefly, overnight *S. pyogenes* cultures were subcultured 1:300 in Tryptic Soy Broth (TSB) medium (Wisent) in 15 ml Falcon tubes and grown for 12 h. In a 1.5 ml tube, 5 µl of subcultures was added to 1.5 ml TSB containing paraquat (Sigma) at a final concentration of 0.5 mM or 1 mM. Tubes were incubated for 18 h, 37°C, 5% CO_2, and the culture densities were determined by measuring the OD_{600}. The same protocol was used to assess culture sensitivity to dithiothreitol (DTT) (Bioshop) at concentrations of 15 mM and 20 mM.

2.8 RAW 264.7 Cell Culture Conditions

RAW 264.7 cells (ATCC® TIB-71), a murine macrophage cell line, were grown to confluence in RPMI 1640 medium (Wisent) supplemented with 10% fetal bovine serum (FBS) (Invitrogen) and 1X penicillin-streptomycin (Invitrogen) in 75 cm^2 flasks (Corning) maintained at 37°C, 5% CO_2. Since these are adherent cells, subculture passages were prepared by aspirating old media, scraping to dislodge cells and diluting in fresh growth media at a subcultivation ratio

of 1:5 every 2-3 days. Viable cell aliquots were preserved in RPMI growth medium supplemented with 5% (v/v) DMSO (Fisher Biotech) at -80°C.

2.9 Gentamicin Protection Assay

RAW 264.7 cells were seeded at a density of 2×10^5 cells per well into a 24-well plate. The following day, cells were washed three times with sterile PBS. Overnight cultures of *S. pyogenes* were subcultured and grown to $OD_{600} = 0.2$. Bacteria were suspended in RPMI + 10% FBS to achieve a concentration of 2×10^6 CFU/ml per well. RAW cells were infected with *S. pyogenes* for 1 h in a 37°C, 5% CO_2 incubator. Each well was then washed 3 times with PBS. To remove any residual extracellular bacterial cells that were not internalized, fresh RPMI + 10% FBS media containing 100 μg/ml gentamicin (Sigma) was added, and the plate was incubated for an additional hour. Aliquots were taken from supernatants and plated to confirm that all extracellular bacteria were killed by the 1 h gentamicin treatment. Following the gentamicin treatment, the plate was washed 3 x with PBS and 1 ml of fresh RPMI + 10% FBS media containing no antibiotics was added to establish the 0-h time point. At the 1 h and 18 h time-points, cells were lysed by 1 ml of sterile 0.001% (w/v) TritonX-100 (Sigma) in 1 X PBS. The resulting lysates were serially diluted and plated to enumerate the intracellular bacteria. The supernatants were also collected, serially diluted and plated to enumerate the extracellular bacteria.

2.10 Cloning and Expression of Recombinant Proteins

Recombinant plasmids to produce N-terminal hexahistidine tagged proteins were constructed by cloning in-frame fragments of the genes into the expression vector pQE-30 (Qiagen). The primers and restriction enzymes used for each gene are listed in Table 3. Plasmids were transformed into *E. coli* XL-1 Blue and selected on LB with ampicillin, and the constructs were confirmed by restriction analysis. The *E coli* pQE-30 rSpeA construct containing the *speA1* whole gene was provided from previous work done in the lab (Lee, unpublished).

To produce His_6-tagged 2037, a 50 ml of overnight culture was diluted into 450 ml of pre-warmed LB and incubated at 37°C, 180 rpm, until mid-exponential phase of growth was obtained. Expression was induced with a final concentration of 1 mM of isopropyl-β-D-thiogalactopyranoside (IPTG), and the culture was incubated at 37°C for an additional 4 h. Cells were harvested by centrifugation (10 000 x g, 10 min) and resuspended in 10 ml column wash buffer (50 mM NaH_2PO_4, 300 mM NaCl, 20 mM imidazole, pH 7). The cells were lysed by sonication for 30s x 30 cycles, with alternating cooling on ice for 30 s intervals. Cell debris was removed from the lysate by centrifugation (27 000 x g, 30 min, 4°C) and the supernatant was applied to a 4 ml His60 Ni Superflow affinity column (Clontech, Mountain View CA, USA) equilibrated with the wash buffer. Unbound proteins were removed with 20 ml of wash buffer and His6-2037 was eluted with 10 ml of elution buffer (50 mM NaH_2PO_4, 300 mM NaCl, 250 mM imidazole) and collected in 1 ml fractions. Purity of the eluted proteins was confirmed by SDS-PAGE and Coomassie blue staining. The His6-SpeA, -2037_{C46A} and -2037_{C49A} cysteine variants were prepared using the same approach.

2.11 Production of Antisera

Antibodies were raised against purified r2037 and rSpeA1 in mice using the same approach: purified recombinant proteins were combined with 2% aluminum hydroxide gel (Sigma) in 1X PBS at 4°C for 24 h. Female BALB/c mice (n =5, Charles River Laboratory, St. Constant, QC, Canada) were immunized via intraperitoneal injection with 10 μg of protein antigen per dose, on days 1, 14, and 21. On day 28, the mice were euthanized and blood was collected by cardiac puncture. To obtain serum, the blood was incubated at 37°C for 1 h, and then on ice at 4°C overnight. Following incubation, serum was collected by centrifugation at 10 000 x g, 10 min and stored at -20°C.

2.12 Alkylation of Proteins

2.12.1 *In vivo* disulfide status

The *in vivo* disulfide status of SpeA was determined through cysteine alkylation. *S. pyogenes* cells from 100 ml overnight culture were pelleted by centrifugation at 14 000 x g, 15 min, 4°C. Proteins in the supernatant were precipitated with 9% (v/v) TCA + 0.18% (v/v) sodium deoxycholate on ice for 30 min, followed by centrifugation (15 000 x g, 15 min, 4°C) and washed twice with acetone. Pellets were then resuspended with 5 mM maleimide-PEG_2-biotin (0.5 kDa) (Bachem) buffered in 100 mM Tris (pH 7.0) and 1% (w/v) SDS. The mixture was incubated for 30 min at room temperature, followed by 10 min at 37°C to allow alkylation to occur. Excess maleimide was removed by TCA precipitation. The resulting pellets were solubilized in 100 mM Tris (pH 7.0) and 1% SDS. To prepare positive controls, TCA precipitated proteins were first reduced with 100 mM DTT in 10 mM Tris (pH 8.1) for 30 min at room temperature prior to the addition of maleimide. To detect biotinlylated proteins, the

samples were boiled in sample buffer and run in duplicate on 15% SDS-PAGE. Proteins were transferred to nitrocellulose membranes. One blot was reacted with avidin alkaline phosphatase (Sigma) to detect alkylated proteins and the second blot reacted with anti-SpeA to determine total SpeA in the samples. All experiments were repeated at least three times to ensure reproducibility.

Densitometry analysis of alkylation was quantified using ImageJ. The proportion of biotinylated protein was calculated by dividing the signal for bands detected by avidin-AP by the signal detected by the anti-SpeA antibody. The fold change between SpeA band intensities was calculated by dividing the relative intensity of the DTT-treated band by the not treated band. The mean fold change was measured from three independent experiments.

2.12.1 *In vitro* disulfide status

The redox state of either the rSpeA or r2037 in an *in vitro* disulfide exchange reaction was determined in a similar manner. Reduced rSpeA and r2037 were prepared by combining 425 µl of protein with 50 mM DTT for 30 min on ice buffered in 100 mM Tris (pH 8). DTT was removed by size exclusion chromatography (SEC) using a 5 cm commercial PD-10 desalting column (Sephadex G-25, GE Life Sciences) equilibrated with 50 mM sodium phosphate buffer (pH 7). Reduced r2037 protein sample was applied to the top of the PD-10 column followed by addition of 2.5 ml 50 mM sodium phosphate buffer and allowed to run though the entire column. At this point, 1 ml of 50 mM sodium phosphate buffer was added and the eluted protein fraction was collected. The eluted protein fraction was collected and kept on ice.

Fully oxidized rSpeA and r2037 were prepared by combining 400 µl of protein with 50 mM oxidized glutathione (Sigma) for 1 h at room temperature buffered in 100 mM Tris (pH 8.8),

200 mM KCl, 1 mM EDTA (Bioshop). Glutathione was then removed by applying the sample to a PD-10 column as described above. Quantification of DTT-reduced proteins and glutathione-oxidized proteins were done using SDS-PAGE with BSA standards and ImageJ analysis as described previously.

To perform the disulfide exchange reaction, 2 nmol of both 2037 (oxidized) and SpeA (reduced) proteins were combined in 0.2 ml of buffer containing 50 mM sodium phosphate (pH 8), 5 mM EDTA, and 100 mM NaCl to achieve final protein concentrations of 10 μM. The mixture was allowed to react at room temperature for either 30 min or 1 h. The same equimolar reaction was set up containing 10 μM of 2037 (reduced) and SpeA (reduced). Proteins were TCA precipitated following incubation. Pellets were then alkylated with 5 mM maleimide-PEG_2-biotin (0.5 kDa) (Bachem) or 20 mM maleimide-PEG_2-biotin (2 kDa) (CreativePEGworks) as described above. Excess maleimide was removed by TCA precipitation and acetone washes. The resulting pellets were solubilized in 100 mM Tris (pH 7.0), 1% SDS. Positive controls were prepared containing 10 μM of either SpeA or 2037 alone in their oxidized or reduced form buffered in 50 mM sodium phosphate (pH 8), 5 mM EDTA. Controls were treated with maleimide for 30 min directly, followed by TCA precipitation as already described. Detection of biotinlylated proteins was done through western blot, identical to the *in vivo* protocol. All experiments were repeated at least three times to ensure reproducibility.

2.13 Enzyme Assays

2.13.1 Oxidative folding of reduced, denatured RNase A

To determine oxidase activity of recombinant proteins, the RNase A refolding assays were carried out as described by Daniels et al., (2010). Recombinant 2037 protein was fully oxidized with 100 mM oxidized glutathione (Sigma) as described above. Glutathione was then removed by dialysis against 100 mM sodium phosphate buffer (pH 7).

Reduced, denatured RNase A was prepared by incubating 5 mg/ml RNase A in 6 M guanidine HCl, 100 mM Tris acetate, 2 mM EDTA, and 130 mM DTT (pH 8), overnight at room temperature. Excess DTT and guanidine HCl were removed by SEC as described above.

Refolding assays were carried out using 7 nmol of r2037 in a redox buffer containing 0.2 mM oxidized glutathione (GSSG), 0.1 mM reduced glutathione (GSH), 2 mM EDTA, in 100 mM Tris acetate, pH 8. Reduced, denatured RNase A (7 nmol) was added and incubated for 2 min prior to the addition of 4.5 mM cCMP substrate (Sigma). Tubes were topped with MilliQ H_20 to reach a volume of 0.7 ml (final protein concentration of 10 μM) and transferred to 1 ml quartz cuvettes. RNase A catalyzed cCMP hydrolysis was measured at A_{296}. Reduced RNaseA alone, without added enzyme, was also included as a control.

2.13.2 Reductase activity

Reductase activity was assessed using an insulin disulfide reduction turbidimetric assay as described by Holmgren (1979). Recombinant 2037 protein was fully reduced by DTT and excess DTT was removed by SEC.

Insulin (Sigma) was prepared at 2 mg/ml by dissolving 20 mg in 10 ml of 100 mM potassium acetate, pH 7.5 and then adjusting the pH to 2-3 with 1.0 M HCl and rapidly titrating the solution to 8.0 with 1.0 M KOH.

Turbidimetric assays were carried out using 7 nmol of purified reduced 2037 combined with 1 μg/μl of insulin and 2 mM EDTA, buffered in 100 mM potassium acetate, pH 7.5. Tubes were topped with MilliQ H_20 to reach a final volume of 0.7 ml and transferred to 1 ml cuvettes. The reaction was started by adding DTT (350 μM) to all cuvettes and any precipitation of insulin was measured at OD_{600} every 5 min for 1 h. Insulin reduction by 350 μM DTT alone, without added enzyme, was also included as a control.

2.13.3 TDOR-substrate complex interaction

The formation of an intermolecular disulfide bond between 2037 and SpeA was assessed in an *in vitro* protocol using potassium ferricyanide ($K_3Fe(CN)_6$). Reduced rSpeA and r2037 were prepared as described above. In a 1.5 ml tube, 2 nmol of 2037 (reduced) and SpeA (reduced) proteins were combined with 5 mM $K_3Fe(CN)_6$ (w/v) (Sigma) in 0.2 ml of 50 mM sodium phosphate buffer (pH 7), and allowed to react for 1 h at 37°C. To detect protein complexes, the reaction samples were analyzed on 15% SDS-PAGE gels under non-reducing conditions, followed by staining with Coomassie blue. The same experimental set-up was used to test heterodimer complexes formed between 2037_{C46A}-SpeA and 2037_{C49A}-SpeA.

2.14 Sequence Analysis

A list of potential *S. pyogenes* TDORs and TDOR substrates was initially generated by Lee (unpublished) using a protocol modified from Daniels et al., (2010) (as described in Davey et al., 2013). The M1 serotype *S. pyogenes* MGAS5005 proteome was downloaded from UniProt (http://www.uniprot.org) and separately grouped into extracytoplasmic versus cytoplasmic proteins using the prediction servers SignalP 3.0 (Bendtsen, Nielsen, Von Heijne, & Brunak,

2004) and LipoP 1.0 (Juncker et al., 2003), which screen for potential secreted proteins and lipoproteins, respectively. Identified extracytoplasmic proteins predicted to encode a signal sequence by either the Neural Network or Hidden Markov Model were considered as extracellular and analyzed further for cysteine content. Extracellular portions of the proteins were identified using the transmembrane prediction server SCAMPI (Bernsel et al., 2008), and proteins with two or more cysteine residues predicted to localize on the outside of the membrane were collected in a list of potential TDORs and natural TDOR substrates. The presence of the distinct catalytic CXXC motif was also used to narrow down potential TDORs, but was not a necessity. Predicted cytoplasmic proteins were mostly discarded; however, those with two or more cysteine residues known to be surface or membrane-associated were also included in the TDOR list. The annotated functions of the genes were obtained from the NCBI protein database.

To generate a TDOR list in the M18 serotype, the protein sequences from predicted M1 TDORs were used as the query for a BLASTP search in the *S. pyogenes* MGAS8232 strain proteome. Homologs that still contained two or more cysteine residues were listed as candidate M18 TDORs. The same BLASTP comparison from M1 *S. pyogenes* was used to compile a list of candidate TDOR substrates in M18. Annotated functions of the MGAS8232 genes were obtained from the NCBI protein database.

2.15 Statistical Analysis

Results were analyzed by one-way analysis of variance with Dunnett post-tests using GraphPad Prism version 6 (GraphPad Software Inc., La Jolla, California). A P value of ≤ 0.05 was considered statistically significant.

CHAPTER 3: Results

3.1 Identification of putative TDORs and TDOR substrates in *S. pyogenes* MGAS8232

Given the recent discovery of a novel TDOR in *S. gordonii*, called SdbA, we first sought to identify potential TDORs within the *S. pyogenes* proteome. A list of candidate TDORs in M1 serotype *S. pyogenes* MGAS5005 was initially generated (Lee, unpublished) using an *in silico* approach where extracytoplasmic and cytoplasmic proteins were grouped separately using the prediction servers SignalP 3.0 and LipoP 1.0 (Bendtsen et al., 2004; Daniels et al., 2010; Juncker et al., 2003). Proteins were analyzed for cysteine content and those with two or more cysteine residues predicted to localize on the outside of the membrane were compiled into a list of potential M1 TDORs (Appendix B). Using this initial list, a BLASTP search in the M18 *S. pyogenes* MGAS823 proteome was conducted, looking for TDOR homologs. Analysis by BLAST search identified 5 candidate M18 TDORs: SpyM18_2037, SpyM18_AhpC, SpyM18_0982, SpyM18_2138 and SpyM18_1572 (Table 5). Of these five, SpyM18_2037, SpyM18_2138 and SpyM18_1572 contain the catalytic CXXC motif, a characteristic of TDOR enzyme active sites. The annotated functions of each protein are described in Table 5 along with their primary amino acid sequences.

Identification of potential substrates was done during the same *in silico* analysis and compiled into a list of M1 TDOR substrates (Appendix C). Likewise, a BLASTP search in the M18 *S. pyogenes* MGAS823 proteome was conducted, looking for substrate homologs compared to M1 protein sequences. Table 6 shows the short-list of candidate protein substrates found in the M18 *S. pyogenes*, including the gene name, known or possible function and number of cysteine residues. The corresponding primary amino acid sequence of each identified M18 substrate can be found in Appendix D. Of note, the *speA* gene was identified as a potential substrate,

Table 5: Candidate TDORs in M18 *S. pyogenes* MGAS8232 strain.

Gene Name (SpyM18)	**Annotated Function***	**Primary Protein Sequence****
2037	Bacteriocin transport	MRPKEKETSMTFEEIVANFIPSSVAEVTSAIASGKDMIVFLGR SS**CPYC**RRFAPKLAQVATDNQKEVYFVDSENAADAAELAAFRE NYQLVTVPALLVSYDQHQRAV**C**DSSLTPDDILAFLTRE
2137 (ahpC)	Alkyl hydroperoxidase	MSLIGKEIAEFSAQAYHDGKFITVTNEDVKGKWAVF**C**FYPADF SFV**C**PTELGDLQEQYETLKSLGVEVYSVSTDTHFVHKAWHDDS DVVGTITYPMIGDPSHLISQAFEVLGEDGLAQRGTFIVDPDGI IQMMEINADGIGRDASTLIDKIHAAQYVRKHPGEV**C**PAKWKEG AETLTPSLDLVGKI
0982	Oxidoreductase	MAQRIIVITGASGGLAQAIVKQLPKEDSLILLGRNKERLEH**C**Y QHIDNKE**C**LELDITNPVAIEKMVAQIYQRYGRIDVLINNAGYG AFKGFEEFSAQEIADMFQVNTLASIHFA**C**LIGQKMAEQGQGHL INIVSMAGLIASAKSSIYSATKFALIGFSNALRLELADKGVYV TTVNPGPIATKFFDQADPSGHYLESVGKFTLQPNQVAKRLVSI IGKNKRELNLPFSLAVTHQFYTLFPKLSDYLARKVFNYK
2138	NADH Oxidase/alkyl hydroperoxidase reductase	MALSPDIKEQLAQYLTLLEADLVLQVSLGDNEQSQKVKDFVEE IAAMSERISIENITLDRQPSFKVAKKGHDSGVVFAGLPLGHEL TSFILALLQVSGRAPKVDQDVIDRIKAIDRPLHFETYVSLT**CH NC**PDVVQALNIMSVLNDKISHTMVEGGMFQDEVKAKGIMSVPT VFLDGEEFTSGRATIEQLLEQIAGPLSEEAFADKGLYDVLVIG GGPAGNSAAIYAARKGLKTGLLAETFGGQVMETVGIENMIGTL YTEGPKLMAEVEAHTKSYDVDIIKAQLATSIEKKENIEVTLAN GAVLQAKTAILALGAKWRNINVPGEDEFRNKGVTY**CPHC**DGPL FEGKDVAVIGGGNSGLEAALDLAGLAKHVYVLEFLPELKADKV LQDRAADTANMTIIKNVATKDIVGDDHVTGLNYTERDSGEDKH LDLEGVFVQIGLVPNTAWLKDSGVNLTDRGEIIVDKHGSTNIP GIFAAGD**C**TDSAYKQIIISMGSGATAAIGAFDYLIRQ
1572	Thioredoxin-like protein; TlpA family	MKKGLLVTTGLA**C**LGLLTA**C**STQDNMAKKEITQDKMSMAAKKK DKMSTSKDKSMMADKSSDKKMTNDGPMAPDFELKGIDGKTYRL SEFKGKKVYLKFWASW**CSIC**LSTLADTEDLAKMSDKDYVVLTV VSPGHQGEKSEADFKKWFQGTDYKDLPVLLDPDGKLLEAYGVR SYPTEVFIGSDGVLAKKHIGYAKKSDIKKTLKGIH

*Annotated descriptions obtained from NCBI protein database
**All cysteine residues are bold and catalytic CXXC motifs are underlined if present

Table 6: Candidate S. pyogenes MGAS8232 extracytoplasmic protein substrates with ≥ 2 cysteine residues.

Gene ID (SpyM18)	Gene Name	Annotated Function*	Cysteine Residues
0393	*speA*	Exotoxin type A; superantigen	3
0201	*speG*	Exotoxin type G; superantigen	3
0547		Conserved bacteriocin-like peptide	2
0975		Putative exfoliative toxin	3
0799	*sagA*	streptolysin S associated protein	7
0803		CPBP family intramembrane metalloprotease	7
2236	*hasA*	Hyaluronate synthase A (HasA)	6
1014	*hylA*	Extracellular hyaluronate lyase	2
0011		Beta-lactamase class A; serine hydrolase	2
1051		Putative D,D-carboxypeptidase, penicillin-binding protein	3
0280	*dacA*	Putative penicillin-binding protein; D-alanyl-D-alanine carboxypeptidase	3
0031		Autolysin; CHAP domain-containing protein	2
1382	*deadD2*	Putative deacetylase	2
1321		putative extramembrane protein; D-alanyl-lipoteichoic acid biosynthesis protein DltD	2
0476		family of actin-ADP-ribosylating toxin	9
1867		heme ABC transporter substrate-binding protein IsdE	5
0197		Cytokinesis protein 3; transglutaminase/protease-like domain	5

*Annotated descriptions obtained from NCBI protein database

containing 3 cysteine residues. This agrees with published reports of the crystal structure and mutational analysis of SpeA showing 2 of the 3 cysteines are involved in forming a stable disulfide bridge (Papageorgiou et al., 1999; Roggiani et al., 1997). Together, this also supports the validity of the *in silico* approach.

3.2 Successful construction of *S. pyogenes* MGAS8232 TDOR mutants

To elucidate the function of each candidate TDOR protein in M18 *S. pyogenes*, mutants defective in the TDOR gene were created by insertional inactivation. The thermosensitive pG$^+$host5 delivery vector is commonly known to have broad application as a mutagenic tool (Kasper, 2013; Maguin, et al 1996). Vectors of the pG$^+$host-based family are thermosensitive derivatives of the *L. lactis* plasmid pWV01, and have been shown to be instrumental for high-efficiency gene inactivation and replacement in Gram-positive bacteria (Leenhouts, Kok, & Venema, 1991; Smidt, Van der Oost, & De Vos, 2001). Key features of the pG$^+$host5 plasmid include: the pBR322 origin replicon for propagation in *E. coli* at 37°C; the pWV01 thermosensitive (Ts) origin for maintenance of the plasmid at 28-30°C in Gram-positive species; a multicloning site originating from pBluescript and an erythromycin resistance gene (Maguin et al., 1996). Accordingly, the pG$^+$host5 plasmid was used and constructed to include the internal portion (300-750 bp) of the targeted TDOR gene, as named in Table 2. Following electroporation of pG$^+$host5 constructs into GAS, transformants were grown under erythromycin selection at 30°C, then 40°C. Chromosomal TDOR gene interruption by homologous recombination was facilitated by this upward shift in temperature to the non-permissive plasmid replication temperature (40°C). Proper integration of the plasmid was confirmed by PCR using one primer that binds to the 5' end of the gene, outside of the cloned internal fragment, and a second primer

that binds a pG$^+$host5 plasmid-specific sequence, as illustrated in Figure 2A. Successful interruption of the *2037* gene was confirmed by PCR amplification of a ~0.4 kb fragment (Figure 2B). Similarly, insertional mutation of the *aphC, 0982, 2138, 1572* whole genes were successfully PCR confirmed by visualization of ~0.6 kb, ~0.7 kb, ~1.2 kb, ~0.7 kb fragments respectively (Figure 2C-F). The M18 wild-type DNA, containing no chromosomal mutation, was included as a negative control in each PCR.

3.3 Mutants show negligible differences in a range of phenotypes compared to parent

3.3.1 No difference in hemolysis

The *sagA* gene encodes for Streptolysin S (SLS), a toxin responsible for the rupture or lysis of RBCs in early stages of GAS infection (Molloy et al. 2011). The SLS toxin contains 7 cysteine residues based on our *in silico* analysis, and is therefore a potential TDOR substrate requiring disulfide bond formation. To test hemolytic activity between wild type and TDOR mutants, cultures were streaked on sheep blood agar (SBA) plates. Observations of hemolytic zones surrounding parent and mutant single colonies showed no difference in hemolysis (Figure 3A). Mutants *Δ2037, ΔahpC, Δ0982, Δ2138 and Δ1572* displayed similarly sized zones of clearance compared to the M18 parent. β-hemolysis was observed uniformly across the entire streaked SBA plates with parent and all five mutant cultures (data not shown). Given the qualitative nature of this result, there is the possibility that SLS is partially misfolded in TDOR mutants or a compensatory factor is producing the hemolysis observed. The role of candidate TDORs in hemolysis was not investigated further.

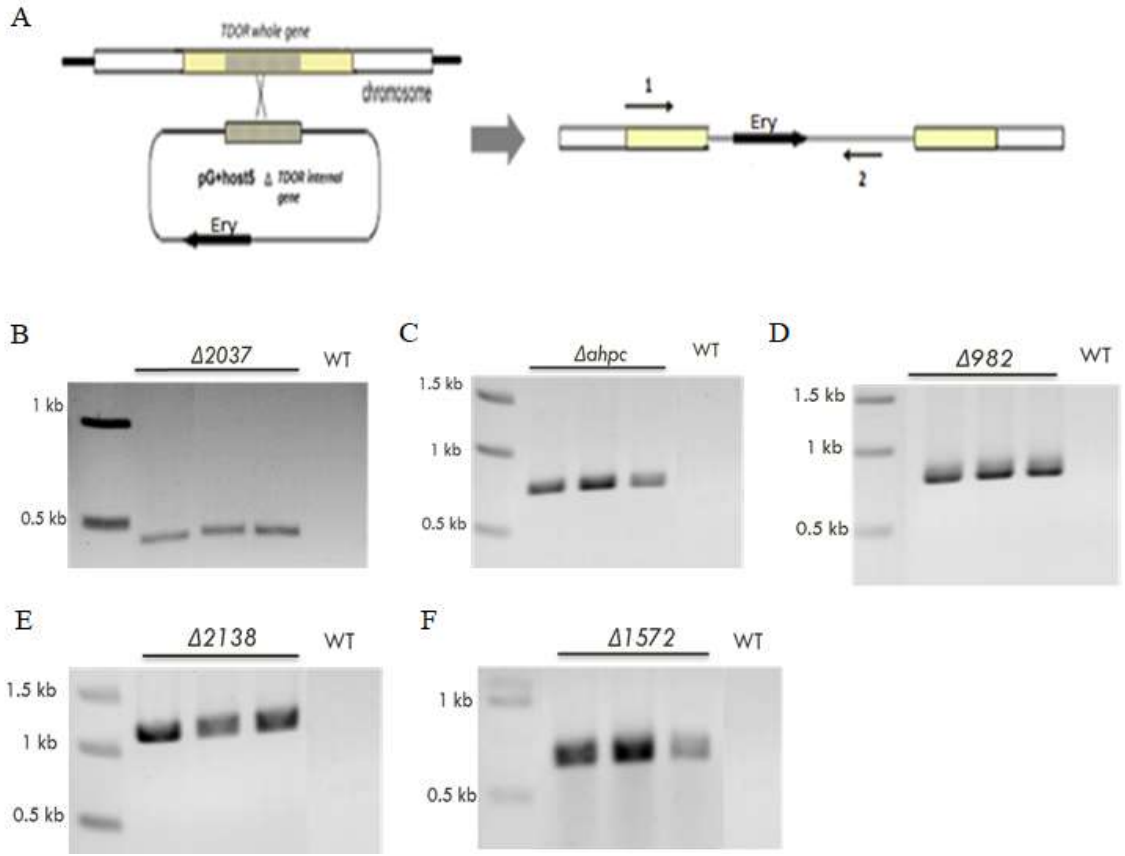

Figure 2: Successful PCR confirmed TDOR mutations in M18 GAS. (A) Schematic illustrating how the insertional disruption of TDOR genes was evaluated. Mutation of chromosomal TDOR gene by integration of the pG$^+$host5 constructs through homologous recombination. Integration of the pG$^+$host5 constructs was confirmed by PCR using representative primers 1 (forward) and 2 (reverse). Primer 1 binds to the 5' end of the TDOR gene outside of the cloned fragment on the plasmid, serving as a reference point. Primer 2 binds to a pG$^+$host5 plasmid-specific internal sequence. (B-F) Agarose gels showing PCR products of *2037, aphC, 0982, 2138, 1572* whole gene interruptions. Three positive mutant clones are shown for each TDOR gene. M18 wild-type DNA, containing no insertional mutation, is included as a negative control in each PCR reaction with designated primers (B-F, *WT* lane). All primer sequences are listed in Table 3.

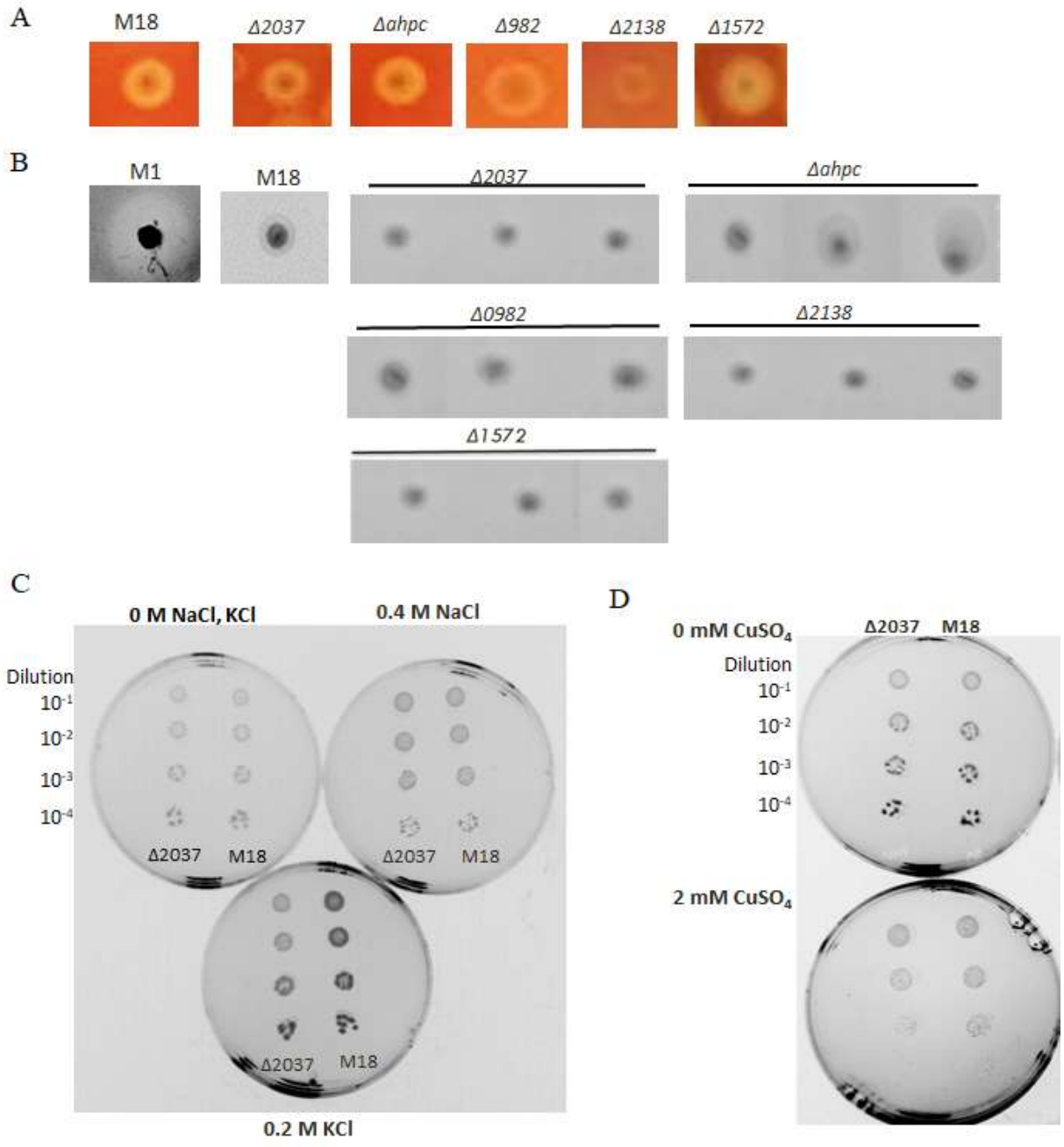
A
M18
Δ2037
Δahpc
Δ982
Δ2138
Δ1572
B
M1
M18
Δ2037
Δahpc
Δ0982
Δ2138
Δ1572
C
0 M NaCl, KCl
0.4 M NaCl
Dilution
10-1
10-2
10-3
10-4
Δ2037
M18
Δ2037
M18
Δ2037
M18
0.2 M KCl
D
0 mM CuSO4
Δ2037
M18
Dilution
10-1
10-2
10-3
10-4
2 mM CuSO4

Figure 3: Qualitative observations of hemolysis, bacteriocin production, salt and copper sensitivities show negligible differences between parent and mutants. (A) Sheep blood agar (SBA) plates streaked with parent and TDOR mutant *Δ2037, ΔahpC, Δ0982, Δ2138, Δ1572* cultures incubated at 37°C, 24 h. Each panel depicts visible zones of hemolysis around colonies. β-hemolysis was observed uniformly across the entire streaked SBA plates with parent and all five mutant cultures (data not shown). (B) Deferred antagonism assay for bacteriocin production by M1 wild-type, M18 parent, and TDOR mutant strains. *S. pyogenes* cultures were stabbed into BHI agar and incubated overnight at 37°C under microaerophilic conditions in candle jars. Plates were overlaid with soft agar containing *L. lactis* as the indicator strain. Zones of inhibition of the indicator strain were evaluated after overnight incubated at 30°C in the candle jars. Triplicate stabbed colonies are shown for each TDOR mutant. (C-D) Growth of M18 parent and TDOR mutant *Δ2037* on representative BHI agar containing either 0.4 M NaCl, 0.2 M KCl or 2 mM $CuSO_4$. *S. pyogenes* cultures were adjusted to OD_{600} of 0.2 and four serial dilutions were made (10^{-1}-10^{-4}) with 10 µl spotted on agar plates. Growth was observed and compared after overnight incubation 37°C. Control plates containing no salt and no copper are included. Experiments done with *ΔahpC, Δ0982, Δ2138, Δ1572* mutants showed similar results to *Δ2037* growth on 0.4 M NaCl, 0.2 M KCl and 2 mM $CuSO_4$ agar (plates not shown). (A-D) All assays were performed three independent times.

3.3.2 No difference in bacteriocin production

Since the *SypM18_2037* gene is annotated as being involved in bacteriocin transport, we sought to compare bacteriocin production in mutant and parent strains. GAS is known to produce Class IIb bacteriocins, which exert optimal antibacterial activity when two peptides are present (Armstrong et al., 2016). These mature two-peptide bacteriocins each have 1 cysteine and can be post-translationally modified by disulfide bond formation (Armstrong et al., 2016). In order to assess bacteriocin production *in vitro*, a standard deferred antagonism assay was done. While the M1 serotype displayed a zone of inhibition surrounding the established colony, no bacteriocin activity was detected from wild-type M18 (strain MGAS8232) or any of the mutant strains (Figure 3B). Triplicate stabbed colonies for mutants *Δ2037, ΔahpC, Δ0982, Δ2138* and *Δ1572* showed no surrounding zones of inhibition (Figure 3B). The inability of M18 GAS to produce bacteriocin *in vitro* has also been reported by Armstrong et al. (2016), who demonstrate that a promoter required for bacteriocin expression was only successfully induced *in vivo*. The role of candidate TDORs in bacteriocin production was not investigated further.

3.3.3 No difference in salt or copper sensitivities

Since candidate TDORs enzymes are predicted to be extracytoplasmic or membrane-associated, sensitivity of mutants to NaCl and KCl was tested. It is possible that mutations of putative TDORs affects the ability of GAS to cope with osmolarity differences caused by general salt stressors. Agar plates were first determined to contain either 0.4 M NaCl or 0.2 M KCl, as these high salt concentrations were still able to support viable M18 parent growth. The *Δ2037, ΔahpC, Δ0982, Δ2138* and *Δ1572* mutants showed similar sensitivities to 0.4 M NaCl and 0.2 M KCl compared to the parent (Figure 3C). Representative plates from *Δ2037* growth are displayed.

Sensitivity to copper was tested next. Copper, a redox-active metal, can catalyze the formation of non-specific disulfide bonds and, in the absence of a functional TDOR, mutants may be unable to rearrange copper-catalysed, non-native disulfide bonds leading to growth differences (Hiniker et al., 2005). However, observations of growth on selective agar plates showed no difference in mutant *Δ2037, ΔahpC, Δ0982, Δ2138* and *Δ1572* sensitivities to 2 mM $CuSO_4$ compared to the parent (Figure 3D). Representative plates from *Δ2037* growth are shown, with copper concentrations likewise determined based on M18 parent viability.

3.3.4 Mutants are sensitive to penicillin G but not other cell-wall/membrane antibiotics

The ability to cope with the effects of cell-wall and cell-membrane targeted antibiotics may be compromised in the absence of a functional TDOR, especially if the predicted TDOR is involved in disulfide bond formation of peptidylglycan synthesis proteins. Penicillin G is a β-lactam antibiotic that irreversibly binds to transpeptidase, also known as penicillin-binding proteins (PBPs), disrupting the final cross-linking steps of cell-wall peptidoglycan (Sauvage et al. 2008). PBP5, encoded by the *dacA* gene, has 3 cysteine residues and was identified as a potential substrate *in silico* (Table 6). Antibiotics vancomycin and bacitracin also work by disrupting GAS cell wall and peptidoglycan synthesis (Hammes & Neuhaus, 1974; Maxted, 1953). Polymyxin B disrupts the structure of bacterial cell membranes by interacting with its phospholipids (Morrison & Jacobs, 1976). Sensitivities to these 4 antibiotics were assessed by disc diffusion assays (Figure 4A) and subsequent measurement of zones of inhibition.

Results from triplicate mean diameters showed that *Δ2037, ΔahpC,* and *Δ2138* mutants were more sensitive to penicillin G at concentrations of 2.5, 1.25 and 0.625 μg/ml compared to

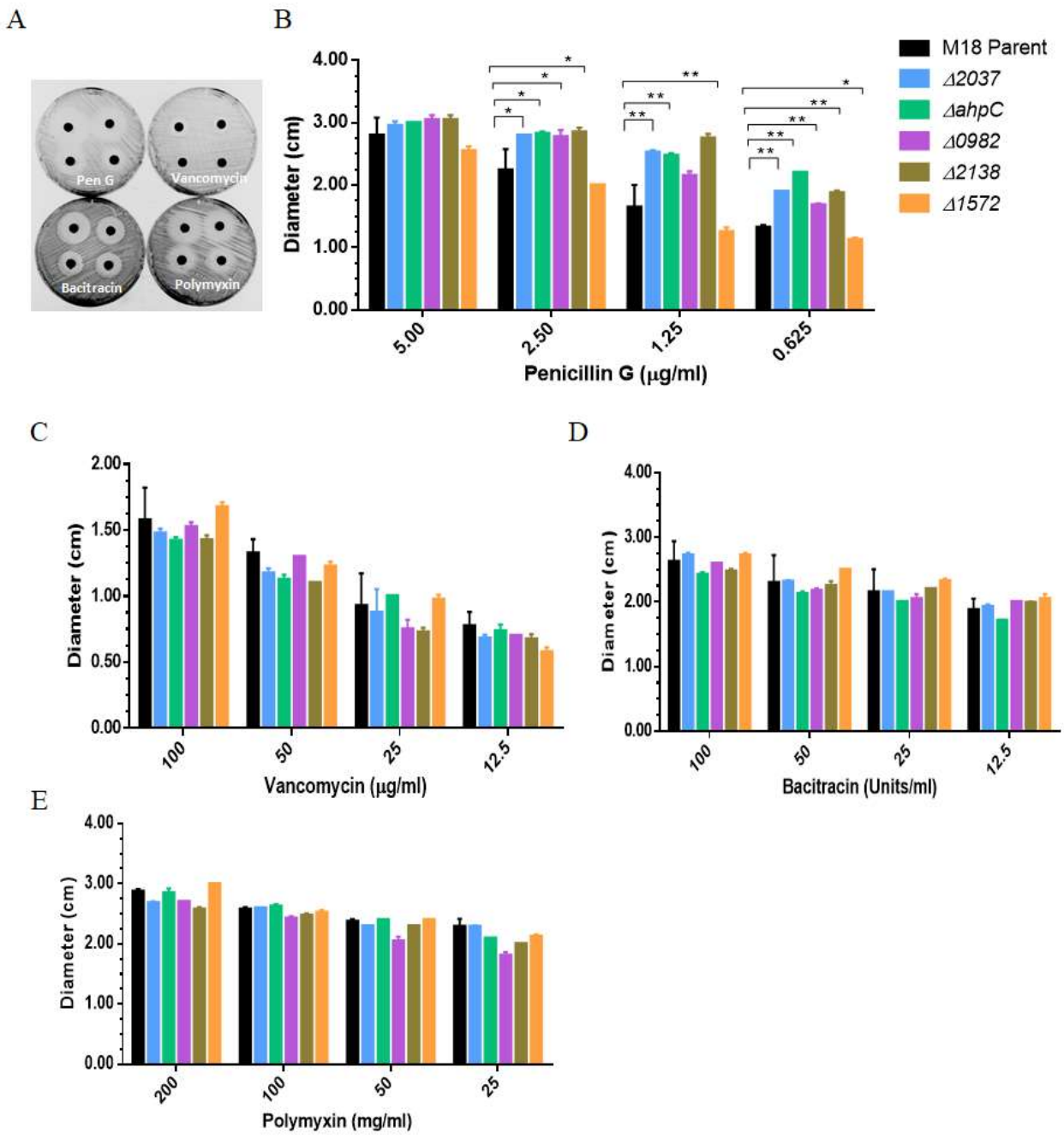
A
Pen G
Vancomycin
Bacitracin
Polymyxin
B
M18 Parent
Δ2037
ΔahpC
Δ0982
Δ2138
Δ1572
Diameter (cm)
4.00
3.00
2.00
1.00
0.00
5.00
2.50
1.25
0.625
Penicillin G (μg/ml)
C
Diameter (cm)
2.00
1.50
1.00
0.50
0.00
100
50
25
12.5
Vancomycin (μg/ml)
D
Diameter (cm)
4.00
3.00
2.00
1.00
0.00
100
50
25
12.5
Bacitracin (Units/ml)
E
Diameter (cm)
4.00
3.00
2.00
1.00
0.00
200
100
50
25
Polymyxin (mg/ml)

Figure 4: Mutants are sensitive to penicillin G but not other cell-wall or cell-membrane specific antibiotics. (A) Representative image of antibiotic disc diffusion plate assay. M18 parent and TDOR mutant *Δ2037, ΔahpC, Δ0982, Δ2138, Δ1572* cultures were adjusted to OD_{600} of 0.2 and evenly distributed on BHI agar plates, covering the entire surface area. Four sterile filter paper discs were placed on top of each plate containing: penicillin G (5, 2.5, 1.25, 0.625 µg/ml), vancomycin (100, 50, 25, 12.5 µg/ml), bacitracin (100, 50, 25, 12.5 U/ml), or polymyxin (200, 100, 50, 25 mg/ml). Growth inhibition zones surrounding the antibiotic discs were measured after overnight incubation, 37°C. Discs with no antibiotic treatment were included as a negative control showing no inhibition zone (data not shown). (B) Graph of mean diameters (cm) of inhibition zones due to penicillin G sensitivities (5, 2.5, 1.25, 0.625 µg/ml). (C-E) Mean diameters of inhibition zones due to vancomycin, bacitracin and polymyxin sensitivities respectively. Error bars represent standard deviation (SD) of triplicate experiments. Asterisks indicate a statistically significant difference (*$P \leq 0.05$; **$P \leq 0.01$; One-way ANOVA).

M18 parent (Figure 4B). *Δ0982* was more sensitive to penicillin G at 2.5, and 0.625 μg/ml while *Δ1572* was more resistant to 0.625 μg/ml compared to parent strain (Figure 4B). No significant difference, however, was found in TDOR mutant sensitivities to defined concentrations of vancomycin, bacitracin or polymyxin compared to parent (Figure 4 C-E). Discs without antibiotic treatment were included as a negative control showing no inhibition zone, and thus confirming the sterile discs themselves do not have antimicrobial properties (data not shown).

3.3.5 No difference in autolytic activity

To further assess any differences in cell-wall biosynthesis and integrity caused by mutation of predicted TDORs, autolytic activity was tested. Autolysis plays a role in many important functions including bacterial growth, remodelling of the cell wall, cell separation, adherence, biofilm formation, and eDNA release. (Davey et al. 2013; Forsberg & Rogers, 1971). In fact, mutation of *S. gordonii* TDOR SdbA showed clear defects in autolysis compared to parent. GAS cell-wall proteins containing cysteine residues have also been identified, such as peptidoglycan deacetylases (*deadD2* gene, 2 cys) and autolysin (2 cys) (Table 6). However, triplicate autolysis assays showed no significant difference in mutant autolytic activity compared to M18 parent. Mean OD_{600} values of *Δ2037, ΔahpC, Δ0982, Δ2138 and Δ1572* mutant strains remained between 95-100% of the initial optical density (Figure 5A).

3.3.6 No difference in capsule production

The *hasA* gene encodes for hyaluronan synthase, an enzyme with 6 cysteines residues responsible for hyaluronic acid (HA) production in GAS capsule composition. Differences in capsule production caused by mutation of predicted TDORs were tested. The amount of HA was

A

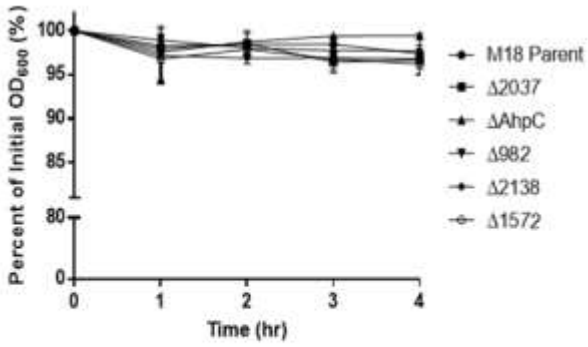

B

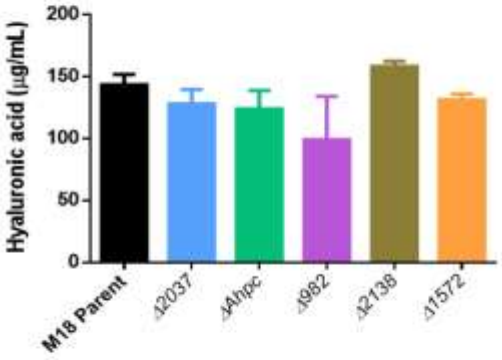

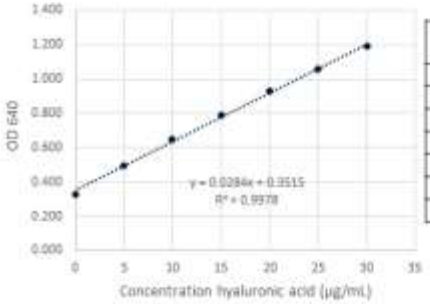

HA standard (μg/mL)	Mean OD (640 nm)
0	0.329
5	0.498
10	0.652
15	0.790
20	0.927
25	1.059
30	1.189

C

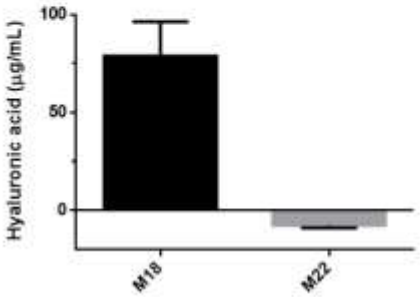

Figure 5: Mutants show no difference in autolytic activity or capsule production. (A) Autolysis of M18 parent and TDOR mutant *Δ2037, ΔahpC, Δ0982, Δ2138, Δ1572* strains monitored over 4 h. *S. pyogenes* cell pellets were suspended in autolytic buffer at 44°C and OD_{600} was measured. Percentages for each time-point were calculated by dividing the OD value by that of the start (time 0) OD_{600} value. Mean percentages are plotted; error bars representing SD of triplicates. (B, left) Quantification of mean capsular hyaluronic acid production from parent and mutant strains. GAS capsule was extracted by chloroform, combined with Stain-All solution, and absorbance measured at 640 nm. (B, right) Absorbance values were compared to a standard curve generated with known concentrations of hyaluronic acid (HA). Mean HA concentration values are plotted with error bars representing SD of three independent experiments performed in triplicate. (C) M22 serotype, a strain that does not produce capsule (Flores et al., 2012), was included as a negative control. Graphs (A, B) shown are representative of three independent experiments performed.

quantified in triplicate assays; however, no difference in capsule production between TDOR mutants and the M18 parent was detected (Figure 5B). The M22 serotype, *S. pyogenes* 10/69 strain, was included as a negative control as it is known to lack the *hasABC* genes necessary for hyaluronic acid capsule biosynthesis (Flores et al., 2012). Consistent with Flores et al. (2012), the M22 wild-type produced no detectable HA, thus supporting our experimental assay validity (Figure 5C).

3.4 Oxidative stress resistance and intracellular survival is compromised in mutant Δ2037

3.4.1 Mutant Δ2037 shows increased sensitivity to oxidative stress compounds *in vitro*

We next asked if the antioxidant system in GAS was compromised in any way by the absence of a functional TDOR. In fact, the SypM18_AhpC is annotated as a peroxidase, and an *ahpC*-deficient *S. pyogenes* was previously shown to be more sensitive to methyl viologen (paraquat) (King et al. 2000). While it is not itself a reactive oxygen species, paraquat acts to increase intracellular levels of toxic superoxides (Lu & Holmgren, 2014). SypM18_2138 is also annotated as a NADH oxidase/peroxide, suggesting a possible player role in the antioxidant system. To this end, we assessed the sensitivity of all 5 TDOR mutants to *in vitro* oxidative-stress-promoting compounds. Based on measured culture densities of growth with 0.5 mM paraquat, *Δ2037*, *Δ0982,* and *Δ1572* mutants showed significant sensitivity to paraquat compared to parent as growth was visibly impaired (Figure 6A). At 1 mM paraquat, all mutants *Δ2037, ΔahpC, Δ0982, Δ2138* and *Δ1572* showed significant paraquat sensitivity, with culture densities well below that of the M18 parent (Figure 6A, $P \leq 0.001$).

The effect of H_2O_2 was tested next, since this is commonly used to complement findings from paraquat sensitivity data. Sensitivity to H_2O_2 was assessed by disc diffusion assays and

A

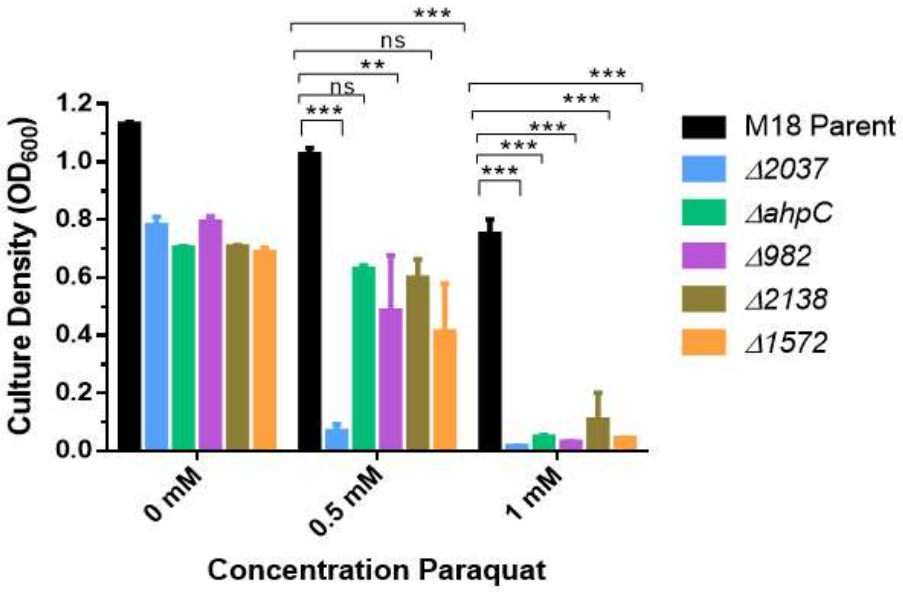
***
ns
**
ns
***
***
***
***
***
***
Culture Density (OD600)
1.2
1.0
0.8
0.6
0.4
0.2
0.0
0 mM
0.5 mM
1 mM
Concentration Paraquat
M18 Parent
Δ2037
ΔahpC
Δ982
Δ2138
Δ1572

B

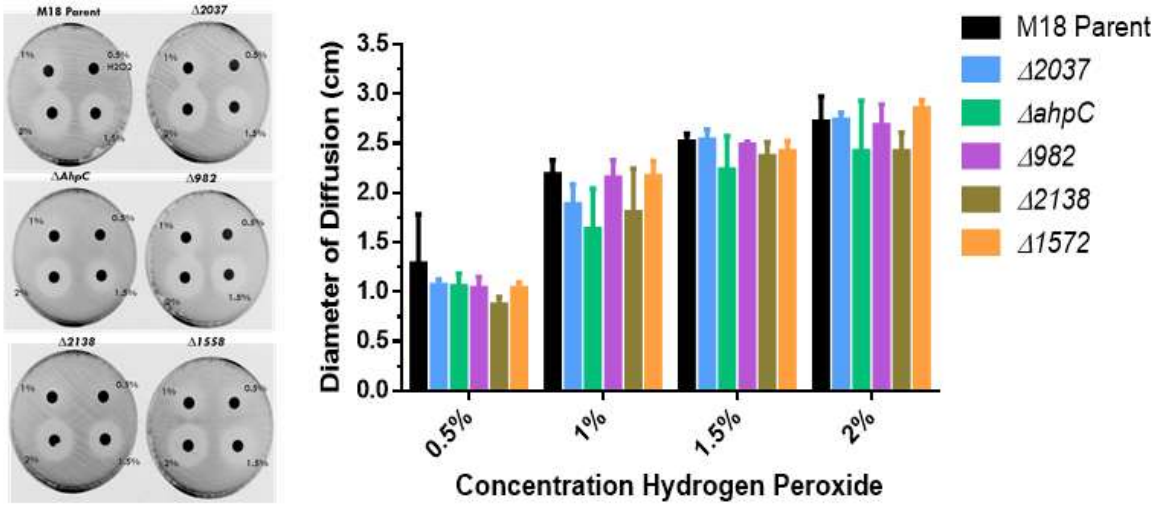
M18 Parent
Δ2037
ΔAhpC
Δ982
Δ2138
Δ1558
Diameter of Diffusion (cm)
3.5
3.0
2.5
2.0
1.5
1.0
0.5
0.0
0.5%
1%
1.5%
2%
Concentration Hydrogen Peroxide
M18 Parent
Δ2037
ΔahpC
Δ982
Δ2138
Δ1572

Figure 6: Mutants show increased sensitivity to paraquat but not hydrogen peroxide. (A) Growth sensitivities of M18 parent and TDOR mutant *Δ2037, ΔahpC, Δ0982, Δ2138, Δ1572* strains to 0, 0.5, 1 mM paraquat. Mean growth was measured by determining the OD_{600} after 18 h of incubation with indicated paraquat concentrations. A representative experiment is shown from five total independent experiments performed. Error bars represent SD of triplicates. Asterisks indicate that a mutant TDOR value is statistically significantly different from the M18 parent (**$P \leq 0.01$; ***$P \leq 0.001$; One-way ANOVA). Where indicated, 'ns' refers to no significance ($P > 0.05$, One-way ANOVA). (B, left) Representative image of hydrogen peroxide disc diffusion plate assay. M18 parent and TDOR mutant *Δ2037, ΔahpC, Δ0982, Δ2138, Δ1572* cultures were adjusted to OD_{600} of 0.2 and evenly distributed on BHI agar plates, covering the entire surface area. Four sterile filter paper discs were placed on top of each plate containing 0.5%, 1%, 1.5% and 2% H_2O_2. Growth inhibition zones surrounding the H_2O_2 discs were examined after overnight incubation, 37°C. (B, right) Graph of mean diameters (cm) of clearance zones due to 0.5%, 1%, 1.5% and 2% H_2O_2 sensitivities in parent and mutant TDOR cultures. Discs without H_2O_2 treatment were included as negative controls showing no zones of inhibition (data not shown). Error bars represent SD of triplicates. A representative experiment is shown from three independent experiments performed.

subsequent measurement of zones of inhibition diameters (Figure 6B). Based on triplicate mean diameters, mutant *Δ2037, ΔahpC, Δ0982, Δ2138* and *Δ1572* showed no significant difference in sensitivity to defined concentrations of H_2O_2 (Figure 6B).

Sensitivity to the reducing agent DTT was also investigated. DTT acts to break existing protein disulfide bonds. At 15 mM DTT, the 5 mutants showed no difference in DTT sensitivity compared to the M18 parent (Figure 7). However at 20 mM, the *Δ2037* mutant showed significant growth impairment whereas *ΔahpC, Δ0982, Δ2138* and *Δ1572* displayed negligible sensitivity differences compared to the parent (Figure 7, $P \leq 0.001$). Notably, the *Δ2037* mutant displays distinct phenotypic differences in assays tested so far, setting it apart from the 4 other candidate TDORs.

3.4.2 Mutant Δ2037 is more susceptible to phagocytic death

To further investigate the difference in oxidative stress resistance of mutants, a survival assay was performed using RAW 264 mouse macrophages. Infection of a human host depends on the ability of GAS to counteract the oxidative stress conditions generated by the release of reactive oxygen species (ROS) from innate immune cells such as monocytes and neutrophils. If TDOR mutants are defective in any part of their antioxidant system, they are expected to be more susceptible to killing by these cells. RAW 264 cells infected with either wild-type, *Δ2037* or *Δ1572* mutant cultures were lysed at the 1 h and 18 hr time-points, followed by serial dilution and enumeration of viable colonies in the lysate (intracellular bacteria) and supernatant (extracellular bacteria). Survival was expressed as the number of colony forming units (CFU) per ml. Compared to the M18 parent, infection with mutant *Δ2037* showed significantly reduced intracellular survival in RAW 264 cell lysates after 1 h and 18 h, suggesting this mutant is more

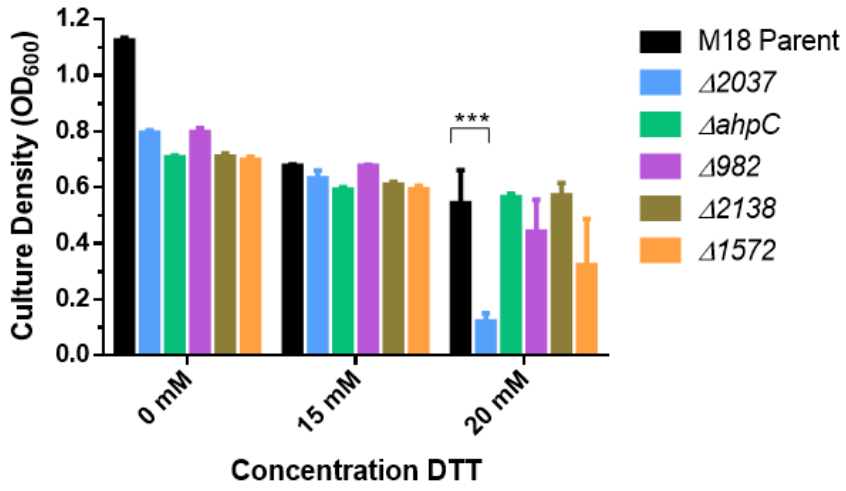

Figure 7: The Δ2037 mutant shows increased sensitivity to DTT compared to the M18 parent. Growth sensitivities of M18 parent and TDOR mutant cultures *Δ2037, ΔahpC, Δ0982, Δ2138, Δ1572* to 0, 15, 20 mM DTT. Mean growth was measured by determining the OD_{600} after 18 h of incubation with indicated DTT concentrations. A representative experiment is shown from five total independent experiments performed. Error bars represent SD of triplicates. Asterisks indicate that a mutant TDOR value is statistically significantly different from the M18 wild-type parent (***$P \leq 0.001$, One-way ANOVA).

susceptible to ROS-driven phagocytic death (Figure 8A and B, $P \leq 0.05$). On the other hand, lysates from *Δ1572* mutant culture infection showed a survival similar to that of the parent M18 (Figure 8A and B). The same trends were seen in extracellular GAS counted from the supernatant 1 h and 18 h post-infection: *Δ2037* showed significantly lower survival while *Δ1572* showed negligible differences in CFUs compared to the parent (Figure 8C and D, $P \leq 0.01$). Growth curve analysis of the M18 parent and mutant *Δ2037* show nearly identical sigmoid curves (Figure 8E), therefore making it unlikely that differences in macrophage survival are due to bacterial growth defects introduced by TDOR gene interruption.

3.5 Redox state of exotoxin SpeA differs in GAS mutants

3.5.1 SpeA exotoxin is produced in all GAS mutants

Given that SpeA has 3 cysteines, 2 of which are involved in a disulfide bridge (Cys87 and Cys98), we investigated SpeA as a potential TDOR substrate (Papageorgiou et al., 1999; Roggiani et al., 1997). To test SpeA production in parent and TDOR mutant cultures, Western blot was done using anti-SpeA antibodies. The results indicate that not only does the M18 parent produce SpeA, but each of the 5 mutants also produces SpeA at similar levels (Figure 9A). Bands from *Δ2037, ΔahpC, Δ0982, Δ2138* and *Δ1572* are shown expressing SpeA at 25 kDa. The same samples were subjected to SDS-PAGE and Coomassie blue staining to assess equal protein loading in all lanes (Figure 9B). Despite showing no differences in SpeA production between parent and mutants, there is the possibility that SpeA could be misfolded and non-functional but still detectable by Western blotting.

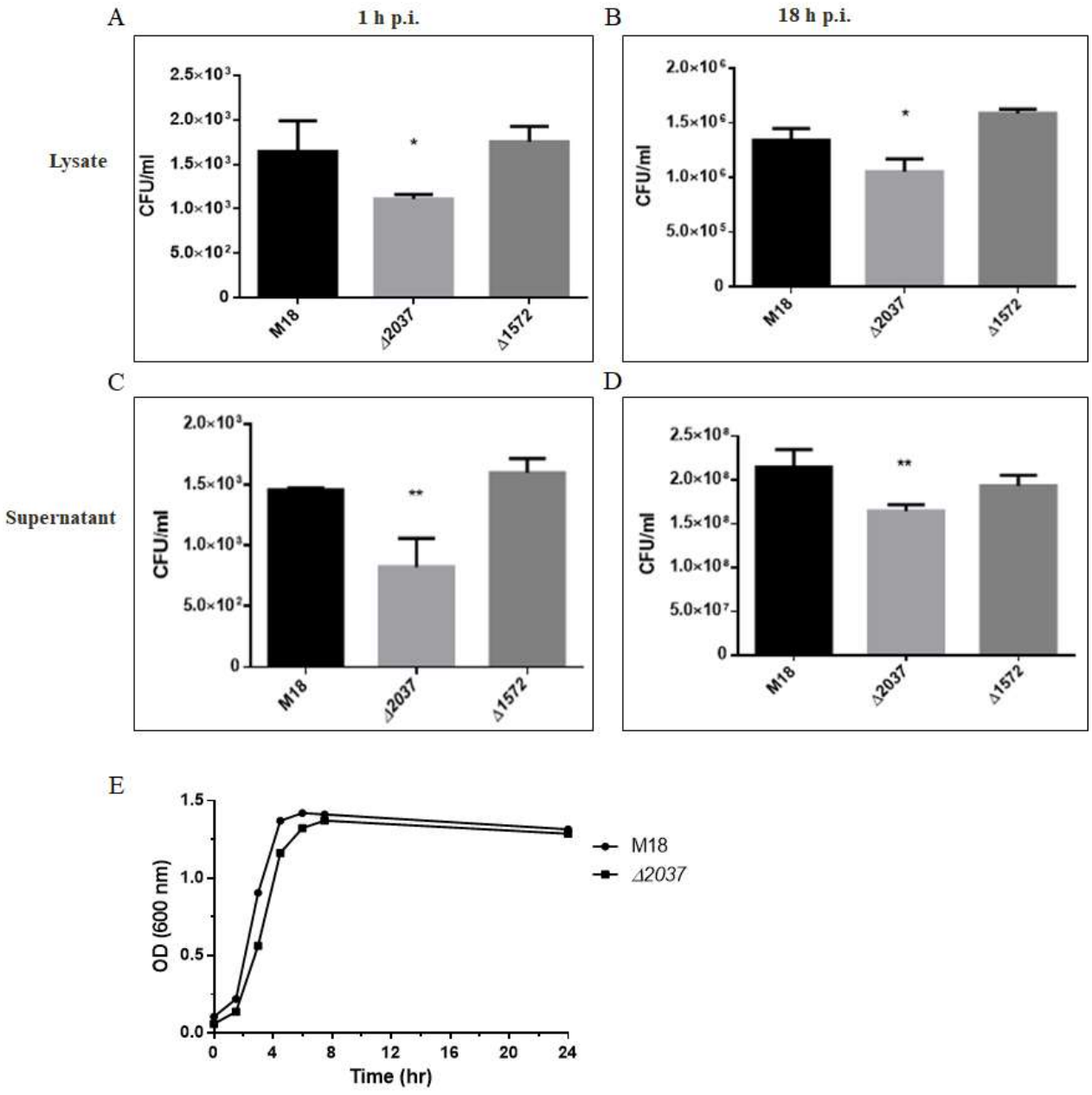
A
1 h p.i.
B
18 h p.i.
Lysate
CFU/ml
2.5×10³
2.0×10³
1.5×10³
1.0×10³
5.0×10²
0
2.0×10⁶
1.5×10⁶
1.0×10⁶
5.0×10⁵
*
M18
Δ2037
Δ1572
C
D
Supernatant
2.0×10³
1.5×10³
1.0×10³
5.0×10²
2.5×10⁸
2.0×10⁸
1.5×10⁸
1.0×10⁸
5.0×10⁷
**
E
OD (600 nm)
1.5
1.0
0.5
0.0
0
4
8
12
16
20
24
Time (hr)
M18
Δ2037

Figure 8: Mutant Δ2037 is more susceptible to phagocytic death by mouse macrophage cells. RAW 264 cells (2×10^5 cells/ml) in RPMI were seeded in a 24-well plates at 37°C, 5% CO_2 for 24 h, followed by infection with either M18 wild-type, *Δ2037* or *Δ1572* mutant *S. pyogenes* cultures. Infected RAW 264 cells were lysed after 1 h (A) and 18 h (B) time-points and the number of colony forming units (CFU) were determined. Supernatants were collected to enumerate the extracellular bacteria after 1 h (C) and 18 h (D). Survival was expressed as the mean number of CFUs per ml. (A-D) Error bars represent SD of triplicates. A representative experiment is shown from three independent experiments performed. Asterisks indicate a statistically significant difference compared to M18 parent (*$P \leq 0.05$; **$P \leq 0.01$; One-way ANOVA). (E) Growth curves of M18 parent and *Δ2037* strains. Error bars represent SD of triplicates.

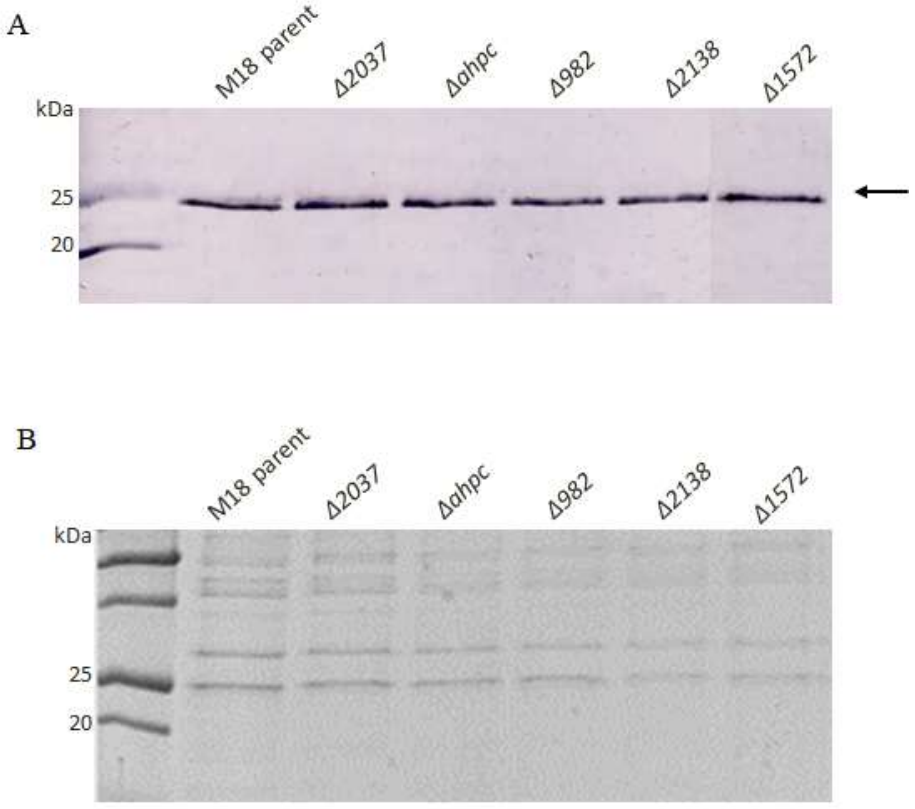

Figure 9: SpeA exotoxin is produced by all GAS M18 mutants. (A) Production of the 25 kDa SpeA protein (arrow) was detected by Western blotting in M18 parent and TDOR mutant *Δ2037, ΔahpC, Δ0982, Δ2138, Δ1572* strains using the anti-SpeA antibody. (B) SDS-PAGE of the same samples stained by Coomassie blue, showing equal loading.

3.5.2 The *in vivo* SpeA redox state differs in mutants

To determine the *in vivo* disulfide status of SpeA in the M18 parent and each TDOR mutant, cysteine alkylation experiments were carried out with maleimide-PEG_2-biotin (0.5 kDa). In this reaction, the maleimide moiety forms a covalent thioether bond with free cysteine thiols, resulting in a biotinylated protein that can be detected with avidin-alkaline phosphatase (avidin-AP). Disulfide bonded cysteines, on the other hand, are blocked from reacting with maleimide. Bands detected with avidin-AP that corresponded to SpeA were identified based on molecular weight (25 kDa). To ensure that the bands aligned, control experiments were carried out by cutting individual lanes of blots in half and reacting with either avidin-AP or anti-SpeA.

Alkylated protein extracts from the same sample were analyzed by Western blotting and reacted with either avidin-AP to detect biotinylated proteins or anti-SpeA. The latter allowed the determination of the total amount of SpeA in the sample, thus serving as a loading control. The results for the parent strain showed a weak band detected by avidin-AP at the same 25 kDa weight as the full length SpeA. However, when samples were reduced with DTT prior to alkylation, there was a marked increase in the intensity of this band, indicating the presence of a disulfide bond (Figure 10A). Quantification of band intensities by ImageJ are plotted in Figure 10B and the mean fold change between the DTT-treated and not treated samples is expressed in Figure 10C. Likewise, SpeA from *Δ0982* and *Δ1572* mutants also showed an increase in intensity with DTT reduction prior to alkylation similar to that of the parent (Figure 10A and B). In contrast, cysteines in SpeA from the *Δ2037, ΔahpC* and *Δ2138* mutant were efficiently alkylated both with and without DTT treatment, indicating the lack of a disulfide bond (Figure 10A and B). Analysis of mean fold changes in band intensities show *Δ2037, ΔahpC* and *Δ2138* mutants are significantly different compared to parent from three independent experiments

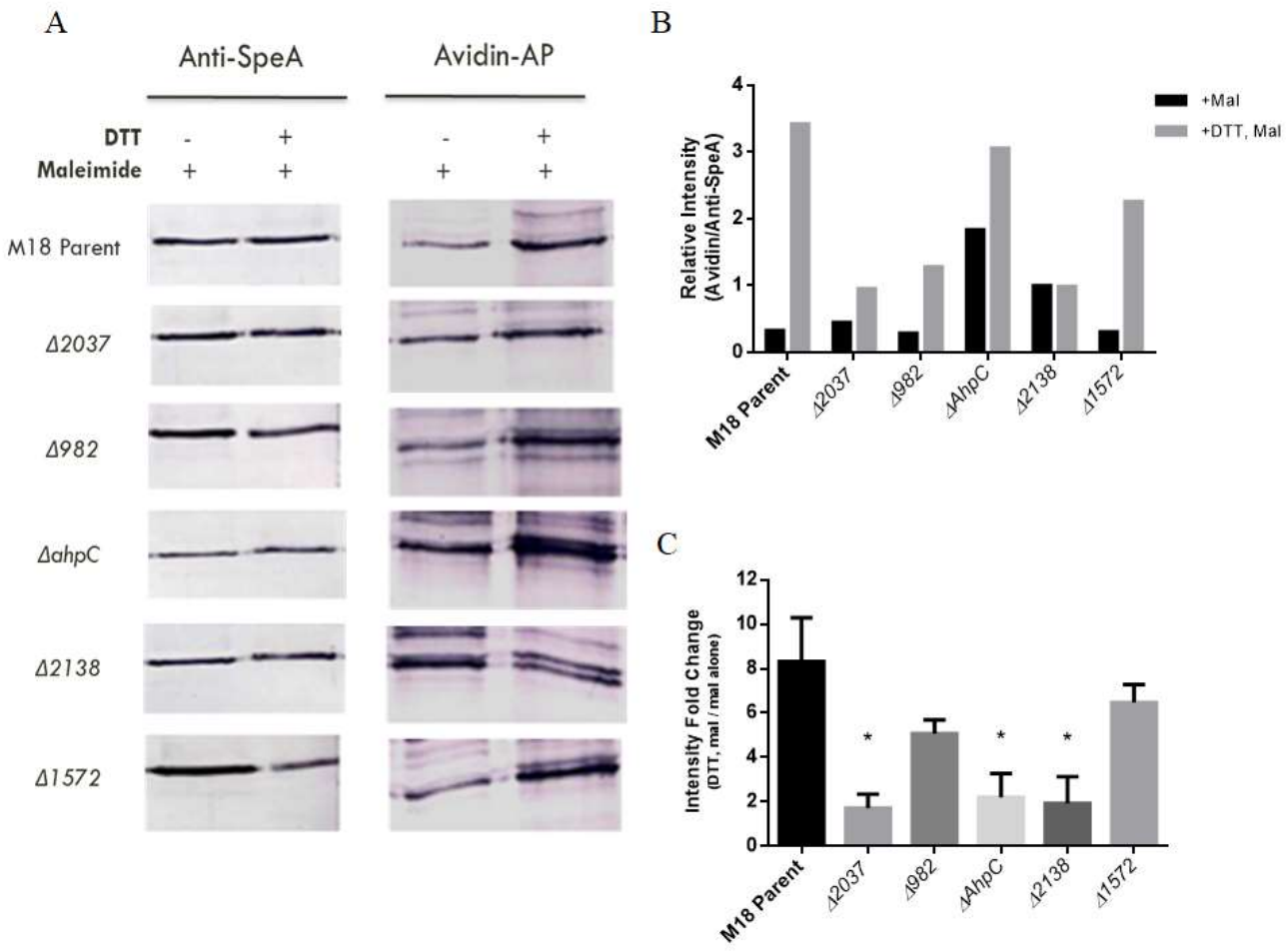
A
Anti-SpeA
Avidin-AP
DTT
Maleimide
M18 Parent
Δ2037
Δ982
ΔahpC
Δ2138
Δ1572
B
Relative Intensity (Avidin/Anti-SpeA)
+Mal
+DTT, Mal
M18 Parent
Δ2037
Δ982
ΔAhpC
Δ2138
Δ1572
C
Intensity Fold Change (DTT, mal / mal alone)
M18 Parent
Δ2037
Δ982
ΔAhpC
Δ2138
Δ1572

Figure 10: Redox state of exotoxin SpeA differs in GAS mutants *in vivo*. (A) Protein extracts from M18 parent and TDOR mutant *Δ2037, ΔahpC, Δ0982, Δ2138, Δ1572* strains were TCA precipitated and reacted with maleimide-PEG2-biotin (Mal). Following alkylation, proteins from a single sample were run in duplicate western blots and reacted with either avidin-AP to detect biotinylated proteins or with anti-SpeA antisera to detect the total SpeA concentration in the sample (loading control). Positive controls were prepared by reducing the samples with DTT prior to alkylation with maleimide. (B) Densitometry analysis of alkylation was carried out using Image J. The amount of alkylated SpeA was normalized by dividing the signal detected with avidin-AP by the signal detected with anti-SpeA. Results are given as relative intensity. Data is representative of three separate experiments. (C) Fold change of the SpeA bands between the DTT-treated and not treated samples. Fold change was calculated from the relative intensity shown in panel B and are means of three independent experiments with SD. Asterisks indicate a statistically significant difference compared to M18 parent strain (*$P \leq 0.05$, One-way ANOVA).

(Figure 10C, $P \leq 0.001$). The background bands present in avidin-AP lanes are a result of using crude bacterial samples with maleimide binding to other proteins containing free thiols. Together, our analyses suggested that the *in vivo* redox state of SpeA differs in certain TDOR mutants. Similar to the parent, SpeA produced by *Δ0982* and *Δ1572* mutants likely have an intact disulfide bond, while the *Δ2037, ΔahpC* and *Δ2138* mutants lacked disulfide bonds entirely.

3.6 Complementation of *2037* restores the *in vivo* redox state of SpeA

3.6.1 Successful generation of a 2037 complement strain

In light of the observed SpeA redox state differences, the contribution of 2037 was further pursued by constructing a 2037 complemented mutant strain. The entire 2037 reading frame was amplified, including predicted promoter and ribosomal-binding site sequences, and ligated to a kanamycin resistance gene. Figure 11A illustrates the PCR confirmed ~1.7 kb ligated fragment which was then cloned into pG^{+}host5. The complement plasmid was isolated from positive *E. coli* transformants that were kanamycin and erythromycin resistant (Figure 11B). Restriction digest using BamHI and EcoRI confirmed the isolated complement construct indeed contained the designed complement fragment, as seen in the ~1.7 kb drop down band (Figure 11B). Following electroporation of the construct into the *Δ2037* mutant, transformants were grown under both kanamycin and erythromycin selection at 30°C, then 40°C. Proper integration of the construct, and thus reintroduction of *2037* back into the genome, was confirmed using primers that bind to the 5' and 3' end of the whole gene (Figure 11C). The ~0.4 kb band corresponding to the 2037 whole gene was clearly seen in the M18 parent and complement strains, but not in the *Δ2037* mutant indicating successful complementation (Figure 11C).

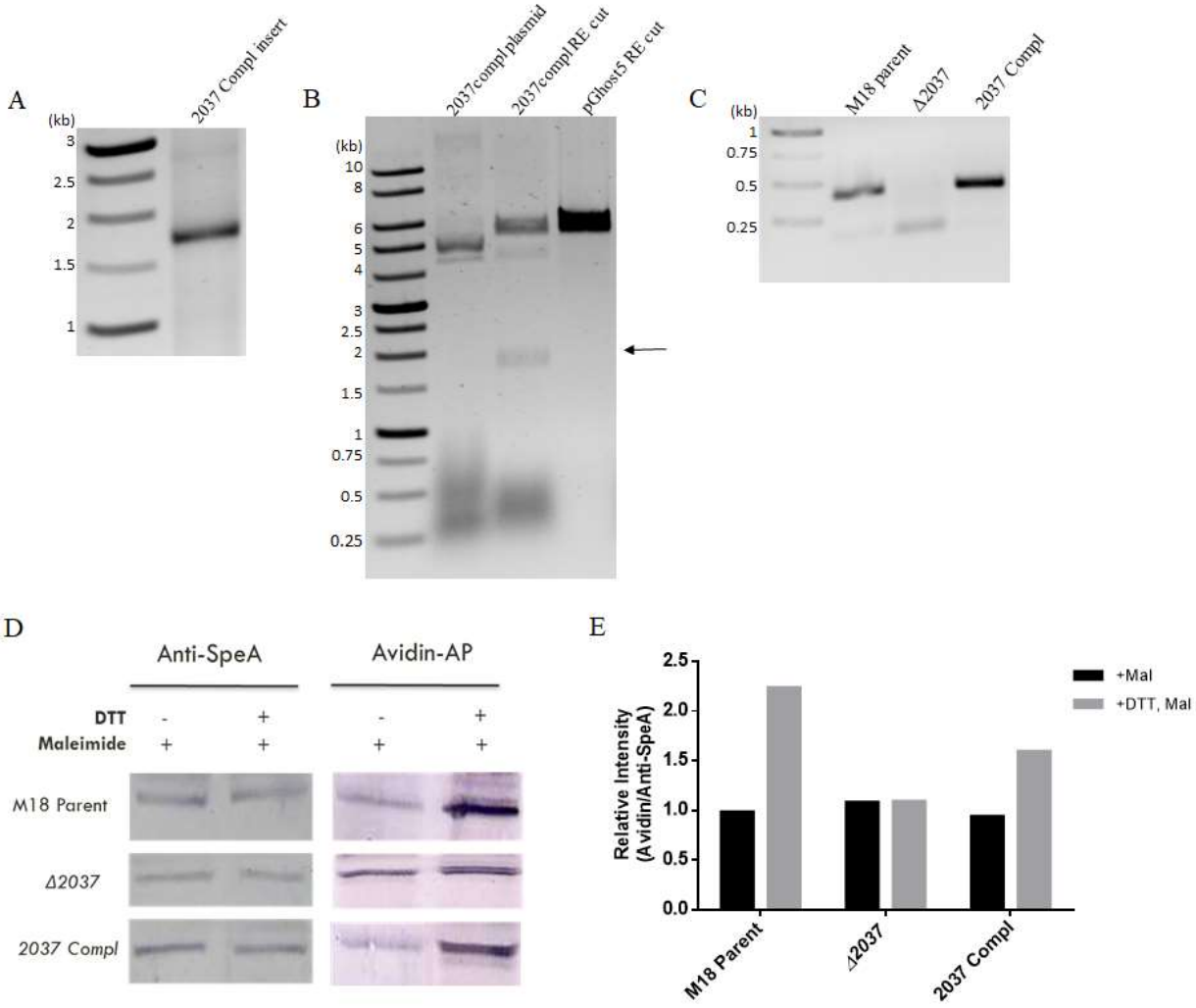
A
2037 Compl insert
(kb)
3
2.5
2
1.5
1
B
2037compl plasmid
2037compl RE cut
pGhost5 RE cut
(kb)
10
8
6
5
4
3
2.5
2
1.5
1
0.75
0.5
0.25
C
M18 parent
Δ2037
2037 Compl
(kb)
1
0.75
0.5
0.25
D
Anti-SpeA
Avidin-AP
DTT
Maleimide
M18 Parent
Δ2037
2037 Compl
E
Relative Intensity (Avidin/Anti-SpeA)
2.5
2.0
1.5
1.0
0.5
0.0
+Mal
+DTT, Mal
M18 Parent
Δ2037
2037 Compl

Figure 11: 2037 complementation restores the redox state of SpeA in *S. pyogenes*. (A) Agarose gel showing PCR constructed complement fragment. The entire 2037 reading frame, along with 300 bp of upstream DNA containing the predicted promoter and ribosomal-binding site sequences, was amplified and ligated to a kanamycin resistance cassette. The final combined amplification product band is seen at ~1.7 kb (*2037 compl insert*). Primers used are found in Table 3. (B) Agarose gel of the 2037 complement pG$^+$host5 plasmid isolated from kanamycin and erythromycin resistant *E. coli* transformants (*2037 compl plasmid*). Double digestion of the complement construct (*2037 compl RE cut*) or the pG$^+$host5 plasmid (*pGhost5 RE cut*) with BamHI and EcoRI. Arrow indicates the expected ~1.7 kb drop down band. (C) Agarose gel of PCR analysis of the 2037 complementation strain. Proper cross-over integration was verified using primers that bind to the 5' and 3' end of the whole gene. (D) Analysis of the redox sate of SpeA in M18 parent and mutant strains. Protein extracts from M18 parent, *Δ2037* mutant and 2037 complemented strain (*2037 compl*) were TCA precipitated and reacted with maleimide-PEG2-biotin (Mal). Following alkylation, proteins from a single sample were analyzed in Western blots reacted with either avidin-AP to detect biotinylated proteins or with anti-SpeA antisera to detect the total SpeA concentration in the sample (loading control). Positive controls were prepared by reducing the samples with DTT prior to alkylation with maleimide. (E) Densitometry analysis of alkylation was carried out using Image J. The amount of alkylated SpeA was normalized by dividing the signal detected with avidin-AP by the signal detected with anti-SpeA. Results are given as relative intensity. Data is preliminary and repeated experiments are necessary.

3.6.2 2037-complementation restores SpeA to the oxidized state

The *in vivo* disulfide statuses of SpeA in the M18 parent, the *Δ2037* mutant and the 2037-complemented mutant were examined by alkylation. Importantly, the 2037 complemented mutant showed an increase in band intensity with DTT reduction prior to alkylation, matching the M18 parent phenotype as displayed in the avidin-AP blot (Figure 11D). This is indicative of a disulfide bond present in SpeA from both the parent and 2037-complemented strains. Whereas cysteines in SpeA from the *Δ2037* mutant were efficiently alkylated both with and without DTT treatment, showing no difference in band intensity, the 2037-complemented mutant reverses this phenotype. Quantification of band intensities by ImageJ are plotted in Figure 11E. These results further reinforce the notion that 2037 plays a direct role in affecting the redox state of SpeA.

3.7 The 2037 enzyme is needed for proper disulfide bond formation in SpeA

3.7.1 Purified 2037 exhibits oxidase activity

We next sought to characterize the functional properties of the 2037 protein. The oxidase activity of r2037 was tested *in vitro* using the RNase A refolding assay. Recombinant 2037 was expressed in *E. coli* and purified by affinity chromatography (Figure 12A). r2037 was incubated with reduced and denatured RNase A and the oxidative folding of RNase A to its active conformation was monitored by cCMP hydrolysis. Based on mean A_{296} values, r2037 successfully catalyzed the correct folding of reduced, denatured RNase A (Figure 12B). Recombinant *S. gordonii* SdbA was included as a positive control since it is known to exhibit oxidase activity (Davey et al. 2013).

The reductase activity of r2037 was tested *in vitro* through an insulin disulfide reduction turbidimetric assay. Reduced 2037 was incubated with insulin and any precipitation of insulin

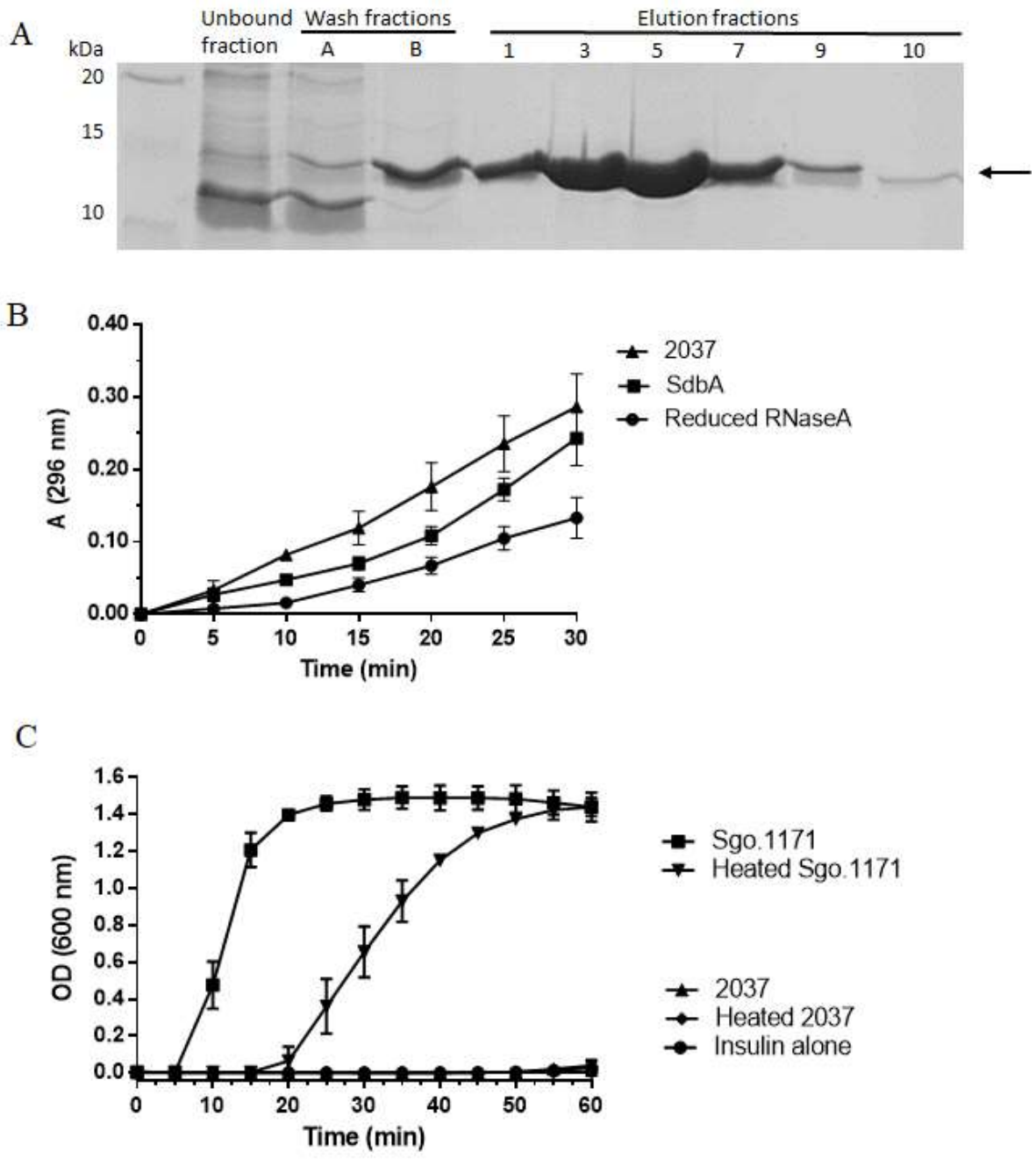
A
kDa
20
15
10
Unbound fraction
Wash fractions
A
B
Elution fractions
1
3
5
7
9
10
B
A (296 nm)
0.40
0.30
0.20
0.10
0.00
0
5
10
15
20
25
30
Time (min)
2037
SdbA
Reduced RNaseA
C
OD (600 nm)
1.6
1.4
1.2
1.0
0.8
0.6
0.4
0.2
0.0
0
10
20
30
40
50
60
Time (min)
Sgo.1171
Heated Sgo.1171
2037
Heated 2037
Insulin alone

Figure 12: Purified 2037 protein exhibits oxidase activity but lacks reductase activity. (A) SDS-PAGE of recombinant 2037 purified from *E. coli* by nickel affinity chromatography (arrow, ~14 kDa). (B) Oxidative folding of reduced, denatured RNase A by the recombinant (r) 2037 and SdbA proteins. r2037 (10 μM) was incubated with reduced RNase A (10 μM) and the cleavage of cCMP was monitored at A_{296}. rSdbA (10 μM) was used as a positive control and reduced RNase A without added enzyme was used as a negative control. Data show the average from three experiments, error bars represent the standard error. (C) Reductase activity of recombinant 2037 and 1171 proteins in an insulin turbidimetric assay. Reduced 2037 (10 μM) was incubated with insulin (10 μM) and any precipitation of insulin caused by reduction was measured at OD_{600}. *S. gordonii* 1171 (10 μM) was used as a positive control. Insulin without added enzyme was used as a negative control along with heat-inactive 2037 and 1171. Data show the average from three experiments, error bars represent the standard error.

caused by reduction was measured. Based on mean OD values, 2037 did not catalyse the precipitation of insulin, showing similar reactivity to the heat-inactivated 2037 tube and insulin alone negative control tube (Figure 12C). Recombinant *S. gordonii* 1171 protein was included as a control since it is known to exhibit reductase activity (Jalal et al., unpublished). The heat-inactive 1171 reaction tube displayed delayed reductase activity. Taken together, these results indicate that 2037 is an oxidoreductase, which is directly involved in the formation of disulfide-bonded proteins in GAS.

3.7.2 Recombinant 2037 oxidizes reduced SpeA *in vitro*

In light of the SpeA redox state differences in mutant *Δ2037 in vivo* and the finding that r2037 has oxidase activity, we investigated the disulfide status of rSpeA in the presence of r2037 under *in vitro* conditions. A disulfide exchange reaction was conducted by combining DTT-reduced rSpeA with glutathione-oxidized r2037 at equimolar concentrations for 30 min and 1 h time points. Sample proteins were precipitated, alkylated with maleimide and analyzed by western blotting with either avidin-AP to detect biotinylated proteins (Figure 13B and D), or anti-SpeA to determine the total SpeA sample amount (Figure 13A and C; loading controls). The reduced and alkylated SpeA control lane showed a strong intensity band detected by avidin-AP with a visible lower doublet banding pattern, while the oxidized and alkylated SpeA control lane showed a much weaker intensity single band indicating the presence of an intact disulfide bond (Figure 13B). Interestingly, rSpeA changes from its initial reduced form to an oxidized form following 30 min incubation with oxidized r2037 (Figure 13B). The rSpeA remained oxidized after 1 hr in reaction with 2037.

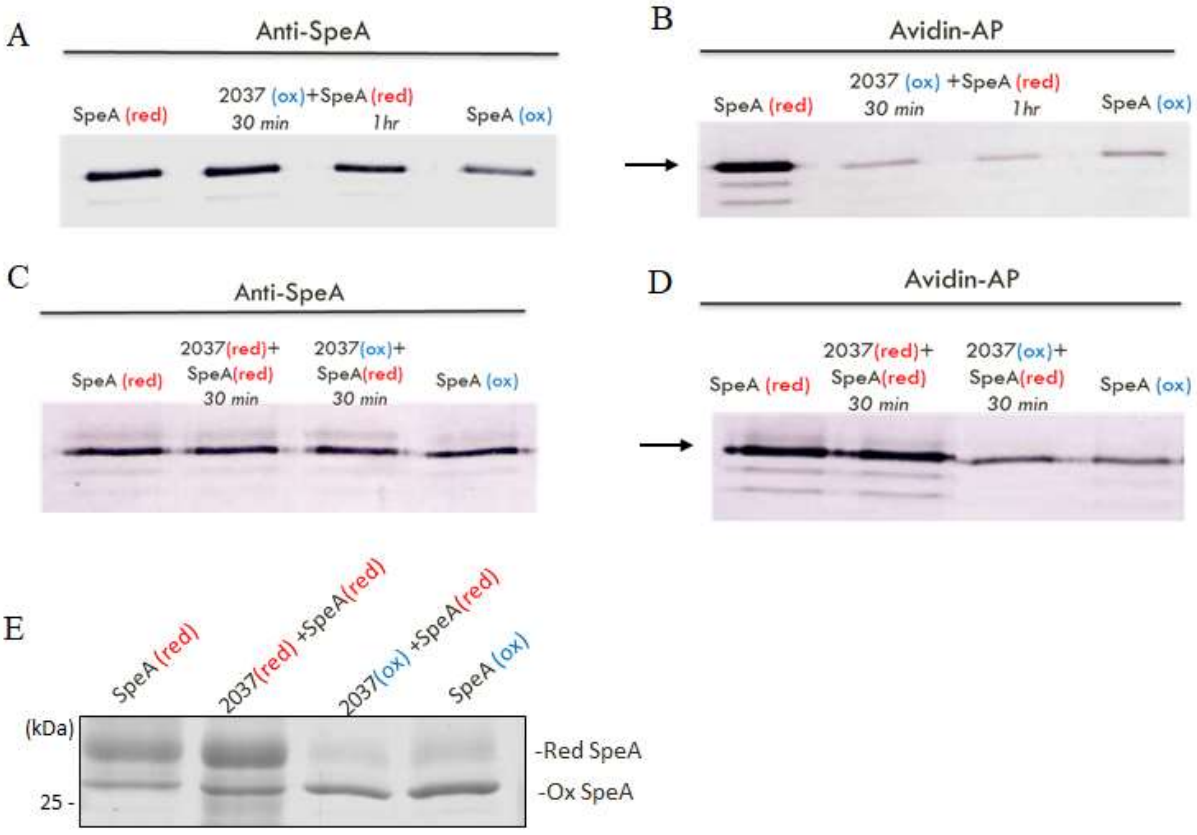
A
Anti-SpeA
SpeA (red)
2037 (ox)+SpeA (red)
30 min
1hr
SpeA (ox)
B
Avidin-AP
SpeA (red)
2037 (ox) +SpeA (red)
30 min
1hr
SpeA (ox)
C
Anti-SpeA
SpeA (red)
2037(red)+ SpeA(red)
30 min
2037(ox)+ SpeA(red)
30 min
SpeA (ox)
D
Avidin-AP
SpeA (red)
2037(red)+ SpeA(red)
30 min
2037(ox)+ SpeA(red)
30 min
SpeA (ox)
E
SpeA (red)
2037(red) +SpeA(red)
2037(ox) +SpeA(red)
SpeA (ox)
(kDa)
25 -
-Red SpeA
-Ox SpeA

Figure 13: rSpeA becomes oxidized in the presence of recombinant 2037. (A, B) Western blot visualization of the disulfide status of rSpeA after incubation with equal molar (10 μM) of oxidized r2037 for 30 min and 1 h. Following TCA precipitation and alkylation with maleimide-PEG2-biotin (mal, 0.5kDa moiety), proteins from a single sample were run in duplicate lanes and reacted with either avidin-AP (B) to detect biotinylated proteins (arrow) or with anti-SpeA antisera (A) to detect the total amount of SpeA in the sample (loading control). (C, D) Western blot of the disulfide status of reduced rSpeA (10 μM, arrow) reacted with either oxidized or reduced r2037 (10 μM) for 30 min. Control lanes containing alkylated reduced and oxidized recombinant SpeA alone are included. Data is representative of three separate experiments. (E) SDS-PAGE of disulfide exchange reaction samples stained by Commassie blue. Following TCA precipitation, protein samples were alkylation with a larger 2 kDa maleimide-PEG2-biotin moiety to observe a shift in band migration. The top bands shows fully reduced and alkylated SpeA at a molecular weight above 25 kDa (*Red SpeA*). The lower bands indicate oxidized and alkylated SpeA at a molecular weight close to 25 kDa (*Ox SpeA*).

To confirm the re-oxidation of reduced rSpeA was due to the activity of r2037 in its oxidized form, a similar disulfide exchange reaction was conducted by combining reduced rSpeA with reduced r2037 at equimolar concentrations for 30 min. Detection by avidin-AP revealed SpeA remained in its reduced state after incubation with reduced 2037, showing the same strong band intensity pattern as the control lane reduced SpeA (Figure 13D). This supports the notion that r2037 must be in its functional oxidized form in order to alter the redox state of SpeA.

Up to this point, differences in SpeA redox state have been determined based on changes in normalized intensity between alkylated protein samples and not based on band migration shifts, which is typically reported in the literature for these types of experiments. In order to corroborate these data, a larger maleimide compound (2 kDa) was used in the same disulfide exchange experiment. SpeA contains 3 cysteines and alkylation with the larger maleimide will add a 2 kDa weight shift to each free thiol group available, leading to visible differences in migration distances on SDS-PAGE. Indeed, upon reaction with reduced 2037, SpeA remained reduced as highlighted in the upper band showing a slower migration (Figure 13E). Upon reaction with oxidized 2037, SpeA becomes oxidized, blocking the maleimide from binding, as highlighted in the faster migrating bands (Figure 13E). This is in line with previous findings based on intensity differences. Control lanes containing reduced and oxidized 2037 alone also display the expected molecular weight shifts upon maleimide treatment. Extra bands visible likely represent incomplete alkylation of a small fraction of proteins, while lane smudges are likely due to the non-specificity of this particular maleimide compound.

Taken together, r2037 and rSpeA appear to act as an enzyme-substrate pair, facilitating an exchange of electrons. In its functional oxidized form, r2037 reforms the disulfide bond in reduced rSpeA *in vitro*.

3.8 Exploring mechanisms of 2037-SpeA interaction by generation of 2037 cysteine point mutants

3.8.1 Successful generation of single-cysteine point mutants in 2037 active site

To better understand the mechanisms of interaction between 2037 and SpeA, single cysteine mutants were generated at the 2037 active site. Since the 2037 enzyme contains the characteristic CXXC catalytic motif, a cysteine (TGT) to alanine mutation (GCT) at position 46 (2037_{C46A}) and position 49 (2037_{C49A}) were created. Final products from overlapping PCR showed distinct sharp bands at the expected fragment size of ~0.4 kb for both cysteine mutants (Figure 14A). These PCR products were individually ligated into a pQE-30 plasmid backbone and transformed in *E. coli*. Positive colonies containing the correct point mutant plasmid constructs were confirmed by colony PCR (Figure 14B). Expression and purification of His6-tagged *r*2037_{C46A} and *r*2037_{C49A} was done through subsequent nickel affinity chromatography. In addition, cysteine point mutations were confirmed by DNA sequencing (Appendix A).

3.8.2 Active site 2037 cysteine mutants show different protein complex formation profiles with SpeA

The generation of these recombinant cysteine variants will allow valuable comparisons between native 2037 and point mutant 2037 interactions with SpeA. Since the point mutants are

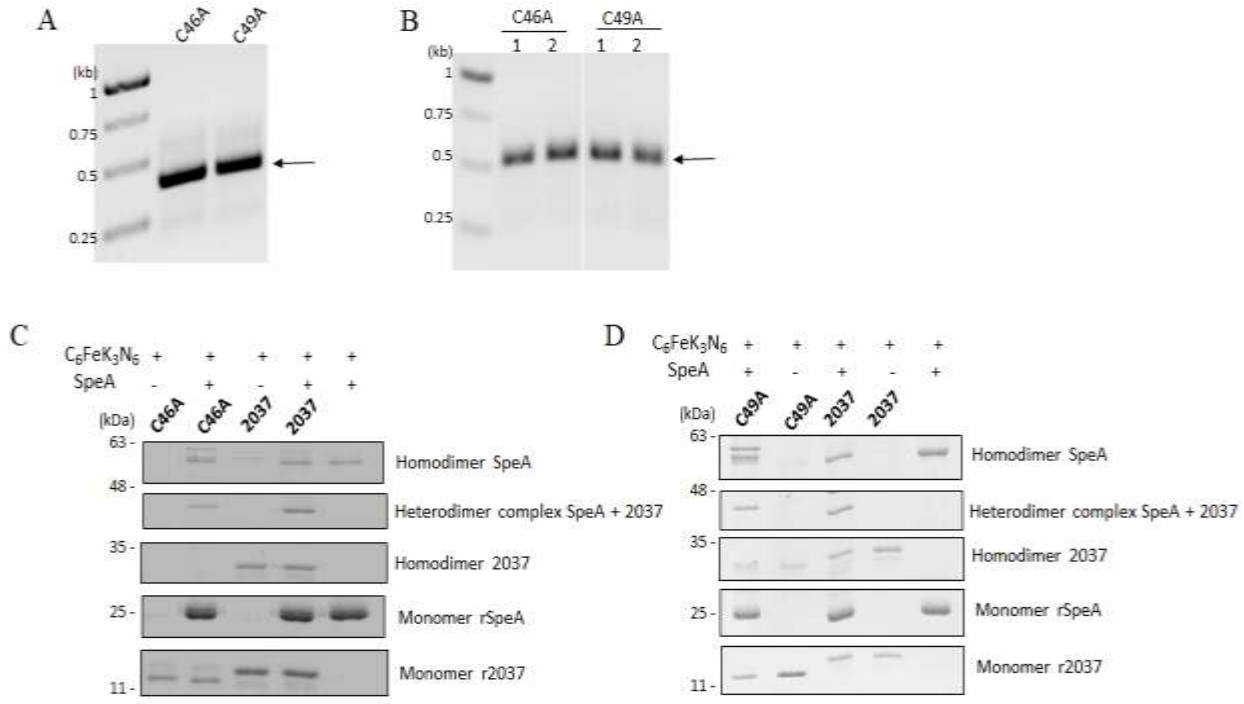

Figure 14: Successfully generated single-cysteine point mutants in 2037 active site may affect complex formation with SpeA. (A) DNA agarose gel showing overlapping PCR products of 2037_{C46A} and 2037_{C49A} point mutants at the expected fragment size of ~0.4 kb (arrow). (B) Agarose gel showing positive *E. coli* transformants containing the 2037_{C46A} - and 2037_{C49A} - pQE-30 plasmid constructs (arrow). Primers used for screening are listed in Table 3. Both cysteine point mutations were further confirmed by DNA sequencing (Appendix A). (C, D) SDS-PAGE analysis of protein complex formation between 2037 and SpeA. Reduced rSpeA was reacted with either native 2037, 2037_{C46A} or 2037_{C49A} in the presence of 5 mM potassium ferricyanide. Under reducing conditions, 2037 runs at 14 kDa and SpeA runs at 25 kDa.

within the 2037 active site, any differences in the ability to form disulfide linked complexes with their substrates can be attributed to the importance of these catalytic cysteine residues. Investigation of heterodimer complex formation between 2037 and SpeA was done through an *in vitro* reaction that combined DTT-reduced rSpeA with either reduced r2037 (wild-type), $r2037_{C46A}$ or $r2037_{C49A}$ at equimolar concentrations in the presence of 5 mM potassium ferricyanide for 1 h. Potassium ferricyanide oxidizes thiol groups, making cysteine residues highly reactive (Wiberg, Maltz, & Okano, 1968). Protein complexes were analyzed by SDS-PAGE under non-reducing conditions and stained with Coomassie blue.

Results from preliminary experiments showed a ~40 kDa band, likely signifying a heterodimer complex between wild-type r2037 (14 kDa) and rSpeA (25 kDa) (Figure 14C). In contrast, a weaker ~40 kDa band was detected in the reaction between $r2037_{C46A}$ and rSpeA. The gel also showed a ~50 kDa band, likely representing the formation of a SpeA homodimer complex during the reaction between wildtype 2037/SpeA (Figure 14C). The same ~50 kDa band was detected in the reaction between 2037_{C46A}/SpeA. Notably, a ~28 kDa band which likely represents the formation of a 2037 homodimer complex was observed in the wild-type 2037/SpeA reaction lane but not in the 2037_{C46A}/SpeA reaction (Figure 14C). A ~25 kDa band representing the SpeA monomer was found in the reaction between 2037/SpeA and 2037_{C46A}/SpeA (Figure 14C). A ~14 kDa band representing the 2037 monomer was found in the reaction between 2037/SpeA and 2037_{C46A}/SpeA (Figure 14C). Control lanes containing either wildtype 2037 alone or 2037_{C46A} alone in the presence of potassium ferricyanide are shown side-by-side. A final control lane containing only SpeA in the presence of potassium ferricyanide is also given.

Similarly, results from preliminary experiments showed the ~40 kDa heterodimer band present in both 2037/SpeA and 2037_{C49A}/SpeA reaction lanes at equal intensities (Figure 14D). The ~50 kDa band representing a SpeA homodimer complex was found in reactions between both 2037/SpeA and 2037_{C49A}/SpeA. Notably, the ~28 kDa band signifying a 2037 homodimer complex was visible in the wildtype 2037/SpeA reaction lane but was only weakly detected in the 2037_{C49A}/SpeA lane (Figure 14D). The ~25 kDa SpeA monomer band was found in reactions between both 2037/SpeA and 2037_{C49A}/SpeA. The ~14 kDa 2037 monomer band was found in reactions between both 2037/SpeA and 2037_{C49A}/SpeA. Control lanes containing either wildtype 2037 alone, 2037_{C46A} alone or SpeA alone in the presence of potassium ferricyanide are also included.

Taken together, disulfide linked complex interactions formed between 2037_{C46A}/SpeA and 2037_{C49A}/SpeA differ compared to parent 2037/SpeA *in vitro*. Of the two active site cysteines, the C46A point mutant had a more contrasting protein profile, showing a weaker intensity ~40 kDa heterodimer band and a missing ~28 kDa band representing 2037 homodimer complex formation. This suggests that the active site 2037 cysteines 46 and 49 may have different reactivates, with the N-terminal cys46 playing a leading role during protein complex formation with SpeA.

CHAPTER 4: Discussion

4.1 Major Findings

Group A *Streptococcus* is an important pathogenic bacterium that strictly infects humans, causing a diverse range of diseases from mild mucosal (pharyngitis) and skin (impetigo) infection, to severe invasive (necrotizing fasciitis) and toxin mediated (toxic shock syndrome) diseases along with non-pyogenic complications (acute rheumatic fever). While there have been exciting advances in GAS virulence factor regulation coupled with massive sequencing efforts to isolate genomes, there are still many questions surrounding the molecular mechanisms of virulence factor production and their role in GAS host-pathogen interactions.

There is evidence that some GAS virulence proteins, including potent superantigenic toxins such as SpeA, are held together by structural disulfide bonds, which are essential for protein stability and activity (Papageorgiou et al., 1999; Roggiani et al., 1997). Disulfide bond formation pathways have not been studied directly in the context of GAS pathogenesis. This lack of knowledge stems from the under-characterized processes of disulfide bond formation in Gram-positive bacteria in general, compared to its Gram-negative counterpart. Gram-positive species tend to make fewer disulfide bonded proteins and sometimes use covalent amide bonds as an alternative (Budzik et al., 2009). Nevertheless, *S. gordonii* SdbA was found to form disulfide bonds in a natural autolysin substrate, with SdbA mutants defective in many physiological processes (Davey et al., 2013); and *C. diphtheriae* MdbA was found to affect disulfide bond formation in diphtheria toxin, with MdbA mutants exhibiting morphological defects and attenuated virulence (Reardon-Robinson et al., 2015).

Along the same lines, a TDOR-mediated pathway in GAS is likewise essential for virulence factor production based on the experimental data presented. An *in silico* approach

coupled with BLASTP analysis identified 5 candidate TDORs in the M18 *S. pyogenes* MGAS823 strain: SpyM18_2037, SpyM18_AhpC, SpyM18_0982, SpyM18_2138 and SpyM18_1572 (Table 5). The same approach identified potential TDOR substrates with more than 2 cysteine residues (Table 6), and this list was used as a guideline with the goal of studying TDOR function in phenotypic assays.

4.1.1 The functions of SpyM18_0982 and SpyM18_1572 remain largely unknown

Two of the predicted TDORs, SpyM18_0982 and SpyM18_1572, exhibited the fewest phenotypic differences in the assays tested. SpyM18_0982 is annotated as a putative oxidoreductase with 3 cysteines but does not have a distinct catalytic CXXC motif. SpyM18_1572 is annotated as a hypothetical protein containing a TlpA-like domain and a catalytic Cys-S-I-Cys motif. The TlpA/ResA/DsbE family of proteins diversely encompasses bacterial disulfide reductases with important roles in cytochrome maturation (Cho & Collet, 2013) and other membrane-associated proteins capable of catalyzing disulfide bonds (Chim et al., 2013). In *S. pneumoniae* for example, TlpA is proposed to work in conjunction with MsrAB and CcdA to reduce oxidized methionines (Andisi et al., 2012). Notably, SpyM18_1572 is located immediately upstream of a protein annotated as a methionine sulfoxide reductase (SpyM18_1571) and located downstream is a cytochrome *c* biogenesis protein CcdA (SpyM18_1573).

Our results show that mutant *Δ0982* displayed increased sensitivity to penicillin G at 2.5 and 0.625 μg/ml concentrations while *Δ1572* was more tolerant to penicillin G at 0.625 μg/ml (Figure 4B) compared to parent. Mechanistically, penicillin inhibits the last steps of peptidoglycan synthesis by binding to high-molecular-weight PBPs (Ferretti et al., 2016). This suggests that our candidate TDORs are somehow involved in the multifaceted regulation of cell

wall metabolism in response to β-lactam antibiotics, resulting in either cell tolerance or cell death (Chaussee, McDowell, Rieck, Callegari, & Chaussee, 2006). Penicillin-mediated killing leads to widespread proteome changes in GAS according to Chaussee et al. (2006), with transcriptional regulators such as Rgg being important for influencing membrane stress responses. It is reasonable to assume that our putative TDORs play a part in these systems and were not identified in our assays.

Increased sensitivity to 0.5 mM and 1 mM paraquat concentrations were seen for both *Δ0982* and *Δ1572* (Figure 6A). This is consistent with SpyM18_1572 as a possible reductase under paraquat-induced intracellular oxidative stress conditions; however, the survival of *Δ1572* was no different in RAW 264 macrophage cell infection experiments compared to parent (Figure 8). Further investigation of *Δ1572* should focus on possible defects in reducing methionine sulfoxide in a reducing pathway similar to that of *S. pneumoniae*. These types of TDORs likely perform unidentified specialized functions within the cell or exhibit functional redundancy that would require multiple mutations to produce observable phenotypes.

4.1.2 The functions of SpyM18_Ahpc and SpyM18_2138 may be closely associated

SpyM18_AhpC is an alkyl hydroperoxidase containing 3 cysteine residues that has been the subject of previous publications. According to King et al. (2000), *ahpC* mutants of *S. pyogenes* HSC5 and JRS4 strains did not demonstrate any increased sensitivity to H_2O_2 when analyzed both by a disk diffusion assay and by determination of minimum inhibitory concentrations (MIC assay); however, *ahpC* mutants did demonstrate increased sensitivity to certain forms of extreme oxidative stress, specifically when cultured in the presence of paraquat. A concentration of 5 mM paraquat had no impact on the growth of the wild-type strains but greatly impaired *ahpC* mutant growth (King et al., 2000). Consistent with this, our results show

that *S. pyogenes* MGAS823 *ΔahpC* is highly sensitive to 1 mM paraquat, but was not sensitive to H_2O_2 in disk diffusion assays (Figure 6). This apparent contradiction may be due to the fact that the continuous production of superoxide-mediated stress by paraquat can result in increased concentrations of H_2O_2 in the culture medium and other reactive by-product species from reaction of H_2O_2 with substrates; whereas exogenously added hydrogen peroxide is reduced over time (King et al., 2000). The capsule of GAS has also been reported to contribute to resistance against H_2O_2 (Henningham et al., 2015). Due to the large amount of capsule produced by the mucoid M18 serotype, this could mask any TDOR-specific phenotype since capsule-mediated aggregation is thought to mechanically shield GAS from destruction by oxygen metabolites like H_2O_2 (Cleary & Larkin, 1979).

SpyM18_2138 is similarly annotated as a putative NADH oxidase/alkyl hydroperoxidase reductase, containing two CXXC motifs and an alkyl hydroperoxide reductase subunit F region (ahpF). Of particular interest is that *2138* is the immediate downstream gene of *ahpC* (*SpyM18_2137*) in the M18 GAS genome. These two genes share high sequence homology with *Salmonella typhimurium* genes encoding AhpC and AhpF. In *S. typhimurium*, AhpC and AhpF together form an alkyl hydroperoxidase system that undergoes a series of electron transfers: AhpC is the peroxide-reducing player that acts as a scavenger of endogenous H_2O_2 in bacteria while AhpF is a separate disulfide reductase protein that regenerates AhpC every catalytic cycle via electrons from NADH (Jönsson, Ellis, & Poole, 2007). Similar to *ΔahpC*, our results indicate that *Δ2138* is hyper-sensitive to 1 mM paraquat, but was not sensitive to H_2O_2 compared to parent (Figure 6). It is very possible that the role of 2138 is coupled with that of AhpC in GAS resistance to oxidative stress, given its closely associated features. It would be interesting to study the effects of a *ΔahpCΔ2138* double mutant created in *S. pyogenes* on resistance to

peroxides. Further investigation is inevitably needed to be better characterize this possible AhpC-AhpF system in GAS and its larger role in the bigger picture of oxidative stress resistance during pathogenic infections.

Both *ΔahpC* and *Δ2138* mutants also showed greater sensitivity to 2.5, 1.25 and 0.625 μg/ml of penicillin G (Figure 4B) and a different SpeA redox state compared to the parent (Figure 10). This suggests that AhpC and 2138 have roles in the cell that may extend beyond resistance to peroxides. It is also possible that 2138 reduces AhpC but affects other protein substrates not yet identified either directly or indirectly.

4.1.3 SpyM18_2037 displays a pleiotropic mutant phenotype

Of the 5 candidate TDORs, SpyM18_2037 exhibited the most prominent phenotypic differences in assays compared to parent, suggesting an important biological function and possible broad substrate specificity. Despite the annotation as a bacteriocin transport accessory protein, 2037 did not affect bacteriocin production in the deferred antagonism assay (Figure 3B). However, the *in vitro* conditions were not ideally suited to study bacteriocin production since even the parent showed no detectable bacteriocins. The inability of M18 GAS to produce bacteriocin *in vitro* has also been reported by Armstrong et al. (2016), who demonstrate that the promoter-driven expression of Class IIb bacteriocins was only successfully induced *in vivo* using an acute nasopharyngeal murine infection model. This therefore highlights the importance of studying GAS bacteriocin gene regulation within appropriate environments. In Gram-positive species, there are several examples of TDOR systems in the literature dedicated to bacteriocin production, including *B. subtilis* 168 BdbAB, and *Streptococcus bovis* HJ50 Sdb1 (Dorenbos et al., 2002; Liu et al., 2009). It is still very possible that 2037 affects production or activity of an unidentified bacteriocin, and one which inhibits bacteria not tested in our assay.

The *Δ2037* mutant showed increased sensitivity to 2.5, 1.25 and 0.625 μg/ml of penicillin G similar to *ΔahpC* and *Δ2138* (Figure 4B). *Δ2037* was the only mutant that displayed increased sensitivity to DTT (Figure 7), suggesting that 2037 may be involved in proper disulfide bond formation of protein substrates needed in growth and cell-wall biosynthesis in a mechanism that is unclear. GAS lacking 2037 appear to display a pleiotropic phenotype resembling that of *S. gordonii* SdbA mutants (Davey et al., 2013). Mutation of *sdbA* was found to trigger upregulation of the CiaRH two-component signaling system involved in cell wall homeostasis in *S. gordonii*, leading to repression of the ComDE quorum sensing system that regulates bacteriocin production (Davey, Halperin, et al., 2016). As well, the ComDE system alone affects expression of over 150 genes and alteration of CiaRH activity is expected to have profound effects on the cell globally (Davey, Halperin, et al., 2016). It is reasonable to believe that 2037 could have a similar global effect on GAS by altering a known or unknown regulatory signaling system.

Of note, all TDOR mutants showed no defects in capsule production and autolysis compared to parent (Figure 5), which was unexpected if a role for maintaining cell wall integrity is proposed. Further investigations are warranted to better understand the basis for many of these phenotypes and their contribution to GAS virulence.

4.1.4 2037 plays a role in resistance to oxidative stress damage

Our findings suggest that 2037 plays a role in GAS resistance to oxidative stress since *Δ2037* was highly sensitive to both 0.5 mM and 1 mM paraquat concentrations (Figure 6A). As well, RAW 264 murine macrophages infected with mutant *Δ2037* showed significantly reduced intracellular survival, suggesting *Δ2037* is more susceptible to ROS-driven phagocytic death (Figure 8). The same trend was seen in extracellular GAS counted from the supernatant 1 h and 18 h post-infection with *Δ2037* showing significantly lower survival (Figure 8). *Δ2037* was not

sensitive to H_2O_2 in disk diffusion assays; however, this matches the phenotype already seen in all other mutants, including *ΔahpC* and *Δ2138* which are annotated peroxidases (Figure 6B). This may speak to possible limitations and inaccuracies of the H_2O_2 disk diffusion agar assay itself, given that it is qualitative in nature. A supporting MIC assay can be done to confirm these findings.

The GAS antioxidant system is complex and our assays have not addressed these pathways in depth. Findings published by King, et al. (2000) revealed that a *ahpC gpoA* double mutant created was even more sensitive to paraquat than the respective single mutants but neither AhpC or GpoA peroxidases were required for normal growth under aerobic conditions, emphasizing that alternative antioxidant pathways/strategies with multiple redundancies exist. Different mechanisms of resistance may be involved in GAS protection from different levels of stress. In *E. coli* for example, peroxide killing is bimodal and tailored to the degree of stress or concentration level of peroxide exposure (Imlay & Linn, 1986). Low-level H_2O_2 exposure leads to DNA damage, while high levels of H_2O_2 directly oxidize many cellular targets (Imlay & Linn, 1986). Damage to different constituents would likely require different types of repair and/or resistance mechanisms (Imlay & Linn, 1986; King et al., 2000).

At this stage, our data points to 2037 as being one of potentially many required components of a GAS cell defense system. To counter oxidative stress at the cell envelope *S. pneumoniae* uses an extracellular methionine sulfoxide reductase (MsrAB2), since ROS-induced oxidation of methionine to methionine sulfoxide can damage proteins (Saleh et al., 2013). The *S. pneumoniae* reducing pathway involves electrons being passed from the cytoplasm → CcdA proteins → extracellular TDORs Etrx1 and Etrx2 → MsrAB2 which then reduces methionine sulfoxide thus repairing the damage (Saleh et al., 2013). It is possible that a similar system

involving 2037 exists where electrons are passed from a cytoplasmic thioredoxin system → an uncharacterized integral protein such as CcdA → 2037, which then reduces downstream substrates. However, this is directly contradicted by the fact that 2037 does not exhibit reductase activity based on our *in vitro* results (Figure 12C). In this case, it might be a combination of other unknown proteins acting with and around 2037 to maintain thiol balance at the cell surface. It appears that a combination of peroxidase gene products are required for optimal resistance.

4.1.5 2037 forms the disulfide bond in exotoxin SpeA

Most strikingly, our results show that 2037 is needed for proper disulfide bond formation in the exotoxin SpeA. In cysteine alkylation experiments, an increase in band intensity with DTT reduction prior to alkylation was seen in the M18 parent, indicating the presence of a disulfide bond in SpeA (Figure 10) that is consistent with crystal structure analysis of SpeA forming a disulfide bridge between Cys87 and Cys98 (Papageorgiou et al., 1999). Cysteines in SpeA from *Δ2037* cultures, in contrast, were efficiently alkylated both with and without DTT treatment indicating the lack of a disulfide bond (Figure 10). Notably, *2037*-complemented mutant showed the return of the SpeA disulfide bond, matching the parent phenotype *in vivo* (Figure 11D and E), strongly suggesting that 2037 is responsible for the formation of the disulfide bond in SpeA.

Accordingly, results from *in vitro* functional assay experiments show that 2037 exhibits oxidase activity (Figure 12B). Disulfide exchange reactions revealed rSpeA changed from its initial reduced form to an oxidized form following 30 min incubation with oxidized r2037 but not reduced r2037 (Figure 13). Thus, r2037 must be in its functional oxidized form in order to oxidize SpeA, lending additional support to *in vivo* findings that 2037 directly contributes to disulfide bond formation.

Given that GAS can produce up to 14 superantigens (SAgs), all with similar structure, 2037 could be involved in collectively forming disulfide bonds for these prominent exotoxins. While SpeA was the main focus, SpeG was identified in our TDOR substrate list and also contains 3 cysteine residues (Table 6). Other known pyrogenic exotoxins include SpeC and SpeH-M (Spaulding et al., 2013). Moreover, SpeA belongs to a family of not only streptococcal superantigens, but also staphylococcal superantigens. This encompasses staphylococcal enterotoxins (SEs) A, B, $C_{1–3}$, D, E, G, H, I, R, and T; the staphylococcal enterotoxin-like (SEls) proteins; and toxic shock syndrome toxin-1 (TSST-1) (Spaulding et al., 2013; Xu & McCormick, 2012). Based on previously reported three-dimensional crystal structure analyses, a disulfide loop is present in all 23 known staphylococcal superantigens except TSST-1 (Hovde et al., 1994; Papageorgiou et al., 1999). Indeed, it is likely that 2037, or another unidentified TDOR-mediated pathway, helps to fold this family of toxins.

Our findings resemble a previously identified TDOR in *C. diphtheriae* called MdbA. Studies by Reardon-Robinson et al. (2015) showed that deletion of *mdbA* was associated with the release of reduced and degraded diphtheria toxin. This phenotype, along with the lack of adhesive pili, had clear consequences on *C. diphtheriae* pathogenesis, as the *ΔmdbA* mutant was attenuated in a guinea pig model of diphtheritic toxemia. While the mechanism is still unclear, MdbA is important for the disulfide bond formation in diphtheria toxin and general folding of other secreted virulence factors (Reardon-Robinson & Ton-That, 2016). Likewise, 2037 altering the SpeA redox state appears to have a negative impact on GAS but more in-depth analyses are needed both at the structural and functional levels.

Given that toxin-mediated diseases such as the STSS are rare and have high mortality rates, it is unlikely that secreted SAgs provide an evolutionary advantage for *S. pyogenes*. An

alternative hypothesis by Kasper et al., (2014) suggested that the true biological function of SAgs is to promote the initial establishment of GAS in humans and SAgs act in a locally immunosuppressive fashion. In fact, a derivative of *S. pyogenes* MGAS8232 in which all six SAgs were deleted (ΔSpeA, ΔSpeC, ΔSpeG, ΔSpeL, ΔSpeM, ΔSmeZ) was attenuated in the humanized mouse model (Kasper et al., 2014). Interestingly, complementation of *speA* regained the ability to colonize humanized mice, and SpeA toxoid immunization provided mice with protection in the intranasal infection model (Kasper et al., 2014). In this context, 2037-mediated disulfide bond formation in SpeA could be important for initial colonization during early stages of entering the host.

The redundancy of SAgs within *S. pyogenes* remains unexplained and poses challenges to studying TDOR-mediated outcomes. An *in viv*o role of SpeA as a virulence factor has been elusive, as a *ΔspeA* mutant strain demonstrated no difference in overall mortality compared to wild-type in a humanized murine model of skin infection (Maamary et al., 2012; Sriskandan et al., 2007). Additionally, in the M89 isolate *S. pyogenes* H293 where SmeZ SAg is dominant, genetic disruption of *smeZ* did not alter bacterial clearance or mortality in a peritoneal infection model (Unnikrishnan et al., 2002). Thus individual SAgs may not contribute to *S. pyogenes* survival during invasive disease in mice, with further possible differences in humans.

4.1.6 2037-SpeA form a heterodimer complex *in vitro* via an unknown mechanism

To further elucidate the mechanism of complex interaction between 2037 and SpeA, cysteine to alanine point mutations at position 46 (2037_{C46A}) and position 49 (2037_{C49A}) were generated in the 2037 active site (Figure 14A and B) and confirmed by DNA sequencing (Appendix A). Results from preliminary data showed a ~40 kDa band, likely signifying a heterodimer complex between r2037 (14 kDa) and rSpeA (25 kDa) (Figure 14C and D). The ~40

kDa heterodimer band was present in both 2037/SpeA and 2037_{C49A} /SpeA reaction lanes at equal intensities; conversely, a weaker intensity ~40 kDa band was detected in the reaction between 2037_{C46A}/SpeA (Figure 14C and D). Other differences included the ~28 kDa band, likely representing a 2037 homodimer complex, which was observed in the wild-type 2037/SpeA reaction but not in 2037_{C46A}/SpeA (Figure 14C). Of the two cysteines, the C46A point mutant had a more contrasting protein profile.

The 2037 point mutants show different profiles of disulfide-linked protein complexes with SpeA, however repetition of the experiment is needed. Furthermore, the active site 2037 cysteines 46 and 49 have different reactivites, with the N-terminal Cys46 possibly playing a distinct role during protein complex formation with SpeA. In *E. coli* DsbA and other related TDORs with oxidase activity, the CXXC motif typically contains an intramolecular disulfide bond that is transferred to substrate proteins, thereby requiring both cysteines for activity (Heras et al., 2009; Inaba & Ito, 2008). DsbA has one cysteine that is accessible and highly reactive while the other residue was buried and unreactive, leading to the formation of an unstable catalytic disulfide bond that explains the high oxidase activity of DsbA (Inaba & Ito, 2008). The same could be true for 2037 where both cysteines are required for oxidation through an intramolecular disulfide bond but with unequal thermodynamic reactivities. Unlike previously described TDORs, characterization of *S. gordonii* SdbA active site showed that SdbA is active with only a single cysteine of the CXXC motif (Davey, Cohen, Leblanc, Halperin, & Lee, 2016). Only variants with a single C-terminal cysteine were active in *S. gordonii* under most conditions which was unexpected given that the C-terminal cysteine is buried, and does not typically interact with substrates (Davey, Cohen, et al., 2016).

Since this study has explored many different experimental avenues, it is important to mention and summarize certain limitations. The generated list of M18 TDORs and their cysteine-containing substrates was limited by the fact that these targets were first found in the M1 proteome, followed by a BLASTP search in the M18 serotype looking for protein homologs. Using the described *in silico* approach with the M18 GAS proteome directly, any additional TDORs and protein substrates that were strain-specific and missed would be identified. Some experiments had low replicate numbers and should be independently repeated to confirm the reproducibility of the data. This is especially important for the preliminary results reported from the 2037 complement and 2037-SpeA hetermodimer complex experiments.

The qualitative nature of the hemolysis, bacteriocin, disc diffusion, salt and copper assays limited the interpretation of these results; it is possible that redundancies of substrate targets exist and that a compensatory factor is producing the phenotype observed, as could be the case for hemolysis since GAS produces SLS and SLO. The bacteriocin assay designed was not suitable to test the M18 serotype and therefore conclusions cannot be properly drawn. It is likewise possible that TDORs have redundant functions in the cell and that creating a mutation of one, does not necessarily lead to an obvious defect.

Although the pG^{+}host plasmid was used successfully for generating the TDOR mutants and is well-documented for high-efficiency gene inactivation in Gram-positive bacteria, polar effects/mutations cannot be entirely ruled out and pose as a limitation. This could negatively affect gene products neighboring or downstream of the intended TDOR gene, especially since the promoter regions of SpyM18_2037, SpyM18_AhpC, SpyM18_0982, SpyM18_2138 and SpyM18_1572 were left undisturbed during insertional inactivation approach. Polar mutations can be misleading and complicates the study of the role of specific TDOR genes in GAS.

At this stage we do not know the additional proteins, if any, that GAS uses to catalyze disulfide bond formation. The identity of potential 2037 redox partner(s) have yet to be identified in GAS as well. Together, our novel findings surrounding 2037 are depicted in a working model scheme (Figure 15). A summary of all phenotypic assays performed is given in Table 7.

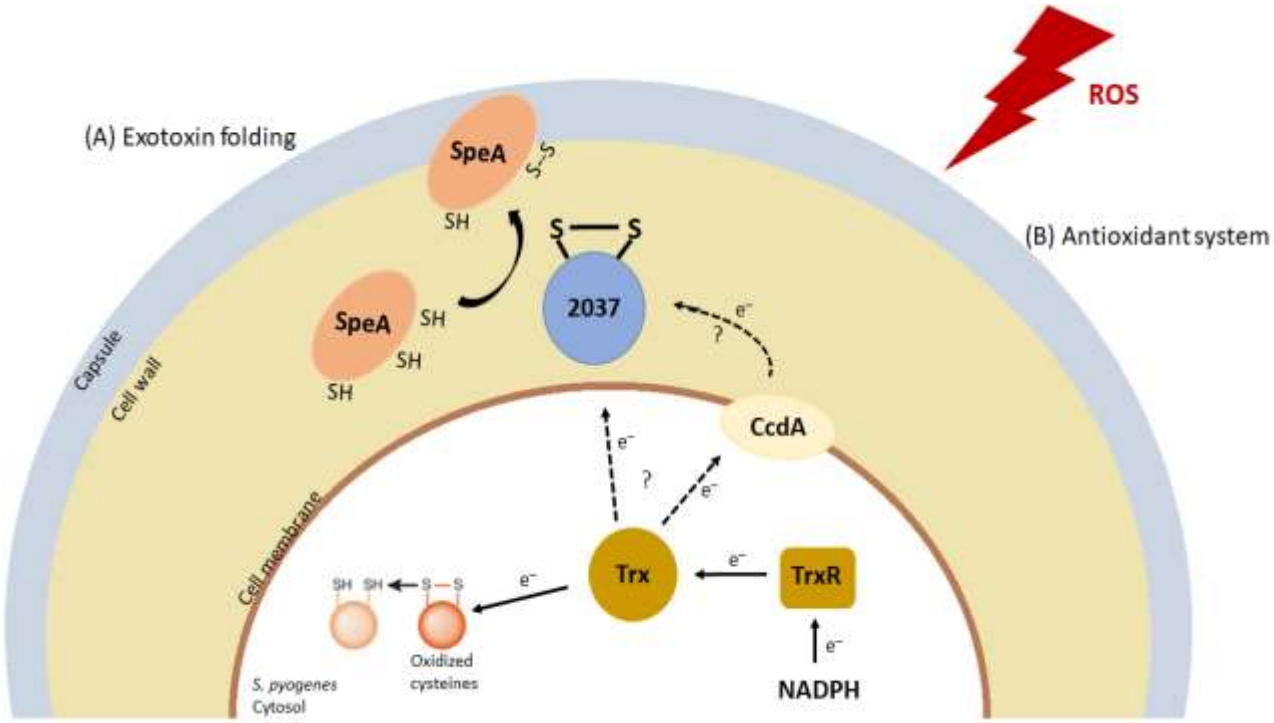

Figure 15: Working model of major findings. Schematic of the GAS cell showing the TDOR enzyme 2037 in the center. (A) In its oxidized form, 2037 is needed to form the disulfide bond in substrate exotoxin SpeA. (B) Under oxidative stress conditions induced by ROS, 2037 is likely involved in maintaining thiol balance at the cell surface by an unknown mechanism. It is possible that a thioredoxin-dependent antioxidant system (Trx, TrxR, NAPDH) in GAS passes electrons (e^-) either directly to 2037 or indirectly through unknown accessary proteins such as CcdA (dashed arrows). Cytosolic thioredoxin is a ubiquitous oxidoreductase that plays a role in repairing oxidized cysteines or by providing reducing equivalents to partner proteins.

Table 7: Summary of phenotypes investigated.

			Difference compared to M18 parent?				
Phenotypic Assay	**Target Substrate/Purpose**	**Cys***	***Δ2037***	***ΔahpC***	***Δ0982***	***Δ2138***	***Δ1572***
Hemolysis	Streptolysin S	7	-	-	-	-	-
Bacteriocin Production	Bacteriocin peptides	2	-	-	-	-	-
Sensitivity to salts (NaCl, KCl)	General cell stress; osmolarity		-	-	-	-	-
Sensitivity to Copper	Non-native disulfide bond rearrangement		-	-	-	-	-
Sensitivity to Penicillin G	Cell wall synthesis enzymes; transpeptidases	2-3	+	+	+	+	+
Sensitivity to other antibiotics	Cell-membrane/cell-wall synthesis enzymes	2-3	-	-	-	-	-
Autolysis	Autolysin, PBPs	2-3	-	-	-	-	-
Capsule Production	Hyaluronate synthase A (HasA)	6	-	-	-	-	-
Sensitivity to Paraquat	Promote intracellular oxidative stress		+	+	+	+	+
Sensitivity to H_20_2	Promote oxidative damage		-	-	-	-	-
Sensitivity to 20 mM DTT	Reduce disulfide bonds		+	-	-	-	-

			Difference compared to M18 parent?				
Phenotypic Assay	**Target Substrate/Purpose**	**Cys***	***Δ2037***	***ΔahpC***	***Δ0982***	***Δ2138***	***Δ1572***
Survival inside macrophage cells	Macrophage-induced ROS		+	TBD	TBD	TBD	-
Exotoxin Production	SpeA	3	-	-	-	-	-
Exotoxin redox state	*In vivo* SpeA disulfide status	3	+	+	-	+	-
Disulfide Exchange Reaction	*In vitro* SpeA disulfide status	3	+	TBD	TBD	TBD	TBD

*Number of cysteine residues, if applicable
'+' denotes a significant difference compared to the parent phenotype
'-' denotes no significant difference
'TBD' data is to be determined

4.2 Future Directions

This is the first reported functional analyses of putative TDORs done in Group A streptococcus. As such, this project lays the foundations for continued investigations of protein disulfide bond formation pathways in GAS, along with other clinically significant bacterial species. Key future directions can largely be divided into three areas: a focus on SpeA, 2037 and the mechanisms of a 2037-SpeA complex interaction.

4.2.1 SpeA

The question remains as to whether the functional activity of SpeA is affected by its altered redox state and future experiments should be designed to address this. SpeA is one of several SAgs secreted by GAS and the *S. pyogenes* MGAS8232 strain in particular encodes 5 other SAgs in its genome. SAgs act by simultaneously binding to MHC class II molecules on host APCs and to the TCR variable β-chain, resulting in non-specific activation of a large number of T cells and massive pro-inflammatory cytokine release. It is possible that the *Δ2037* mutant lacking the disulfide bond in SpeA has impaired T cell stimulation and a different cytokine expression profile compared to wild-type. This is greatly supported by toxicity analyses of SpeA done by Roggiani et al. (1997) showing that individual cysteine residues changed to serine had diverse effects on SpeA properties. Cysteines 87 and 98 are linked by a disulfide bond in SpeA, and point mutants C87S and C98S had severely reduced mitogenic ability (Roggiani et al., 1997). Cys 87 and 98 were also important for the lymphocyte proliferative activity of SpeA *in vitro*, further emphasizing the notion that the disulfide linkage confers conformational stability that effects SpeA function (Roggiani et al., 1997).

It is unknown if the missing disulfide bond in SpeA of the *Δ2037* mutant changes the overall binding affinity of SpeA with the TCR and MHC class II molecule. Previous data have

shown the disulfide loop between Cys87 and Cys98 is important for SpeA1 interactions with both MHC and TCR variable β-chain in the M1 serotype (Kline & Collins, 1997). The proximity of the disulfide loop to the antigen-binding groove also needs to be considered (Kline & Collins, 1997; Roggiani et al., 1997).

Differences in GAS survival caused by the *Δ2037* mutation should be further investigated using *in vivo* models. As previously described in literature, an HLA-expressing humanized mouse can be used for nasopharyngeal infections with GAS, and these humanized mice are better representative models of natural routes of infection compared to other animal models (Ito et al., 1996; Nooh, El-Gengehi, Kansal, David, & Kotb, 2007; Wilkening & Federle, 2017). An *in vivo* environment may be more suitable for studying GAS antioxidant defenses and possible virulence attenuation due to misfolded superanitgens, as was the case for bacteriocin production. Certainly, the role of 2037 in GAS pathogenesis needs to be explored in humanized mouse infections before any clinical significance can be attributed.

4.2.2 2037-SpeA complex interactions

The interaction of 2037_{C46A} and 2037_{C49A} point mutants with SpeA needs to be explored in GAS directly, with a good starting point being the *in vivo* alkylation experiments. The potassium ferricyanide used *in vitro* oxidizes thiol groups by making any cysteine residue highly reactive, but is not ideally representative of true protein-protein interactions that happen in the cell. Based on known TDOR structural activity in *S. gordonii* SdbA, it is expected that one of the two single cysteine point mutations will render 2037 inactive, likely the N-terminal cys46, and will prevent 2037 from interacting with SpeA. Along with studying single point mutants, generation of a successful double cysteine point mutant (2037_{AXXA}) at the active site will provide valuable insight on the 2037-SpeA complex. Studying the interaction of 2037_{AXXA} with SpeA

should be explored both *in vitro* and *in vivo*. It is expected that the double mutant will render 2037 catalytically inactive, preventing binding to SpeA and therefore having no effect on SpeA redox state.

To better understand the catalytic mechanism of 2037, analyses should focus on solving its crystal structure. 2037 has 3 cysteine residues in total, 2 involved in the CXXC motif that participate in a disulfide bond and a third that is nearby. It is unclear if 2037 favorably forms homodimers or if the third cysteine is in any way involved in enzyme function. SpeA has 3 cysteine residues as well, which could add another layer of complexities when studying 2037-SpeA interactions. With 3 cysteines in each respective protein, there are likely a combination of disulfide-linked protein formation complexes that are possible each with different conformational stabilities. By replacing the cysteines that are not expected to participate in disulfide bonding in both SpeA and 2037 with another amino acid, this could be a way to specifically study the disulfide transfer between TDOR and substrate. These are only few of many exciting future directions.

4.3 Conclusion

Our results have identified 2037 as a novel TDOR enzyme in GAS. Mutation of *2037* results in a pleiotropic phenotype indicating an important biological function and possible broad substrate specificity. 2037 plays a role in GAS resistance to oxidative stress but the mechanism is unclear as to how it helps maintain thiol balance at the cell surface. Most strikingly, 2037 in its oxidized form was found to introduce a disulfide bond in the exotoxin SpeA. This is the first report of an enzyme being directly involved in the proper folding of a distinct GAS

superantigenic toxin and highlights the importance of studying protein-folding-pathways in pathogenic Gram-positive bacteria.

From a clinical perspective, an improved understanding of individual virulence factor production at the molecular level can lead to better models of GAS disease progression, which may ultimately lead to better treatment and drug intervention strategies. Studying TDOR-mediated pathways could pave the way for new vaccine targets that offer an alternative to antibiotics. Indeed, the development of a safe and effective commercial human vaccine for the prophylaxis of GAS disease still remains a high priority (Walker et al., 2014).

References

Ahn, S. J., & Burne, R. A. (2006). The atlA operon of Streptococcus mutans: Role in autolysin maturation and cell surface biogenesis. *Journal of Bacteriology*, *188*(19), 6877–6888.

Amiri-Jami, M., Lapointe, G., & Griffiths, M. W. (2014). Engineering of EPA/DHA omega-3 fatty acid production by Lactococcus lactis subsp. cremoris MG1363. *Applied Microbiology and Biotechnology*, *98*(7), 3071–3080.

Andisi, V. F., Hinojosa, C. A., de Jong, A., Kuipers, O. P., Orihuela, C. J., & Bijlsma, J. J. E. (2012). Pneumococcal gene complex involved in resistance to extracellular oxidative stress. *Infection and Immunity*, *80*(3), 1037–1049.

Armstrong, B. D., Herfst, C. A., Tonial, N. C., Wakabayashi, A. T., Zeppa, J. J., & McCormick, J. K. (2016). Identification of a two-component Class IIb bacteriocin in Streptococcus pyogenes by recombinase-based in vivo expression technology. *Scientific Reports*.

Arthur, J. R. (2001). The glutathione peroxidases. *Cellular and Molecular Life Sciences*, *57*(13), 1825–1835.

Belotserkovsky, L., Baruch, M., Peer, A., Dov, E., Ravins, M., Mishalian, I., … Hanski, E. (2009). Functional analysis of the quorum-sensing streptococcal invasion locus (sil). *PLoS Pathogens*, *5*(11). https://doi.org/10.1371/journal.ppat.1000651

Bendtsen, J. D., Nielsen, H., Von Heijne, G., & Brunak, S. (2004). Improved prediction of signal peptides: SignalP 3.0. *Journal of Molecular Biology*, *340*(4), 783–795.

Bernsel, A., Viklund, H., Falk, J., Lindahl, E., von Heijne, G., & Elofsson, A. (2008). Prediction of membrane-protein topology from first principles. *Proceedings of the National Academy of Sciences*, *105*(20), 7177–7181.

Bessen, D. E. (2010). NIH Public Access, *9*(4), 581–593. https://doi.org/10.1016/j.meegid.2009.03.00.Population

Betschel, S. D., Borgia, S. M., Barg, N. L., Low, D. E., & De Azavedo, J. C. S. (1998). Reduced Virulence of Group A Streptococcal Tn916 Mutants That Do Not Produce Streptolysin S. *Infection and Immunity*, *66*(4), 1671–1679.

Birnboim, H. C., & Doly, J. (1979). A rapid alkaline extraction procedure for screening recombinant plasmid DNA. *Nucleic Acids Research*, *7*(6), 1513–1523.

Bisno, A. L. (1991). Group A Streptococcal Infections and Acute Rheumatic Fever. *New England Journal of Medicine*, *325*(11), 783–793.

Budzik, J. M., Poor, C. B., Faull, K. F., Whitelegge, J. P., He, C., & Schneewind, O. (2009). Intramolecular amide bonds stabilize pili on the surface of bacilli. *Proceedings of the National Academy of Sciences*, *106*(47), 19992–19997.

Carapetis, J. R., Steer, A. C., Mulholland, E. K., & Weber, M. (2005). The global burden of group A streptococcal diseases, *5*(November), 685–694.

Chaussee, M. A., McDowell, E. J., Rieck, L. D., Callegari, E. A., & Chaussee, M. S. (2006). Proteomic analysis of a penicillin-tolerant rgg mutant strain of Streptococcus pyogenes. *Journal of Antimicrobial Chemotherapy*, *58*(4), 752–759.

Chim, N., Harmston, C. A., Guzman, D. J., & Goulding, C. W. (2013). Structural and biochemical characterization of the essential DsbA-like disulfide bond forming protein from Mycobacterium tuberculosis. *BMC Structural Biology*, *13*(1).

Cho, S.-H., & Collet, J.-F. (2013). Many Roles of the Bacterial Envelope Reducing Pathways. *Antioxidants & Redox Signaling*, *18*(13), 1690–1698. https://doi.org/10.1089/ars.2012.4962

Cleary, P. P., & Larkin, A. (1979). Hyaluronic acid capsule: Strategy for oxygen resistance in group A streptococci. *Journal of Bacteriology*, *140*(3), 1090–1097.

Cole, J. N., Pence, M. A., von Köckritz-Blickwede, M., Hollands, A., Gallo, R. L., Walker, M. J., & Nizeta, V. (2010). M protein and hyaluronic acid capsule are essential for in vivo selection of covRS mutations characteristic of invasive serotype M1T1 group A Streptococcus. *mBio*.

Crater, D. L., & Van de Rijn, I. (1995). Hyaluronic acid synthesis operon (has) expression in group A streptococci. *Journal of Biological Chemistry*, *270*(31), 18452–18458.

Cross, A. S. (2008). What is a virulence factor? *Critical Care (London, England)*, *12*(6), 196. https://doi.org/10.1186/cc7127

Cunningham, M. W. (2008). Pathogenesis of group a streptococcal infections and their sequelae. In *Advances in Experimental Medicine and Biology* (Vol. 609, pp. 29–42).

Dalton, T. L., & Scott, J. R. (2004). CovS inactivates CovR and is required for growth under conditions of general stress in Streptococcus pyogenes. *J Bacteriol*, *186*(12), 3928–3937.

Daniels, R., Mellroth, P., Bernsel, A., Neiers, F., Normark, S., Von Heijne, G., & Henriques-Normark, B. (2010). Disulfide bond formation and cysteine exclusion in gram-positive bacteria. *Journal of Biological Chemistry*.

Davey, L., Cohen, A., Leblanc, J., Halperin, S. A., & Lee, S. F. (2016). The disulfide oxidoreductase SdbA is active in Streptococcus gordonii using a single C-terminal cysteine of the CXXC motif. *Molecular Microbiology*, *99*(2), 236–253.

Davey, L., Halperin, S. A., & Lee, S. F. (2016). Mutation of the streptococcus gordonii Thiol-disulfide oxidoreductase SdbA leads to enhanced biofilm formation mediated by the CiaRH two-component signaling system. *PLoS ONE*.

Davey, L., Halperin, S. A., & Lee, S. F. (2016). Thiol-Disulfide Exchange in Gram-Positive Firmicutes. *Trends in Microbiology*.

Davey, L., Ng, C. K. W., Halperin, S. A., & Lee, S. F. (2013). Functional analysis of paralogous thiol-disulfide oxidoreductases in Streptococcus gordonii. *Journal of Biological Chemistry*, *288*(23), 16416–16429.

Dorenbos, R., Stein, T., Kabel, J., Bruand, C., Bolhuis, A., Bron, S., … Van Dijl, J. M. (2002). Thiol-disulfide oxidoreductases are essential for the production of the lantibiotic sublancin 168. *Journal of Biological Chemistry*, *277*(19), 16682–16688.

Dumoulin, A., Grauschopf, U., Bischoff, M., Thöny-Meyer, L., & Berger-Bächi, B. (2005). Staphylococcus aureus DsbA is a membrane-bound lipoprotein with thiol-disulfide oxidoreductase activity. *Archives of Microbiology*, *184*(2), 117–128.

Dunny, G. M., Lee, L. N., & LeBlanc, D. J. (1991). Improved electroporation and cloning vector system for gram-positive bacteria. *Applied and Environmental Microbiology*, *57*(4), 1194–1201.

Eneli, I., & Davies, H. D. (2007). Epidemiology and outcome of necrotizing fasciitis in children: an active surveillance study of the Canadian Paediatric Surveillance Program. *The Journal of Pediatrics*, *151*(1), 79–84, 84.e1.

Facklam, R. F., Martin, D. R., Lovgren, M., Johnson, D. R., Efstratiou, A., Thompson, T. a, … Beall, B. (2002). Extension of the Lancefield classification for group A streptococci by addition of 22 new M protein gene sequence types from clinical isolates: emm103 to emm124. *Clinical Infectious Diseases : An Official Publication of the Infectious Diseases Society of America*, *34*(1), 28–38.

Ferretti, J. J., Stevens, D. L., & Fischetti, V. a. (2016). Streptococcus pyogenes: Basic Biology to Clinical Manifestations. *Streptococcus Pyogenes: Basic Biology to Clinical Manifestations*, 1–15.

Fischer, A., & Montal, M. (2007). Crucial role of the disulfide bridge between botulinum neurotoxin light and heavy chains in protease translocation across membranes. *Journal of Biological Chemistry*, *282*(40), 29604–29611.

Flores, A. R., Jewell, B. E., Fittipaldi, N., Beres, S. B., & Musser, J. M. (2012). Human disease isolates of serotype M4 and M22 group A streptococcus lack genes required for hyaluronic acid capsule biosynthesis. *mBio*, *3*(6).

Fontaine, M. C., Lee, J. J., & Kehoe, M. A. (2003). Combined contributions of streptolysin O and streptolysin S to virulence of serotype M5 Streptococcus pyogenes strain Manfredo. *Infection and Immunity*.

Forsberg, C., & Rogers, H. J. (1971). Autolytic enzymes in growth of bacteria. *Nature*, *229*(5282), 272–273.

Gennaris, A., & Collet, J. F. (2013). The "captain of the men of death", streptococcus pneumoniae, fights oxidative stress outside the "city wall." *EMBO Molecular Medicine*, *5*(12), 1798–1800.

Hammes, W. P., & Neuhaus, F. C. (1974). On the mechanism of action of vancomycin: inhibition of peptidoglycan synthesis in Gaffkya homari. *Antimicrobial Agents and Chemotherapy*, *6*(6), 722–728.

Han, H., & Wilson, A. C. (2013). The two CcdA proteins of Bacillus anthracis differentially affect virulence gene expression and sporulation. *Journal of Bacteriology*, *195*(23), 5242–5249.

Henningham, A., Döhrmann, S., Nizet, V., & Cole, J. N. (2015). Mechanisms of group A Streptococcus resistance to reactive oxygen species. *FEMS Microbiology Reviews*.

Heras, B., Kurz, M., Jarrott, R., Shouldice, S. R., Frei, P., Robin, G., … Martin, J. L. (2008). Staphylococcus aureus DsbA does not have a destabilizing disulfide: A new paradigm for bacterial oxidative folding. *Journal of Biological Chemistry*, *283*(7), 4261–4271.

Heras, B., Shouldice, S. R., Totsika, M., Scanlon, M. J., Schembri, M. A., & Martin, J. L. (2009). DSB proteins and bacterial pathogenicity. *Nature Reviews Microbiology*.

Hertzog, B. B., Kaufman, Y., Biswas, D., Ravins, M., Ambalavanan, P., Wiener, R., … Hanski, E. (2018). A Sub-population of Group A Streptococcus Elicits a Population-wide Production of Bacteriocins to Establish Dominance in the Host. *Cell Host and Microbe*, *23*(3), 312–323.e6.

Hiniker, A., Collet, J. F., & Bardwell, J. C. A. (2005). Copper stress causes an in vivo requirement for the Escherichia coli disulfide isomerase DsbC. *Journal of Biological Chemistry*, *280*(40), 33785–33791.

Hoge, C. W., Schwartz, B., Talkington, D. F., Breiman, R. F., MacNeill, E. M., & Englender, S. J. (1993). The changing epidemiology of invasive group A streptococcal infections and the emergence of streptococcal toxic shock-like syndrome. A retrospective population-based study. *JAMA : The Journal of the American Medical Association*, *269*(3), 384–389.

Holmgren, A. (1979). Thioredoxin catalyzes the reduction of insulin disulfides by dithiothreitol and dihydrolipoamide. *Journal of Biological Chemistry*, *254*(19), 9627–9632.

Hossain, M. S., & Biswas, I. (2011). Mutacins from Streptococcus mutans UA159 are active against multiple streptococcal species. *Applied and Environmental Microbiology*, *77*(7), 2428–2434.

Hovde, C. J., Marr, J. C., Hoffmann, M. L., Hackett, S. P., Chi, Y. -i, Crum, K. K., … Bohach, G. A. (1994). Investigation of the role of the disulphide bond in the activity and structure of staphylococcal enterotoxin C1. *Molecular Microbiology*, *13*(5), 897–909.

Imlay, J. A., & Linn, S. (1986). Bimodal pattern of killing of DNA-repair-defective or anoxically grown Escherichia coli by hydrogen peroxide. *Journal of Bacteriology*, *166*(2), 519–527.

Inaba, K., & Ito, K. (2008). Structure and mechanisms of the DsbB-DsbA disulfide bond generation machine. *Biochimica et Biophysica Acta - Molecular Cell Research*. https://doi.org/10.1016/j.bbamcr.2007.11.006

Ireland, N. (CBC N. (2017). Invasive Group A strep cases rising, but the reason is a medical mystery. Retrieved April 16, 2018, from http://www.cbc.ca/news/health/invasive-group-a-strep-flesh-eating-medical-mystery-1.4566806

Ito, K., Bian, H. J., Molina, M., Han, J., Magram, J., Saar, E., … Nagy, Z. A. (1996). HLA-DR4-IE chimeric class II transgenic, murine class II-deficient mice are susceptible to experimental allergic encephalomyelitis. *The Journal of Experimental Medicine*, *183*(6), 2635–2644.

Jönsson, T. J., Ellis, H. R., & Poole, L. B. (2007). Cysteine reactivity and thiol-disulfide interchange pathways in AhpF and AhpC of the bacterial alkyl hydroperoxide reductase system. *Biochemistry*, *46*(19), 5709–5721.

Juncker, A. S., Willenbrock, H., von Heijne, G., Brunak, S., Nielsen, H., & Krogh, A. (2003). Prediction of lipoprotein signal peptides in Gram-negative bacteria. *Protein Science*, *12*(8), 1652–1662.

Kaplan, E. L. (1980). The group A streptococcal upper respiratory tract carrier state: An enigma. *The Journal of Pediatrics*, *97*(3), 337–345.

Kaplan, E. L. (2004). The Group A Streptococcal Upper Respiratory Carrier Diagnosis and Management. In *Streptococcal Pharyngitis Optimal Management* (p. 69).

Kasper, K. J. (2013). Systematic Assessment of the Contribution of Superantigens to Nasopharyngeal Colonization in a Mouse Model of Streptococcal Infection, (February). Retrieved from http://ir.lib.uwo.ca/etd/1120

Kasper, K. J., Zeppa, J. J., Wakabayashi, A. T., Xu, S. X., Mazzuca, D. M., Welch, I., … McCormick, J. K. (2014). Bacterial Superantigens Promote Acute Nasopharyngeal Infection by Streptococcus pyogenes in a Human MHC Class II-Dependent Manner. *PLoS Pathogens*, *10*(5).

King, K. Y., Horenstein, J. A., & Caparon, M. G. (2000). Aerotolerance and peroxide resistance in peroxidase and PerR mutants of Streptococcus pyogenes. *Journal of Bacteriology*, *182*(19), 5290–5299.

Kline, J. B., & Collins, C. M. (1997). Analysis of the interaction between the bacterial superantigen streptococcal pyrogenic exotoxin A (SpeA) and the human T-cell receptor. *Molecular Microbiology*, *24*(1), 191–202.

Koroleva, I. V., Sjöholm, A. G., & Schalen, C. (1998). Binding of complement subcomponent Clq to Streptococcus pyogenes: Evidence for interactions with the M5 and FcRA76 proteins. *FEMS Immunology and Medical Microbiology*, *20*(1), 11–20.

Kreikemeyer, B., McIver, K. S., & Podbielski, A. (2003). Virulence factor regulation and regulatory networks in Streptococcus pyogenes and their impact on pathogen-host interactions. *Trends in Microbiology*. https://doi.org/10.1016/S0966-842X(03)00098-2

Laemmli, U. K. (1970). Cleavage of structural proteins during the assembly of the head of bacteriophage T4. *Nature*, *227*(5259), 680–685.

Lancefield, R. C. (1962). Current knowledge of type-specific M antigens of group A streptococci. *Journal of Immunology (Baltimore, Md. : 1950)*, *89*, 307–313.

Lee, S. F., & Davey, L. (2017). Disulfide Bonds: A Key Modification in Bacterial Extracytoplasmic Proteins. *Journal of Dental Research*. https://doi.org/10.1177/0022034517725059

Leenhouts, K. J., Kok, J., & Venema, G. (1991). Lactococcal plasmid pWVO1 as an integration vector for lactococci. *Applied and Environmental Microbiology*, *57*(9), 2562–2567.

Liu, G., Zhong, J., Ni, J., Chen, M., Xiao, H., & Huan, L. (2009). Characteristics of the bovicin HJ50 gene cluster in Streptococcus bovis HJ50. *Microbiology*, *155*(2), 584–593.

Lu, J., & Holmgren, A. (2014). The thioredoxin antioxidant system. *Free Radical Biology and Medicine*. https://doi.org/10.1016/j.freeradbiomed.2013.07.036

Lynskey, N. N., Goulding, D., Gierula, M., Turner, C. E., Dougan, G., Edwards, R. J., & Sriskandan, S. (2013). RocA Truncation Underpins Hyper-Encapsulation, Carriage Longevity and Transmissibility of Serotype M18 Group A Streptococci. *PLoS Pathogens*, *9*(12), 1–15.

Maamary, P. G., Zakour, N. L. B., Cole, J. N., Hollands, A., Aziz, R. K., Barnett, T. C., … Walker, M. J. (2012). Tracing the evolutionary history of the pandemic group A streptococcal M1T1 clone. *FASEB Journal*, *26*(11), 4675–4684.

Maguin, E., Prévost, H., Ehrlich, S. D., Gruss, A., & Ge, L. De. (1996). Efficient insertional mutagenesis in lactococci and other gram-positive bacteria . These include : Efficient Insertional Mutagenesis in Lactococci and Other Gram-Positive Bacteria. *Microbiology*, *178*(3), 931–935.

Maxted, W. R. (1953). The use of bacitracin for identifying group A haemolytic streptococci. *Journal of Clinical Pathology*, *6*(3), 224–226. Retrieved from http://www.pubmedcentral.nih.gov/articlerender.fcgi?artid=1023624&tool=pmcentrez&rendertype=abstract

Meima, R., Eschevins, C., Fillinger, S., Bolhuis, A., Hamoen, L. W., Dorenbos, R., … Bron, S. (2002). The bdbDC operon of Bacillus subtilis encodes thiol-disulfide oxidoreductases required for competence development. *Journal of Biological Chemistry*, *277*(9), 6994–7001.

Möller, M. C., & Hederstedt, L. (2008). Extracytoplasmic processes impaired by inactivation of trxA (thioredoxin gene) in Bacillus subtilis. *Journal of Bacteriology*, *190*(13), 4660–4665.

Molloy, E. M., Cotter, P. D., Hill, C., Mitchell, D. A., & Ross, R. P. (2011). Streptolysin S-like virulence factors: the continuing sagA. *Nature Reviews Microbiology*.

Morrison, D. C., & Jacobs, D. M. (1976). Binding of polymyxin B to the lipid A portion of bacterial lipopolysaccharides. *Immunochemistry*, *13*(10), 813–818.

Moses, A. E., Wessels, M. R., Zalcman, K., & Albertí, S. (1997). Relative contributions of hyaluronic acid capsule and M protein to virulence in a mucoid strain of the group A Streptococcus . Relative Contributions of Hyaluronic Acid Capsule and M Protein to Virulence in a Mucoid Strain of the Group A Streptococcus, *65*(1), 64–71.

Nelson, J. W., & Creighton, T. E. (1994). Reactivity and Ionization of the Active Site Cysteine Residues of DsbA, a Protein Required for Disulfide Bond Formation in Vivo. *Biochemistry*, *33*(19), 5974–5983.

Nooh, M. M., El-Gengehi, N., Kansal, R., David, C. S., & Kotb, M. (2007). HLA Transgenic Mice Provide Evidence for a Direct and Dominant Role of HLA Class II Variation in Modulating the Severity of Streptococcal Sepsis. *The Journal of Immunology*, *178*(5), 3076–3083.

Pancholi, V., Boël, G., & Jin, H. (2010). Streptococcus pyogenes Ser/Thr kinase-regulated cell wall hydrolase is a cell division plane-recognizing and chain-forming virulence factor. *Journal of Biological Chemistry*, *285*(40), 30861–30874.

Papageorgiou, A. C., Collins, C. M., Gutman, D. M., Kline, J. B., O'Brien, S. M., Tranter, H. S., & Acharya, K. R. (1999). Structural basis for the recognition of superantigen streptococcal pyrogenic exotoxin A (SpeA1) by MHC class II molecules and T-cell receptors. *EMBO Journal*, *18*(1), 9–21.

Parks, T., Smeesters, P. R., & Steer, A. C. (2012). CURRENT OPINION IN INFECTIOUS DISEASES. *Streptococcal Skin Infection and Rheumatic Heart Disease*.

Picard, A. (The G. and M. (2018). Streptococcus outbreak in Canada is part of a larger story. Retrieved April 16, 2018, from https://www.theglobeandmail.com/opinion/streptococcus-outbreak-in-canada-is-part-of-a-larger-story/article37121621/

Public Health Agency of Canada. (2014). National Laboratory Surveillance of Invasive Streptococcal Disease in Canada Annual Summary 2013, 0–61. Retrieved from http://www.healthycanadians.gc.ca/publications/drugs-products-medicaments-produits/2014-streptococcus/index-eng.php

Quach, D., Van Sorge, N. M., Kristian, S. A., Bryan, J. D., Shelver, D. W., & Doran, K. S. (2009). The ciar response regulator in group b streptococcus promotes intracellular survival and resistance to innate immune defenses. *Journal of Bacteriology*, *191*(7), 2023–2032.

Reardon-Robinson, M. E., Osipiuk, J., Jooya, N., Chang, C., Joachimiak, A., Das, A., & Ton-That, H. (2015). A thiol-disulfide oxidoreductase of the Gram-positive pathogen Corynebacterium diphtheriae is essential for viability, pilus assembly, toxin production and virulence. *Molecular Microbiology*, *98*(6), 1037–1050.

Reardon-Robinson, M. E., & Ton-That, H. (2016). Disulfide-bond-forming pathways in Gram-positive bacteria. *Journal of Bacteriology*. https://doi.org/10.1128/JB.00769-15

RF, B., JP, D., RR, F., & al, et. (1993). Defining the group a streptococcal toxic shock syndrome: Rationale and consensus definition. *JAMA*, *269*(3), 390–391. Retrieved from http://dx.doi.org/10.1001/jama.1993.03500030088038

Roggiani, M., Stoehr, J. A., Leonard, B. A. B., & Schlievert, P. M. (1997). Analysis of toxicity of streptococcal pyrogenic exotoxin A mutants. *Infection and Immunity*.

Saleh, M., Bartual, S. G., Abdullah, M. R., Jensch, I., Asmat, T. M., Petruschka, L., Hammerschmidt, S. (2013). Molecular architecture of streptococcus pneumoniae surface thioredoxin-fold lipoproteins crucial for extracellular oxidative stress resistance and maintenance of virulence. *EMBO Molecular Medicine*, *5*(12), 1852–1870.

Sauvage, E., Kerff, F., Terrak, M., Ayala, J. A., & Charlier, P. (2008). The penicillin-binding proteins: Structure and role in peptidoglycan biosynthesis. *FEMS Microbiology Reviews*. https://doi.org/10.1111/j.1574-6976.2008.00105.x

Seaver, L. C., & Imlay, J. A. (2001). Alkyl hydroperoxide reductase is the primary scavenger of endogenous hydrogen peroxide in Escherichia coli. *Journal of Bacteriology*, *183*(24), 7173–7181.

Sievers, F., Wilm, A., Dineen, D., Gibson, T. J., Karplus, K., Li, W., Higgins, D. G. (2011). Fast, scalable generation of high-quality protein multiple sequence alignments using Clustal Omega. *Molecular Systems Biology*, *7*. https://doi.org/10.1038/msb.2011.75

Smidt, H., Van der Oost, J., & De Vos, W. M. (2001). Development of a gene cloning and inactivation system for halorespiring Desulfitobacterium dehalogenans. *Applied and Environmental Microbiology*, *67*(2), 591–597.

Smoot, J. C., Barbian, K. D., Van Gompel, J. J., Smoot, L. M., Chaussee, M. S., Sylva, G. L., Musser, J. M. (2002). Genome sequence and comparative microarray analysis of serotype M18 group A Streptococcus strains associated with acute rheumatic fever outbreaks. *Proceedings of the National Academy of Sciences of the United States of America*, *99*(7), 4668–4673.

Spaulding, A. R., Salgado-Pabón, W., Kohler, P. L., Horswill, A. R., Leung, D. Y. M., & Schlievert, P. M. (2013). Staphylococcal and streptococcal superantigen exotoxins. *Clinical Microbiology Reviews*, *26*(3), 422–447.

Spellerberg, B., & Brandt, C. (2016). Laboratory Diagnosis of Streptococcus pyogenes (group A streptococci). *Streptococcus Pyogenes : Basic Biology to Clinical Manifestations*, *13*(6), 206–210. Retrieved from http://www.ncbi.nlm.nih.gov/pubmed/26866238

Sriskandan, S., Faulkner, L., & Hopkins, P. (2007). Streptococcus pyogenes: Insight into the function of the streptococcal superantigens. *International Journal of Biochemistry and Cell Biology*. https://doi.org/10.1016/j.biocel.2006.08.009

Sriskandan, S., Unnikrishnan, M., Krausz, T., & Cohen, J. (1999). Molecular analysis of the role of streptococcal pyrogenic exotoxin A (SPEA) in invasive soft-tissue infection resulting from Streptococcus pyogenes. *Molecular Microbiology*, *33*(4), 778–790.

Steer, A. C., Law, I., Matatolu, L., Beall, B. W., & Carapetis, J. R. (2009). Global emm type distribution of group A streptococci: systematic review and implications for vaccine development. *The Lancet Infectious Diseases*. https://doi.org/10.1016/S1473-3099(09)70178-1

Theodore, T. S., & Calandra, G. B. (1981). Streptolysin S activation by lipoteichoic acid. *Infection and Immunity*, *33*(1), 326–328.

Towbin, H., Staehelin, T., & Gordon, J. (1979). Electrophoretic transfer of proteins from polyacrylamide gels to nitrocellulose sheets: procedure and some applications. *Proceedings of the National Academy of Sciences*, *76*(9), 4350–4354.

Unnikrishnan, M., Altmann, D. M., Proft, T., Wahid, F., Cohen, J., Fraser, J. D., & Sriskandan, S. (2002). The Bacterial Superantigen Streptococcal Mitogenic Exotoxin Z Is the Major Immunoactive Agent of Streptococcus pyogenes. *The Journal of Immunology*, *169*(5), 2561–2569.

Walker, M. J., Barnett, T. C., McArthur, J. D., Cole, J. N., Gillen, C. M., Henningham, A., Nizet, V. (2014). Disease manifestations and pathogenic mechanisms of group A Streptococcus. *Clinical Microbiology Reviews*, *27*(2), 264–301.

Wegmann, U., O'Connell-Motherway, M., Zomer, A., Buist, G., Shearman, C., Canchaya, C., Kok, J. (2007). Complete genome sequence of the prototype lactic acid bacterium Lactococcus lactis subsp. cremoris MG1363. *Journal of Bacteriology*, *189*(8), 3256–3270.

Wiberg, K. B., Maltz, H., & Okano, M. (1968). Mechanism of the Ferricyanide Oxidation of Thiols. *Inorganic Chemistry*. https://doi.org/10.1021/ic50062a045

Wilkening, R. V., & Federle, M. J. (2017). Evolutionary Constraints Shaping Streptococcus pyogenes–Host Interactions. *Trends in Microbiology*, *25*(7), 562–572.

Xu, S. X., Kasper, K. J., Zeppa, J. J., & McCormick, J. K. (2015). Superantigens modulate bacterial density during staphylococcus aureus nasal colonization. *Toxins*, *7*(5), 1821–1836.

Xu, S. X., & McCormick, J. K. (2012). Staphylococcal superantigens in colonization and disease. *Frontiers in Cellular and Infection Microbiology*, *2*(April), 1–11.

Yu, C. E., & Ferretti, J. J. (1989). Molecular epidemiologic analysis of the type A streptococcal exotoxin (erythrogenic toxin) gene (speA) in clinical Streptococcus pyogenes strains. *Infection and Immunity*, *57*(12), 3715–3719.

Zaoutis, T., Attia, M., Gross, R., & Klein, J. (2004). The role of group C and group G streptococci in acute pharyngitis in children. *Clinical Microbiology and Infection*, *10*(1), 37–40.

Zuverink, M., Chen, C., Przedpelski, A., Blum, F. C., & Barbieri, J. T. (2015). A heterologous reporter defines the role of the tetanus toxin interchain disulfide in light-chain translocation. *Infection and Immunity*, *83*(7), 2714–2724.

Appendix A

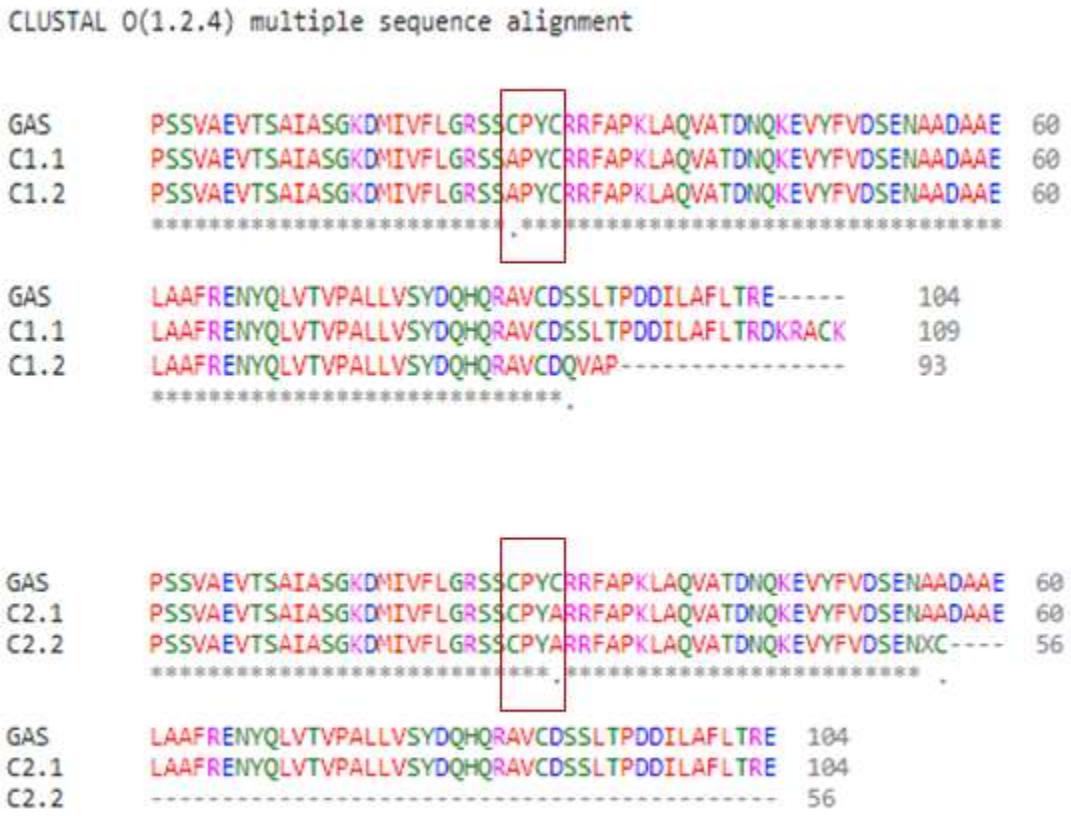

Figure 16: Cysteine point mutant DNA sequencing results from the McGill University and Génome Québec Innovation Centre were translated to primary amino acid sequences and aligned with Clustal Omega (Sievers et al., 2011). 'GAS' denotes the M18 parent sequence. 'Cl.1' and 'C1.2' denote the C46A point mutant sequence amplified with 2037 forward primer 1 or reverse primer 2 respectively. 'C2.1' and 'C2.2' denote the C49A point mutant sequence amplified with 2037 forward primer 1 or reverse primer 2 respectively. *Boxed* areas indicate the location of the CXXC active site. *Asterisks* indicate identical amino acids, and single dots indicate non-similar residues, thus confirming the cysteine to alanine point mutants generated.

Appendix B

Table 8: M1 *S. pyogenes* MGAS5005 strain predicted TDORs list.

Gene Name	**Primary Protein Sequence**
Spy_1678	MTFEEIVANFIPSSVAEVTSAIASGKDMIVFLGRSS**CPYC**RRFA PKLAQVATDNQKEVYFVDSENAADAAELAAFRENYQLVTVPALLVSYDQHQRAV **C**DSSLTPDDILAFLTRE
Spy_1768 (ahpc)	MSLIGKEIAEFSAQAYHDGKFITVTNEDVKGKWAVF**C**FYPADFSFV**C**PTELGDL QEQYETLKSLGVEVYSVSTDTHFVHKAWHDDSDVVGTITYPMIGDPSHLISQAF EVLGEDGLAQRGTFIVDPDGIIQMMEINADGIGRDASTLIDKIHAAQYVRKHPG EV**C**PAKWKEGAETLTPSLDLVGKI
Spy_0726	MAQRIIVITGASGGLAQAIVKQLPKEDSLILLGRNKERLEH**C**YQHIDNKE**C**LEL DITNPVAIEKMVAQIYQRYGRIDVLINNAGYGAFKGFEEFSAQEIADMFQVNTL ASIHFA**C**LIGQKMAEQGQGHLINIVSMAGLIASAKSSIYSATKFALIGFSNALR LELADKGVYVTTVNPGPIATKFFDQADPSGHYLESVGKFTLQPNQVAKRLVSII GKNKRELNLPFSLAVTHQFYTLFPKLSDYLARKVFNYK
Spy_1769	MALSPDIKEQLAQYLTLLEADLVLQVSLGDNEQSQKVKDFVEEIAAMSERISIE NITLDRQPSFKVAKKGHGSGVVFAGLPLGHELTSFILALLQVSGRAPKVDQDVI DRIKAIDRPLHFETYVSLT**CHNC**PDVVQALNIMSVLNDKISHTMVEGGMFQDEV KAKGIMSVPTVFLDGEEFTSGRATIEQLLEQIAGPLSEEAFADKGLYDVLVIGG GPAGNSAAIYAARKGLKTGLLAETFGGQVMETVGIENMIGTLYTEGPKLMAEVE AHTKSYDVDIIKAQLATSIEKKENIEVTLANGAVLQAKTAILALGAKWRNINVP GEDEFRNKGVTY**CPHC**DGPLFEGKDVAVIGGGNSGLEAALDLAGLAKHVYVLEF LPELKADKVLQDRAAKTNNMTIIKNVATKDIVGEDHVTGLNYTERDSGEDKHLD LEGVFVQIGLVPNTAWLKDSGVNLTDRGEIIVDKHGSTNIPGIFAAGD**C**TDSAY KQIIISMGSGATAAIGAFDYLIRQ
Spy_1283	MKKGLLVTTGLA**C**LGLLTA**C**STQDNMAKKEITQDKMSMAAKKKDKMSTSKDKSM MADKSSDKKMTNDGPMAPDFELKGIDGKTYRLSEFKGKKVYLKFWASW**CSIC**LS TLADTEDLAKMSDKDYVVLTVVSPGHQGEKSEADFKKWFQGTDYKDLPVLLDPD GKLLEAYGVRSYPTEVFIGSDGVLAKKHIGYAKKSDIKKTLKGIH

Appendix C

Table 9: *S. pyogenes* M1 strain MGAS5005 extracytoplasmic protein substrates with ≥ 2 cysteine residues

Gene name or ID	Annotated function*	Cysteine residues
speA2	Enterotoxin, superantigen	3
speE	Enterotoxin, superantigen	2
speG	Enterotoxin, superantigen	2
silD	Uncharacterized	2
Spy_0720	Putative exfoliative toxin	3
sagA	*Streptolysin S*	7
sagE	Streptolysin S self-immunity protein	4
hasA	Hyaluronan synthase	6
hylA	Extracellular hyaluronate lysae	2
Spy_0010	Beta-lactamase	2
dacA	Penicillin-binding protein	3
dacA2	Penicilin-binding protein	3
Spy_0028	Autolysin, CHAP domain amidase	2
Spy_1118	Peptidoglycan N-acetylglucosamine deacetylase	2
Spy_1370	Putative deacetylase	2
dltD	D-alanyl-lipoteichoic acid biosynthesis protein	2
spyA	C3 family ADP-ribosyltransferase	6
Spy_1528	Ferrichrome-binding protein	2
Spy_0180	S-layer homology domain	4
Spy_0210	Uncharacterized	4
*gap***	Glyceraldehyde-3-phosphate dehydrogenase	2

*Annotated description obtained from NCBI protein database

**Glyceraldehyde-3-phosphate dehydrogenase does not have a signal sequence but it is known to be found on the surface of *S. pyogenes*.

Appendix D

Table 10: *S. pyogenes* M18 strain MGAS8232 TDOR substrates with ≥ 2 cysteine residues

Gene ID (SpyM18)	Primary Protein Sequence
0393	MENNKKVLKKMVFFVLVTFLGLTISQEVFAQQDPDPSQLHRSSLVKNLQNIYF LYEGDPVTHENVKSVDQLLSHDLIYNVSGPNYDKLKTELKNQEMATLKDKNVD IYGVEYYHLCYLCENAERSACIYGGVTNHEGNHLEIPKKIVVKVSIDGIQSLS FDIETNKKMVTAQELDYKVRKYLTDNKQLYTNGPSKYETGYIKFIPKNKESFW FDFFPEPEFTQSKYLMIYKDNETLDSNTSQIEVYLTTK
0201	MAKFILEFFNILTIIILSCVFSYGSQLAYADENLKDLKRSLRFVYNITPCDYE NIEIAFVTTNSIHINTKQKRSECILYVDSIVSLGITDQFIKGDKVDVFGLPYN FSPPYVDNIYGGIVKHSNQGNKSLQFVGILNQDGKETYLPSEAVRIKKKQFTL QEFDFKIRKFLMEKYNIYDSESRYTSGSLFLATKDSKHYEVDLFNKDDKLLSR DSFFKRYKDNKIFNSEEISHFDIYLKTH
0547	MTGMAGAAQGVTVCAQTGVFIPWQGYILCGAAGAATNIIWPH
0975	MKHLKNPPLVMSGLALGTLSFGNLLATYVSIFSYLGILAALFIYGILLVGMVR NLNDTKMQLRQPLIASVFPTFFMTGMLLSSLFLKVTGGCWLGFLTWWLFFLGN LVLIAYYQYRFVFSFSWDNVFPSWSVLFVGIAMAALTAPASRQFLLGQVIFWV CLLLTAVILPFMAKKTYGIGLGQAVMPNISTFCAPLSLLSASYLATFPRPQVG MVIFLLVSSQLLYAFVVVQLPRLLNRPFNPGFSAFTFPFVISATSLKMTLSFL GWQGLGWQVLLLGEVLLATALVTYVYGAYLRFLFQNK
0799	MLKFTSNILATSVAETTQVAPGGCCCCCTTCCFSIATGSGNSQGGSGSYTPGK
0803	MPLSIQCLNLCFLLVTFCPSIPMQAIFGKEDSGYAFNLIGFLRATLIYDILAL VSIYVLSPQITLSLESIDSKTFFMGLVFCVLIVLIELVFLHGLRCWQKKQWLP ATFSFVGTTNDWSKIGYPLLLALFEEMIYRFLWFNILAFQWHLPTIIVLIVTS FCYALNHLLMGKSIFYAKLVTGIIYGSIYMLTSQLWLVVIMHVGGNLLVECLS HLQTKKKKEVT
2236	MPIFKKTLIVLSFIFLISILIYLNMYLFGTSTVGIYGVILITYLVIKLGLSFL YEPFKGKPHDYKVAAVIPSYNEDAESLLETLKSVLAQTYPLSEIYIVDDGSSN TDAIQLIEEYVNREVDICRNVIVHRSLVNKGKRHAQAWAFERSDADVFLTVDS DTYIYPNALEELLKSFNDETVYAATGHLNARNRQTNLLTRLTDIRYDNAFGVE RAAQSLTGNILVCSGPLSIYRREVIIPNLERYKNQTFLGLPVSIGDDRCLTNY AIDLGRTVYQSTARCDTDVPFQLKSYLKQQNRWNKSFFRESIISVKKILSNPI

Gene ID (SpyM18)	Primary Protein Sequence
	VALWTIFEVVMFMMLIVAIGNLLFNQAIQLDLIKLFAFLSIIFIVALCRNVHY MVKHPASFLLSPLYGILHLFVLQPLKLYSLCTIKNTEWGTRKKVTIFK
1014	MNTYFCTHHKQLLLYSNLFLSFAMMGQGTAIYADTLTSNSEPNNTYFQTQTLT TTDSEKKVVQPQQKDYYTELLDQWNSIIAGNDAYDKTNPDMVTFHNKAEKDAQ NIIKSYQGPDHENRTYLWEHAKDYSASTNITKTYRNIEKIAKQITNPESCYYQ DSKAIAIVKDGMAFMYEHAYNLDRENHQTTGKENKENWWVYEIGTPRAINNTL SLMYPYFTQEEILKYTAPIEKFVPDPTRFRVRAANFSPFEASSGNLIDMGRVK LISGILRKDDLEISDTIKAIEKVFTLVDEGNGFYQDGSLIDHVITNAQSPLYK KGIAYTGAYGNVLIDGLSQLIPIIQKTKSPIEADKMATIYHWINHSFFPIIVR GEMMDMTQGRSISRFNAQSHVAGIEALRAILRIADMSEEPHRLALKTRIKTLV TQGNAFYNVYDNLKTYHDIKLMKELLSDTSVPVQKLDSYVASFNSMDKLALYN NKHDFAFGLSMFSNRTQNYEAMNNENLHGWFTSDGMFYLYNNDLGHYSENYWA TVNPYRLPGTTETEQKPLEGTPENIKTNYQQVGMTSLSDDAFVASKKLNNTSA LAAMTFTNWNKSLTLNKGWFILGNKIIFVGSNIKNQSSHKAYTTIEQRKENQK HPYHAYVNNQPVDLNNQLVDFTNTKSIFLESDDSAQNIGYYFFKPTTLSISKA LQTGKWQNIKADDKSPEAIKEVSNTFITIMQNHTQDDDRYAYMMLPNMTRQEF ENYISKLDIDLLENNDKLAAVYDHDSQQMHVIHYEKKATMFSNHNLSHQGFYS FPHPVKQNQQ
0011	MRKLLAAMLMTFFLTPLPVISTEKKLIFSKNAVYQLKQDVVQSTQFYNQLPSN PNLYQETCAYKDSDLTLPAGRLGVNQPLLIKSLVLNKESLPVFELADGTYVEA NRQLIYDDIVLNQVDIDSYFWTQKKLRLYSAPYVLGTQTIPSSFSFAQKVHAT QMAQTNHGTYYLIDDKGWASQEDLVQFDNRMLKVQEMLLQKYNNPNYSIFVKQ LNTQTSAGINADKKMYAASISKLAPLYIVQKQLQKKKLAENKTLTYTKDVNHF YGDYDPLGSGKISKIADNKDYRVEDLLKAVAQQSDNVATNILGYYLCHQYDKA FRSEIKALSGIDWDMEQRLLTSRSAANMMEAIYHQKGQIISYLSNTEFDQQRI TKNITVPVAHKIGDAYDYKHDVAIVYGNTPFILSIFTNKSTYEDITAIADDVY GILK
1051	MIKRWAILFFVVLACSGLGKTVLAADFQVGAEHAIVVEVDSGRVLYEKDAKTP DAIASLTKLVTAYLVLDKVNSGQLQLSDQVNLSDYAFELTTDSSLSNVPFDQK TYSVQDLLEATLVASSNSAAIALAEKVAGSEPNFVAQMRAQLSRWGITSGKIL NASGLPNEVLKDHRYPGSALEEENMLSAQDVAIVTMHLLEDFPEILEITKQTE VDFAGNSIKSFNQLLPGMAKGRAGVDGLKTGTTDLAGHCLVVTSIENGMRVIT VILNADGSDKNQNTRFEQANRLLDYVARTYCRRKILKKGSLVLERSLPIQDGQ VKELPVSVAEDVTIILQQGEQVPKPKQFMISETSLLAPITKGEVVAYLTSPRI TDQSVRYLKEPKRIPLKASQSLKKASDLQLWWRDFLEKRR

Gene ID (SpyM18)	Primary Protein Sequence
0280	MIKRLISLVVIALFFAASTVSGEEYSVTAKHAIAVDLESGKVLYEKDAKEVVP VASVSKLLTTYLVYKEVSKGKLNWDSPVTISNYPYELTTNYTISNVPLDKRKY TVKELLSALVVNNANSPAIALAEKIGGTEPKFVDKMKKQLRQWGISDAKVVNS TGLTNHFLGANTYPNTEPDDENCFCATDLAIIARHLLLEFPEVLKLSSKSSTI FDGQTIYSYNYMLKGMPCYREGVDGLFVGYSKKAGASFVATSVENQMRVITVV LNADQSHEDDLAIFKTTNQLLQYLLINFQKVQLIENNKPVKTLSVLDSPEKTV KLVAQNSLFFIKPIHTKTKNTVHITKKSSTMIAPLSKGQVLGRATLQDKHLIG QGYLDTPPSINLILQKNISKSFFLKVWWNRFVRYVNTSL
0031	MKKFHRFLVSGVILLGFNGLVPTMPSTLISQQENLVHAAVLGDNYPSKWKKGN GIDSWNMYIRQCTSFAAFRLSSANGFQLPKGYGNACTWGHIAKNQGYPVNKTP SIGAIAWFDKNAYQSNAAYDHVAWVADIRGDTVTIEEYNYNAGQGPERYHKRQ IPKSQVSGYIHFKDLSSQTSHSYPRQLKHISQASFDPSGTYHFTTRLPVKGQT SIDSPDLAYYEAGQSVYYDKVVTAGGYTWLSYLSFSGNRRYIPIKEPAQSVVQ NDNTKPSIKVGDTVTFPGVFRVDQLVNNLIVNKELAGGDPTPLNWIDPTPLDE TDNQGKVLGNQILRVGEYFTVTGSYKVLKIDQPSNGIYVQIGSRGTWVNADKA NKL
1382	MKKLNVILVGLLSILMLSLAIVFINRWKLNEDSQRIVLAEKKKNTSDLVIKAV KHIKKDQKDYYYFSPIKQADDFFVDNLPVSLYKKKNSDKELILVKPKLQSSHL RSVNTLTISKIVYQKKFFHLAKKSEKVISTYHVTDNLKPFQVKDLVSGHLERI QEEVEKKYPNAGFNSDKYNGLKESNSLLSDGFEVKSGNLIFDKKLTIPLTTLF DVINPDFLANSDRAAYDNYRTYKEQHPKKLVALTFDDGPDPTTTPQVLDILAK YQAKGTFFMIGSKVVNNENLTKRVSDAGHEIANHTWDHPNLTNLSVSEIQHQV NMTNQAIEKACGKKPRYLRPPYGATNATVQQSSGLTQMLWTVDTRDWENHSTD GIMTNVKNQLQPGGVVLMHDIHQTTINALPTVMEYLKAEGYECVTVSELYAHQ
1321	MLKRLWLILGPLLIAFVLVVITIFSFPTQLDHSIAQEKANAVAITDSSFKNGL IKRQALSDETCRFVPFFGSSEWSRMDSMHPSVLAERYKRSYRPFLIGKRGSAS LSHYYGMQQITNEMQKKKAIFVVSPQWFTVQGINPSAVQMYLSNTQVIEFLLK ARTDKESQFAAKRLLELNPGVSKSNLLKKVSKGKSLSRLDRAILKCQHQVALR EESLFSFLGKSTNYEKRILPRVKGLPKVFSYKQLNALATKRGQLATTNNRFGI KNTFYRKRIAPKYNLYKNFQVNYSYLASPEYNDFQLLLSEFAKRKTDVLFVIT PVNKAWADYTGLNQDKYQAAVRKIKFQLKSQGFHRIADFSKDGGESYFMQDTI HLGWNGWLAFDKKVQPFLETKQPVPNYKMNPYFYSKIWANRKDLQ
0476	MLKKRYQLAMILLLSCFSLIWQTEGLVKLFVCEHYERAVCEGTPAYFTFSDQK GAETLIKKRWGKGLVYPRTEQEAMAAYTCQQAALINTSLDKTKGELSQLTPEL

Gene ID (SpyM18)	Primary Protein Sequence
	RDQVAQLDAATHRLVIPWNIVVYRYVYETFLRDIGVSHADLTSYYRNDQFDPH ILCKIKLGTRYTKHSFMSTTALKNGAMTHRPVECASVSKKGPKQPLSSLIRLC LQRLSSCFQEAVSWRSLELTCHRTTKSST
1867	MTKVVIKQLLQVIVVFMISLSTMTNLVYADKGQIYGCIIQRNYRHPISGQIED SGGEHSFDIGQGMVEGTVYSDAMLEVSDAGKIVLTFRMSLADYSGNYQFWIQP GGTGSFQAVDYNITQKGTDTNGTTLDIAISLPTVNSIIRGSMFVEPMGREVVF YLSASELIQKYSGNMFAQLVTETDNSQNQEVKDSQKPVDTKLGESQDESHTGA MITQNKPKANSSNNKSLSDKKILPSKMGLTTSLELKKEDKFRSKKDLSIMIYY FPTFFLMLGGFAVWVWKKRKKMIKRCKGIGLVLMAFFLVACVNQHPKTAKETE QQRIVATSVAVVDICDRLNLDLVGVCDSKLYTLPKRYDAVKRVGLPMNPDIEL IASLKPTWILSPNSLQEDLEPKYQKLDTEYGFLNLRSVEGMYQSIDDLGNLFQ RQQEAKELRQQYQDYYRAFQAKRKGKKKPKVLILMGLPGSYLVATNQSYVGNL LDLAGGENVYQSDEKEFLSVNPEDMLAKEPDLILRTAHAIPDKVKVMFDKEFA ENDIWKHFTAVKEGKVYDLDNTLFGMSAKLNYPEALDTLTQLFDHVGDHP
0197	MGVMMKQKIKILTVIGLMTVGMSACHNTSKPSNTDSVFSLTGKKRQQIVKQVR QRYYFQQLSKTEQENYLTLYDSLAQFREIISLTPASTKSLIKTIDAFVMDNPE FYWITSADYRFEFSDQTVFVTFPIPEDAKNVYQDLQAIGNDIVANMPSKDRYE QVKYFYEVIIRDTDYNKKAFEAYQSGSQAQVASNQDIKSVFIDHLSVCNGYAQ AFQFLCQKAGIPVAYIRGTGTSQQPQQSFAHAWNAVQINNTYYGVDVTWGDPV FDNHLSHQKQGTINYSFLCLPDHLMALSHQPSKDIAFNTKERFENVWTIPSCT DDSLLYSKRHQSYISTFDSDAILASLENQLLNRQEPLSLQFAHQDDYQQMVTD LTTNQTGYHNLFNQYWNNYTGFTYGLLPETLSISFASRN